ADVANCED MASTERS IN STRUCTURAL ANALYSIS
OF MONUMENTS AND HISTORICAL CONSTRUCTIONS

Master's Thesis

Ajoy Kumar Das

Safety assessment of Mallorca cathedral

UNIVERSITAT POLITÈCNICA DE CATALUNYA

University of Minho

Education and Culture

Erasmus Mundus

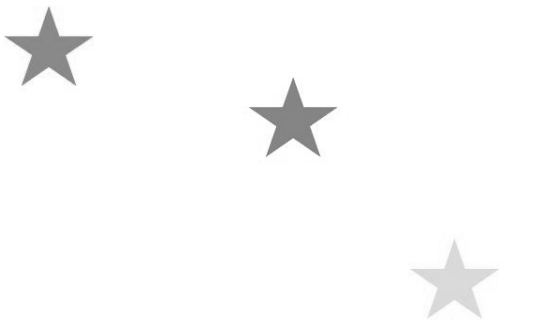

ADVANCED MASTERS IN STRUCTURAL ANALYSIS
OF MONUMENTS AND HISTORICAL CONSTRUCTIONS

Master's Thesis

Ajoy Kumar Das

Safety assessment of Mallorca cathedral

Supervisor

Prof. Pere Roca Fabregat

This Masters Course has been funded with support from the European Commission. This publication reflects the views only of the author, and the Commission cannot be held responsible for any use which may be made of the information contained therein.

Spain, 2008

Declaration

This thesis under European Erasmus Mundus Master's Program is the outcome of the study done at Universitat Politechnica de Catalunya Construction Department between April, 2008 and July, 2008. I declare that it is the result of my own work and contains no material that has been accepted for the award of any other degree or diploma in any educational institution and, to the best of my knowledge and belief, it contains no material previously published or written by another person, except where due reference is made in the text of the thesis.

Signed: ……..

Abstract

Safety analysis of a cultural heritage structure has been performed. After a making a detail account of past alterations, damage and present state, a 3D numerical model of a typical bay of the structure had been prepared in GID (ver. 8). To implement a realistic behaviour of material, a non-linear material model so called tension compression distributed damage model has been utilized. Analysis has been performed in COMET. The results include analysis both for gravity load and seismic load. An overall assessment of the ultimate vertical load carrying capacity (although a little realistic but gives a sense of safety psychologically) and structural behaviour at an earthquake demand displacement has been done to explain the safety condition of the structure.

Acknowledgement

I am grateful to my supervisor Prof. Pere Roca for his persistent technical guidance and encouragement throughout the period of my thesis work. I would also like to thank Luca Pela for giving me valuable information on the basics of the study.

I would like to express my gratitude to the European Commission for selecting me and providing me financial support through out the master's program.

I wish to take this opportunity to thank CIMNE, UPC, Barcelona for providing us the temporary licence of the GID software, utilized for the analysis.

I am thankful to all of my master's colleagues for their consistent mental support. My special thanks to Juan Murcia and Roberto Cuzzilla for valuable discussions with me.

I also want to thank my parents for inspiration, in spite of being far away from me.

Contents

1

Introduction

1.1 Historical aspect of masonry

Masonry construction is symbolizes the era when cave dwellers started stepping towards civilized life. Primitive man, eventually, discovered the methodology to arrange stones in such a way that could provide relief from the struggling life of cave. Formed naturally, the existing stones proved its strength and effectiveness for better habitat. Building houses became popular among ancient habitants. Primitive houses were built just by careful arrangements of the stones, no mortars or jointing materials were used. Circular stone huts, partially dug into the ground, dating from prehistoric times have been found in the Aran Islands, Ireland. By the 4th millennium BC, Egypt had developed an elaborate stone masonry technique, culminating in the most extravagant of all ancient structures, the pyramids.

Stone masonry was replaced by the clay brick masonry constructions in some part of the ancient world like in western Asia between the Tigris and Euphrates, lacked stone outcroppings but was rich in clay deposits. For example, the masonry structures of the Assyrian and Persian empires were constructed of sun-dried bricks faced with kiln-burned, sometimes glazed, units.

Mankind gained a lot of experience in the construction process. Different ideas came out in the form of construction typologies that prevented premature failure of constructions, which took a long time

to be understood. For example, prior to the arch, all builders in stone had been handicapped by the stone's breaking under its own weight when supported on widely separated piers or walls. The Egyptians had roofed temples with stone slabs but had been forced to place the supporting columns close together. The Greeks had used wooden roof beams covered with thin stone; such beams were subject to weather and fire. The arch introduced by Romans avoided tension entirely, keeping all the masonry in compression, from the keystone to the piers. Stone in compression has great strength, and the Romans built huge arched bridges and aqueducts in large numbers. Therefore innovative placing of stones in the form of arches gave a brilliant solution to failure under its own weight and became a breakthrough in the history of masonry construction. Extending their arch into a tunnel, they invented the barrel vault, with which they successfully roofed such buildings as the Temple of Venus in Rome. Several arches intersecting at a common keystone could be used to form a dome, such as that of the Pantheon in Rome (see Figure 1.1a). Two intersecting barrel vaults gave rise to the groin vault, which was used in some of the great Roman public baths.

The Roman arch underwent a significant modification in the middle ages in the evolution of the pointed arch, which provided a strong skeleton resting on well-spaced piers. The massive, rigid masonry structures of the Romans gave way to soaring vaults supported by external flying buttresses (external bracing). The use of smaller-sized stones and thick mortar joints created an elastic, slender structure that stressed the masonry to its fullest. The bearing of unit upon unit required the use of mortar to distribute the contact stresses.

With the advent of Gothic forms, masonry construction in a historic sense had solved the problem of spanning space entirely by material in compression, the most effective design formula suitable to stone. With time mankind captured idea of putting stone pieces in such a form that it rendered flat ceiling as can be seen in Mughal architecture in India. Agra Fort, India (construction completed in 1573 AD) is a great example having flat roofed ceiling (Figure 1.1b).

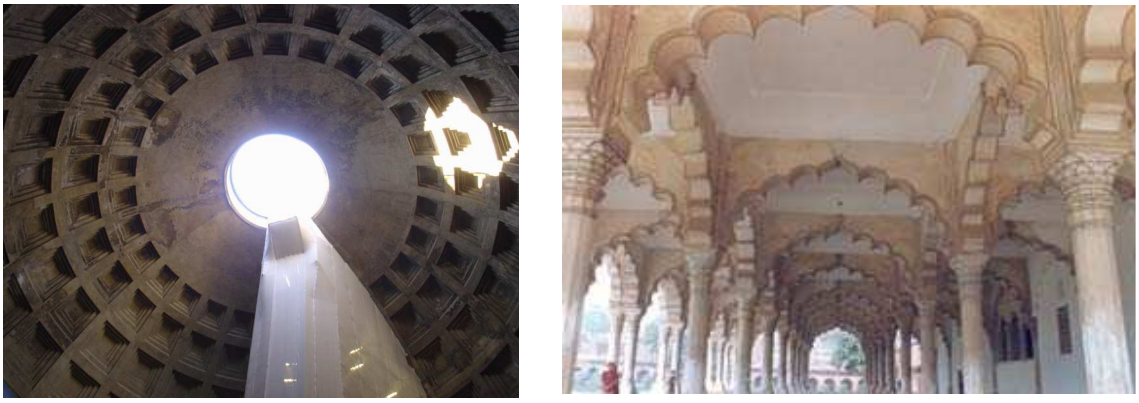

(a) (b)

Figure 1.1: (a) Roof of Panthenon (27 B.C.), Rome, Italy; (b) Flat roof in Agra Fort (1573 A.D.), Agra, India.

With the introduction of the truss in the 16th century, the rise of scientific structural analysis in the 17th century, and the development of high-tensile resistant materials (steel and reinforced concrete) in the 19th century, the importance of masonry as a material declined. In the fourth decade of twentieth century, discovery of concrete almost took the position of masonry as it provide more flexibility to form at site and also overcame the drawback regarding the lack of tensile strength on masonry. Reinforcement became part and parcel of concrete to improve the strength. In this way attention to the study and standpoint of masonry became weaker through the previous century.

1.2 Importance of structural analysis of masonry

Though masonry construction signifies for the mankind to step into civilization, a very difficult task can be to make the research to find the time of initiation of masonry construction practice by our ancestors. In turn, throughout the centuries masonry had been an art of construction. By means of its evolution till nineteenth century, masonry reached to its crown by overcoming its drawbacks (e. g. utilizing the masonry compressive stress). Though this superior position has been captured by reinforced concrete and steel very recently, almost all the architectural beauties are still in possession of masonry constructions, though older but retaining the sustainability. From the second half of the previous century tourism related to these historical constructions became a rapid growing industry in Europe. Tourism also increased in the East Asia, northern Africa. A significant part of the gross national income in some countries is now coming from tourism. Irrespective to ancient architectural heritage (for example, see Figure 1.2a) or modern heritage (for example, see Figure 1.2b) there are huge rush from all part of the world to see the architectural attractions.

(a)

(b)

Figure 1.2: (a) Colosseum (80 A.D.), Rome, Italy; (b) Agra Taj Mahal (1650 AD), Agra, India.

As the constructions in ancient times were mostly based on traditional influences, there was no hard and fast rule. Therefore analytical study of these structures came to attention of the researchers very recently in the last few decades of the twentieth century after several natural hazards caused significant damages to some heritage constructions. Till date the progress of the research in this field is not satisfactory for understanding the behaviour of masonry. The reason can be lack of awareness and insufficient fund reserved towards the conservation of the heritage structures. Other can be due to a small number of experts working in this field. Also it should be acknowledged undoubtedly that present curriculum of study of structural engineering is more oriented to modern materials. None the less from macro-level to micro-level of study of masonry behaviour demands a very good insight to focus in the behaviour.

In this perspective masonry demands for research to achieve the following goals:

Due to lack of research, the current codes of practice are underdeveloped and there is a lack of knowledge about the behavior of this composite material. The fundamental point of today's research in structural masonry is thus to *rationalize the engineering design of structural masonry* (Lourenco, 1996). A better understanding can result if the analytical procedures are followed closely with the experimental studies for validation.

Material should be described thoroughly and should be supported by comparing with significant number of experiment results. For this deformation controlled experiments on small to large-scale masonry including masonry samples will be effective. Using this material description a reliable and accurate numerical model can be developed for understanding the overall behaviour of large constructions. As a most important requirement recently discovered properties, like softening and dilatancy, being virtually absent in the masonry literature, play a crucial role in the nonlinear processes. Nonlinear finite element analyses will always be helpful for the *validation of the design of complex masonry structures under complex loading conditions* (Lourenco, 1996). In particular computations beyond the limit load down to a possibly lower residual load are needed to assess the safety of the structure. Aside from failure analysis, also the serviceability limit states can be successfully validated with numerical analyses, e.g. crack control and prevention for restrained shrinkage and differential movements.

Through the knowledge gained upon understanding the material behaviour and implementing these into computer codes, it is a must do responsibility to verify the safety of the ancient architectural constructions and to preserve them with minimal intervention for source of social, cultural inspiration of the mankind.

Another important goal shall be to erect a standpoint for implementing masonry constructions using locally available materials in the underdeveloped countries, as masonry is itself a environmental friendly, long lasting material which several advantages (e.g. sound, thermal insulating) over other construction materials. Also the masonry construction cost can kept reasonable limit upon using proper design and construction strategies.

1.3 Objectives of the thesis

The present study focuses on the understanding of behaviour of well known French-Gothic cathedral at Palma in the Mallorca island in the Mediterranean sea. In the name of the island the cathedral is called Mallorca Cathedral. Built over for more than two hundred years, the cathedral had been brought to the attention of researchers in several occasions. Following are two groups presented to summarise objectives will be carried out in the current study:

Main objectives

A three dimensional numerical model of representative single bay of the cathedral will be prepared in GID using four nodded tetrahedral elements. Tension-compression distributed damage model (referred only as distributed damage model in elsewhere) will be employed for numerical simulation of materials. The solution will be performed in COMET (Coupled Mechanical Thermal Analysis) developed by CIMNE, Barcelona. The analysis will look for the following main objectives:

(i) Dynamic identification to idealize the geometry and structural behaviour (e.g. by adjusting the elastic parameters) by modal analysis.

(ii) Analysis for real gravity load considering linear and non-linear material model to justify the suitability of the numerical model with non-linear material, which will be used in subsequent analyses.

(iii) Developing a partial idea of maximum vertical load carrying capacity of the structure using non-linear material model (although this has a very little significance in realistic sense).

(iv) Find out the lateral load carrying capacity employing non-linear static analysis (step by step horizontal force proportional to gravity) and modal pushover analysis (step by step displacement according to fundamental mode shape).

(v) Parametric analysis to find the effect of tensile strength on lateral load carrying capacity using non-linear static analysis.

(vi) Application of performance based seismic analysis (i.e. Capacity Spectrum Method) to understand the performance of the structure for a particular seismic demand.

Partial objectives

As one of the partial objectives, modal analysis of the three dimensional numerical model will be performed in DIANA 9.2. The modal parameters obtained will be compared with the existing information (both numerical and experimental) of the global model of the structure. Changing the elastic parameters will help to obtain the behaviour of the present model closer to experimental behaviour. Other partial objectives will summarize the background information and time to time study of the cathedral that will sustain the interest for the present study. A brief note on the tension-compression distributed damage model will be presented to put light on the material simulation. Also brief discussion will be made on the performance based seismic analysis (Capacity Spectrum Method), which is relatively new for masonry.

1.4 Thesis organisation

A brief overview has been presented in this chapter on the common lack of understanding of the masonry that makes the stand point of some earlier researches weaker. A brief discussion has been made on the importance of researches on masonry in present days. As well as for the existing historical constructions, the modern study should look for better understanding of the masonry behaviour that will motivate for future constructions using naturally available masonry.

Chapter 2 will provide a very basic conception on numerical modelling of masonry structures employing finite elements approach (both for macro- and micro-modelling approach). This will contain the geometrical and structural idealization of masonry constructions. A brief summary of different kind of nonlinear material modelling will discuss the specificity of the models for a particular construction material. At the end of the chapter a brief idea on the performance based seismic analysis of structures, which is relatively new to masonry constructions, will supplement the procedure to find performance of structures for a particular seismic demand.

Chapter3 includes complementary information on Mallorca cathedral to build the background knowledge of history of construction and alteration in different historical periods. How the present shape of the structure has evolved from small scale initial construction – this will be discussed keeping reference to available resources. As a most important part, past seismic events in the island has also been presented.

Chapter 4 summarises the previous structural analysis of Mallorca cathedral. This includes conclusions inferred by different authors based on their studies. This chapter will be referred in many occasions while in discussing the present analysis results in chapter 5.

Chapter 5 will contain the methodology of analysis and results that are mentioned in section 1.4. One important difference from previous analysis done by previous author (Clemente, 2007) is consideration of low fracture energy both for tension and compression, which would give more realistic modelling of the material. Among the possible out comes, the vertical load at collapse (though it does not have much realistic sense) and maximum lateral load carrying capacity will come to be lesser than that obtained by Clemente, 2007. Capacity spectrum method, based on performance based seismic analysis, will give clear interpretation of the structural behaviour. It will also be interesting to see the impact of the tensile strength on the lateral collapse of the structure. It is worth mentioning that there are no reliable data to consider tensile strength, rather it is adopted on empirical basis.

Chapter 6 will contain the general conclusions on the study of the structure. A brief discussion will be made on the safety of the structure both for current condition and future seismic hazard. Finally there will be a possible directions of future improvement of the research.

2

Structural analysis of historical constructions

2.1 Introduction

Ancient heritage constructions, built utilizing the philosophic sense and traditional practice, is a major challenge to sophisticated modern procedures. It has been admitted undoubtedly by the experts in this field that the complexity is inherent within the construction itself. The branching of advanced knowledge for studying modern structures, applied in this field is relatively new. And analysis of historical constructions is still a complex issue (Lourenço, 2001, 2005; Roca, 2001, 2004; Modena, 2004; Binda, 2005). A very insignificant research has been done so far to derive a common simple procedure in order to have the idea of mechanical properties of historical materials. More over the material of construction are observed to vary from part to part of the structure built in different period. Depending on the availability, different materials can be found in different parts of the structure although even if built at the same period. Another important factor is that the change of material properties over time. Therefore the research done so far in this field is not adequate to take all these material issues into any empirical procedure that could be helpful for other studies. Apart from the complexity of material characterization there are several complexity associated with the structure itself. For most of the ancient constructions geometrical information are not adequate.

Construction sequences had not been recorded clearly. Invisible damage and micro cracks change the behaviour of the structure, which instigates to suspicion to the material properties even though they are well representative of the same. Some times historical natural hazards (earthquake, cyclone, soil settlements etc.) that caused damage to the structure had not been archived for its future use.

Therefore analysis of the historical structures is mainly challenged by the material and the structural characterization. Once these are understood, it needs to adopt suitable method for both qualitative and quantitative understanding of the structural behaviour and thereby surmising possible safety of the structure. From ancient study of simple analytical procedure (thrust-line analysis) to modern sophisticated numerical analysis, there are different procedures (depending on the aim and complexity of the structure involved) of the structural modelling that could be well representative for its analysis. At the same time it has been depicted by authors that a complex analysis may not necessarily produce a result better than a simplified model (Lourenco, 2002). Therefore before applying any method the analyst must impose his careful judgements into the structural model.

The present chapter deals the available modelling strategies of historical masonry structure. A brief light has been put into the numerical modelling of materials which are in case of masonry structures highly nonlinear. A small description has been made on the formulation of material selected (chapter 5) for the analysis of Mallorca cathedral. Finally a brief note introduces the methodology of capacity spectrum method that has been employed to assess the seismic strength of the cathedral (same chapter).

2.2 Numerical modelling strategies of masonry structures

Masonry is a composite material consisting of units of bricks or stone blocks and mortar, a weak material joining the individual units at their interface. These two materials have distinct characteristics of their own. Therefore the representation of the materials for the simulation of the structure globally is a bit complex. The approaches for its numerical representation mainly focus on two different ways of modelling namely modelling of individual components of units and mortar called micro-modelling and simplified modelling considering masonry as a composite material called macro-modelling. Depending on the type and size of the structure and the result intended the following strategies are taken into consideration (see Computations of Masonry Structures, Lourenço, 2002).

***Detailed micro-modelling**:* Here the concept lies in representing the units and mortars as continuum elements whereas unit-mortar interface is represented by discontinuum elements. In this approach, material parameters such as Young's modulus, Poisson's ratio and inelastic properties

(optional) of both unit and mortar are taken into account. The interface, which is actually a plane of potential crack/slip, is modelled with initial dummy stiffness to avoid interpenetration of the continuum. Therefore this enables the combined action of unit, mortar and interface to be studied under magnification (Figure 2.1**a**).

Simplified micro-modelling: In this approach, each joint that consists of mortar and the two unit–mortar interfaces, considered as an average interface while the units are expanded in order to keep the geometry unchanged (Figure 2.1b). Masonry is thus considered as a set of elastic blocks bonded by potential fracture/slip lines at the joints. Since the Poisson effect of the mortar is not included in this kind of modelling, the accuracy of results is lost.

Macro-modelling: Macro-modelling approach is simplified by means of abolishing the difficulty of distinctive characteristics of unit, mortar and unit-mortar interface, and introducing the concept of homogeneous anisotropic continuum into the masonry as a whole (Figure 2.1**c**).

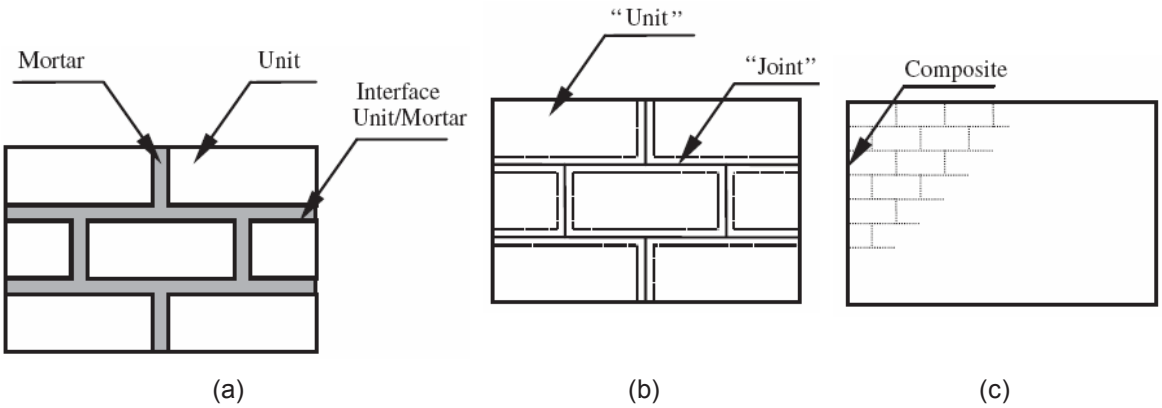

Figure 2.1: Masonry modeling: (a) detailed micro-modelling, (b) simplified micro-modelling, (c) macro-modelling (Lourenço, 2002).

Consideration of above mentioned methods for structural modelling varies from situation to situation depending on the size of the structure and purpose of analysis. Therefore it is not justifiable to make comparison of different methods. When the local behaviour of a structural masonry is a prime concern of understanding macro-modelling plays an efficient tool in that case. Macro-modelling is applicable for structures consisting of solid wall and sufficiently large dimensions such that variation of stresses across or along the micro-level is insignificant (can be considered as uniform). But macro-modelling has a great advantage over micro-modelling in the sense that it consumes less time and computer memory to carry out an optimal analysis.

2.2.1 Finite element models for continua (macro-modelling)

Mostly in all the ancient structures the complexity in geometry is associated with massive structural parts like pier, buttresses combined with arches and vaults. Finite Elements Method is an efficient method in modern time to represent suitably a historical structure in two-dimension and three dimensions overcoming these geometrical complexity. But main difficulty of implementation of macro-modelling is still prominent because of the lack of comprehensive experimental data explaining pre or post-peak behaviour. Another fact is complexity that is still needs to be overcome to formulate adequately anisotropic inelastic property of material. Formulation of the behaviour of isotropic quasi-brittle materials considers, generally, different inelastic criteria for tension and compression. The model introduced by Lourenco et al. (1998) recently extended to accommodate shell masonry behaviour, combines the advantages of modern plasticity concepts with a powerful representation of anisotropic material behaviour, which includes different hardening/softening behaviour along each material axis.

2.2.2 Discontinuum models (micro-modelling)

Masonry joint is the plane of weakness in the interface of units. The representation of the joints and the units in a numerical model needs a specific algorithm leading to rigorous analysis tool. This kind of analysis is adequately used for small structures where the state of stress and strain has sharp variation. Characteristic properties of each of the units, mortar and interface are required in this case. Finite Elements Method can be used as an efficient tool for the analysis of micro-models. This approach is still limited to research and small models as it needs more computational cost. As all the possible features of constituents materials and their interface is taken into consideration, this kind of analysis must include the failure mechanisms namely cracking of joints, sliding, cracking of the units and crushing of masonry.

2.2.3 Idealization of geometry

It is well accepted opinion about the inherent complexity of historical structures. Therefore geometrical idealization should be done in a simplest way up to the extent where it would be sufficient enough for the analysis. Careful judgement made by Lourenço (2002) includes the following:

- fully three-dimensional models are usually very time-consuming with respect to preparation of the model, to perform the actual calculations and to analyse the results. In the case of the widely spread finite element method, several authors use eight node bricks, with one element over the thickness of the walls or vaults. The errors associated with such a

discretization are very large, even in the case of a linear elastic analysis, yielding meaningless results;

- the results of models incorporating shell elements are fairly difficult to analyse owing to the variation of stresses along the thickness of the elements. In addition, the large thickness of the structural elements may yield a poor approximation of the actual state of stress;
- increasing the detail and size of the model might result in a large amount of information that blurs the important aspects.

The author pointed towards simplification of geometry by (a) using two-dimensional models rather than three-dimensional models; (b) avoiding the use of shell elements in areas important for the global behaviour of the structure; and (c) modelling structural parts and details instead of modelling complete and large structures.

2.2.4 Idealization of structural behaviour

Idealization of structural behaviour lies in the idealization of the constituent material of the structure. Commonly adopted behaviour for analysis is elastic behaviour (with or without taking into account the redistribution of stresses), plastic behaviour and nonlinear behaviour. Linear elastic analysis assumes that the material obeys Hooke's law. This is hardly the case for masonry under tension, which cracks at very low stress levels.

Nonlinear analysis is the most powerful method, able to trace the complete response of a structure from the elastic range, through cracking and crushing, up to complete failure. There are different possibilities of nonlinearity, namely, physical (related to the nonlinearity of the material), geometric (related to the fact that the point of application of loads changes with the increase of actions, and that structures buckle due to instability) and contact (related to the addition or removal of supports, or to the change of contact between bodies with the increase of actions). These nonlinearities can be combined efficiently in structural analysis. It may be used for both ultimate limit states (ULS) and serviceability limit states (SLS).

Plastic analysis or limit analysis aims at evaluating the structural load at failure. It is to be used only for verification of ULS and, theoretically, the material must exhibit a ductile response. This method can be assumed as adequate for the analysis of historical masonry structures if a zero tensile stress is assumed. The plastic analysis is based either on the lower-bound (static) method or on the upper-bound (kinematic) method. Its application to larger structures is rather cumbersome, and the issue of structural safety is difficult to solve. The inherent difficulty in the use of this tool is the selection of an adequate collapse mechanism for a given load combination. For traditional masonry structures, such as the buildings in historic centres, the method is readily applicable to analysis and strengthening. For more complex and unique monumental structures, this method is still of interest

to calculate strengthening, once the relevant collapse mechanisms are identified and the structural behaviour is understood from nonlinear analysis.

Finally, it need mention that linear elastic finite element models have been widely used for analysing historic structures. Sometimes, cracks have been included in the model, by assuming a zero stiffness set of elements in areas where cracks already exist in the structure Lourenço (2002), or in areas where the linear elastic calculation predicts high tensile stresses. The use of linear elastic analysis seems debatable, taking into account the advanced tools today available to solve engineering problems.

2.2.5 Modelling of material

Due to highly nonlinear behaviour of masonry a suitable criteria needs to be implemented in the computer codes to have acceptable and reliable solution. However a very sophisticated constitutive model makes sense only when the main objective of the analysis is to follow with the best possible accuracy of the post-failure behaviour at all points of a structure. Considering full scale ancient masonry structures it is quite hard to completely define the equilibrium path, particularly in the post-peak behaviour. Currently, to simulate the non linear behaviour of masonry, different constitutive models can be employed. For modelling continua (macro-modelling), one can opt, as, for example, smeared cracking with decomposed strain, total strain based models, plasticity based models, damage formulations. For cracking in discontinua, interface models based on decomposed relative displacements, total relative displacements, plasticity based approaches and other models are available. The attention will now focus on continuum models since these can be satisfactorily employed for macro-modeling schemes. The concept of *smeared cracking* will be outlined since it is strictly connected with the constitutive models described in the following section. In comparison with the discrete cracking, mainly employed in micro-modeling strategies and based on a σ–τ yield domain, with the smeared cracking approach the elastic domain is bounded in terms of principal stresses. The effect of a crack (or shear plane) is *spread out* over the area that belongs to an integration point, and the concepts of crack/stress displacements are substituted with those of crack/stress *strains.* Main advantages of the concept are that no special interface elements are needed in order to define the cracked stage, and there are no restrictions with regard to the direction and location of cracks. Though the smeared crack model has originally been developed for global analysis of large scale reinforced concrete structures, now with the advent of fracture mechanics, it became clear that smeared crack models could also be applied to detailed analysis of individual crack localizations. In the following, a description of the different continuum constitutive models will be provided.

Decomposed-strain based smeared crack models

The strain is decomposed into a part representing the non-cracked material and a part that belongs to the crack. These models are conceptually elegant as they allow for the separate treatment of softening for the cracks and elasticity and/or plasticity for the continuum between the cracks, as in equation (2.1).

$$\varepsilon = \varepsilon^{el} + \varepsilon^{crk} + \varepsilon^{cru} \tag{2.1}$$

where:

ε is the total strain vector

ε^{el} is the strain elastic component

ε^{crk} is the strain cracking component

ε^{cru} is the strain crushing component

The strain decomposition includes secant unloading/reloading both for the mode I (tensile) and mode II (shear) (Figure 2.2). Another advantage is that the strain of the material between the cracks can be sub-decomposed into e.g. an elastic part, a creep part, a plasticity part and/or a thermal part. This allows for the combination of cracking with other nonlinear phenomena. Furthermore, the crack strain can be decomposed into the local crack strains of a number of cracks at different orientations. This gives the possibility to handle non-orthogonal multidirectional cracking.

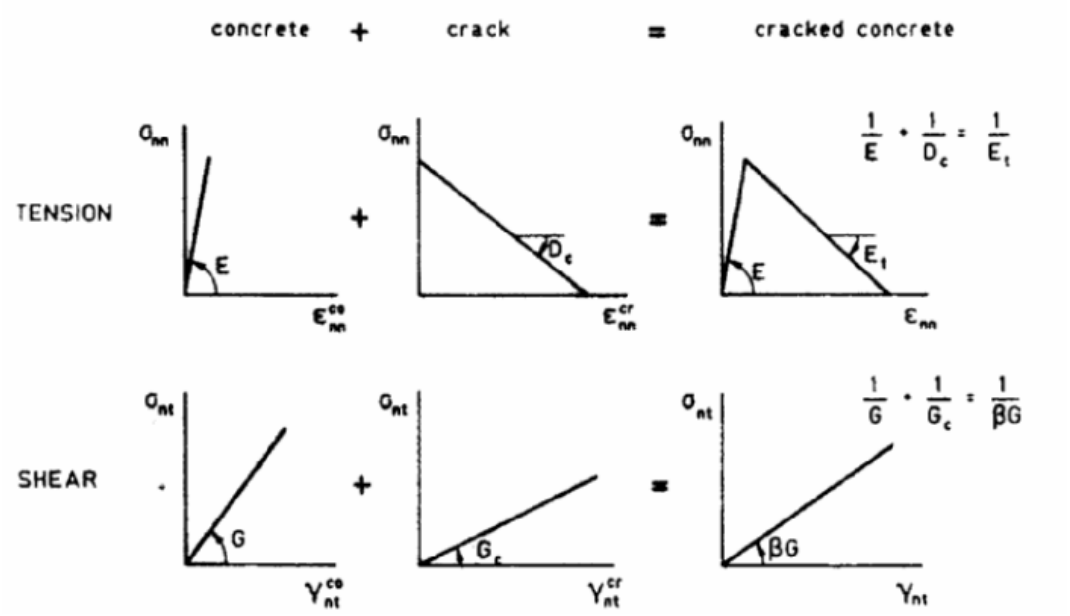

Figure 2.2 Smeared cracking with decomposed strain (Rots, 2002 referred by Casarin, 2006)

As failure modes in tensile regime, Rankine plasticity model and multiple fixed smeared crack models can be used. A popular decomposed strain model for compressive crushing is a plasticity model, e.g. Drucker-Prager or in plane stress the Von Mises yield criterion. The models for tension and compression can be combined, so that we arrive either at a full Rankine-Von Mises plasticity model, or a combination of the multiple fixed-smeared crack model for tension with Von Mises plasticity for compression. Though the model is thus conceptually attractive, the difficulty lies in the implementation and parameter choices. Two practical disadvantages are to be mentioned. First, the algorithmic aspects are complicated. The model needs internal iterations to handle state changes like unloading, closing and reopening, to handle nonlinear softening diagrams and to handle the combination with plasticity for compression strut action. When multiple cracks occur this internal iteration procedure may fail and even sub-stepping cannot always guarantee success. Secondly, the user's choices for shear retention functions and inter-crack threshold angles are not obvious, which may e.g. result in a too stiff response, stress-locking or uncontrollable principal stress rotation (Casarin, 2006).

Total-strain based models

A stress-total strain relation is defined for the continuum, in either fixed or rotating axes. These models present a decreased possibility of including sophisticated crack laws, being however appealing from an engineering point of view, because both tension and compression are captured within the same framework, via the stress-strain laws for tension and compression respectively. The total-strain based fixed model is an extended fixed, orthogonal crack model, and the total strain based rotating model is an extended rotating, orthogonal crack model. For the fixed version, shear retention parameters are required, whereas the rotating version uses an implicit shear term to provide co-axiality between the rotating principal stress and strain. The internal state is then fully described by the components of the updated strain vectors and internal variables. The basic assumption in a total-strain based model is that the constitutive relationship are evaluated in a rotated, local coordinate system defined by an assumption for the crack initiation. The global strain update is given by

$$\varepsilon_{xy} = \varepsilon_{xy} + \Delta\varepsilon_{xy} \tag{2.2}$$

The local strain vector is now determined as

$$\varepsilon_{ns} = T({}^{\tau}\phi)\varepsilon_{xy} \tag{2.3}$$

With φ the angle between the global coordinate system, *xy*, and the local coordinate system, *ns*, determined for the fixed version at the time τ in correspondence of the first occurrence of the

violation of the failure condition in tension, and constantly updated ($\tau = t + \Delta t$) for the rotating version. In a plane stress situation (Figure 2.3), the angle is given by equation (2.4):

$$ {}^{\tau}\phi = \frac{1}{2}\arctan\frac{{}^{\tau}\gamma_{xy}}{{}^{\tau}\varepsilon_{xx} - {}^{\tau}\varepsilon_{yy}} \tag{2.4} $$

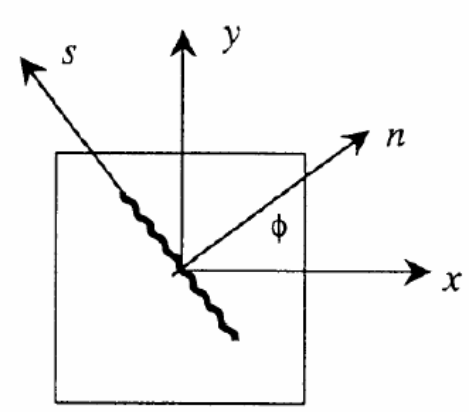

Figure 2.3: Local and global coordinate system (Feenstra et al., 2001 referred by Casarin, 2006).

Given the angle between the local and global coordinate system the strain transformation matrix is given by

$$ T = \begin{bmatrix} \cos^2\phi & \sin^2\phi & \sin\phi\cos\phi \\ \sin^2\phi & \cos^2\phi & -\sin\phi\cos\phi \\ -2\sin\phi\cos\phi & 2\sin\phi\cos\phi & \cos^2\phi - \sin^2\phi \end{bmatrix} \tag{2.5} $$

The stress vector in the local coordinate system is given by the general relationship

$$ \sigma_{ns} = D(\varepsilon_{ns})\varepsilon_{ns} \tag{2.6} $$

With the assumption of a co-rotational concept between the local strain vector and the local stress vector the updated stress vector in the global coordinate system is given by

$$ \sigma_{xy} = T({}^{\tau}\phi)^T \sigma_{ns} \tag{2.7} $$

With these equations the whole concept of total strain-based models is explained, with the only need to specify the constitutive relationship in the local coordinate system. It is emphasized that these equations are equal for the fixed and the rotating version of the total strain-based models. The formulation of the constitutive model in the local coordinate system, equation (2.6), is possible in a large number of ways. This approach is attractive to practicing engineers who think in terms of stress-strain relations and can plug these in directly. There is no need to input abstract yield functions or sophisticated crack laws. The concept of a stress-strain relation can be used both for softening or stiffening in tension and for non linear behaviour and crushing in compression. Moreover, from an implementation and algorithmic point of view, the model is purely explicit and does not require internal iterations. After updating a number of internal state variables, the stress is computed directly from the strain. Local convergence problems or closing/reopening difficulties do not exist. On the other hand, with such formulation only orthogonal cracks can be modelled. Non-orthogonal multi-directional cracking cannot be included, even if this limitation is not very serious, due to the difficulty connected with the parameter choices for non orthogonal cracking, and to the fact that many engineering problems only involve orthogonal cracking. Another disadvantage is that combinations with creep, shrinkage and thermal strains are not straightforward due to the description in terms of lumped total strain. Here, the decomposed model is to be preferred. The rotating crack model can be derived as a special case of the decomposed multi-directional model assuming a zero inter-crack threshold angle, so that a new crack under slightly different angle is initiated in each step while the previous cracks unload elastically. Regarding the choice of fixed versus rotating, fit can be said that for localized cracking the rotating model is to be preferred. It provides less stress-locking than the fixed version. For smeared cracking in reinforced structures, explicit shear across fixed cracks can be relevant. If so, the fixed model provides more possibilities to model that, although the choices for shear retention functions are not obvious considering their interrelation with possible uncontrollable principal stress rotations (Casarin, 2006).

Plasticity based crack models

Several standard elastic-plastic constitutive laws have been developed to model materials presenting quasi brittle behaviour, starting with the simple "no tension" law described and used in. Other plasticity models commonly used in analysing masonry are the Drucker-Prager and Mohr-Coulomb laws. Even the von Mises constitutive model has sometimes been used. Rankine-Von Mises and Rankine-Drucker Prager crack-crush models including softening for the two domains were developed by Feenstra (1993) referred by Casarin (2006). The advantage is that the additive strain decomposition and general theory of elasto-plasticity can be used. The implementation and algorithmic aspects follow a concise format, and it has been demonstrated that quadratic convergence can be achieved for a number of localized fracture problems. However, other experiences exist with spontaneous divergence, probably due to local internal convergence

problems or problems with maintaining the global consistent (negative) tangent stiffness. An advantage of the plasticity based models is that they can be extended to orthotropic material, still using the same principles. This was developed and carefully evaluated by Lourenço (1996) for masonry, with Rankine-Hill criteria. Also the framework of the decomposed smeared crack model allows for extension to orthotropic elastic and fracture behavior. Another advantage of a plasticity formulation is that it allows for a transparent extension to creep, shrinkage and thermal effects. A disadvantage of plasticity based models is the inherent elastic unloading/reloading. A secant approach back to the origin, as included in the decomposed as well as total-strain based smeared crack models, is a better approximation of the real unloading behavior for quasi-brittle material. Figure 2.4 gives and example in tension.

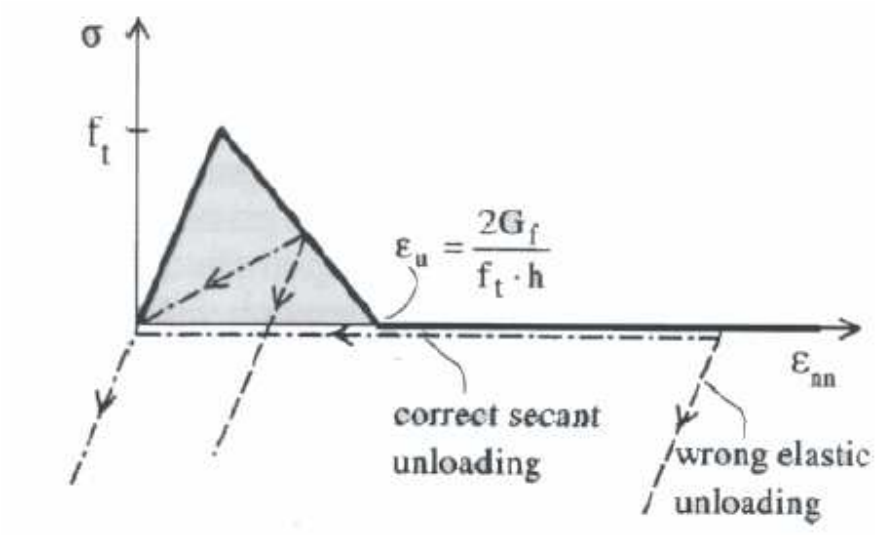

Figure 2.4: Secant and elastic unloading options (Rots, 2002 as referred by Casarin, 2006).

On purpose, in Figure 2.4 the unloading behavior for a fully open crack is included, i.e. a crack for which the strain is far beyond the ultimate strain of the tensile softening diagram. This ultimate strain for tension-softening is based on the crack band model which reads for a linear diagram: (2 G_f) / (f_t h) with G_f the fracture energy, f_t the tensile strength and h the crack band width which is related to finite element size and lay-out. Often, researchers evaluate models for small-scale notched beams. Then, h is small, and consequently ε_u is large, so that one does not pass the ultimate point of the diagram easily. For large-scale structures, however, h is large and ε_u relatively small. The Rankine plasticity model with elastic unloading then gives a response which is far from the real unloading behavior that passes almost along the origin. Non-proportional loadings and erroneous results may be found with the elastic unloading option. Plasticity models should be extended with damage options to improve this behaviour (Casarin, 2006).

Damage based models

Damage constitutive models have only recently been used for the applications to masonry structures. The isotropic damage modelling approach is based on the simplifying assumption that the stiffness degradation is isotropic, i.e., stiffness modulus corresponding to different directions decrease proportionally and independently of direction of loading. The unloading is of secant type, and it was demonstrated that stress-locking does not occur and that curved mode-I fractures can be simulated accurately. A disadvantage of isotropic damage models is that also the compression strut action parallel to the crack degrades to zero. This makes these models impractical for reinforced concrete where the compression strut action is crucial. Recent development in the formulation of damage-based constitutive models applied to continuum models can be found in present studies, where different in-plane damage mechanisms, involving both mortar and blocks, are considered and the damage process is governed by evolution laws based on an energetic approach derived from fracture mechanics and on a non-associated Coulomb friction law. The failure domain is analysed considering different orientations of the bed joints relative to the loading direction(Casarin, 2006).

2.3 Selective formulation

The present section puts light into the formulation that will be used in chapter 5 for the analysis of Mallorca cathedral. The current formulation is a derivation utilizing the concept of isotropic damage model and takes into consideration two scalar internal variables to monitor the local damage under tension and compression, respectively. This provides a simple constitutive model which captures the overall non-linear behaviour including strain-hardening/softening response, stiffness degredation and retardation under multiple stress reversals and the rate dependency. Masonry being a highly nonlinear material exhibiting dramatic softening (i.e. with very low tensile/compressive fracture energy) this model can reproduce the behaviour in a more realistic way. Also for the analysis of large scale constructions this model is considered effective as it manifest the damages directly on the in the structural model. Furthermore one of the most valuable features of this model intended to be used in large scale computations is that this model holds the possibility of implementation in a strain-driven form which leads to an almost closed form algorithm to integrate the stress tensor in time.

2.3.1 Tension-compression distributed damage model

The model is based on the effective stress concept ($\overline{\boldsymbol{\sigma}}$), defined as the stress associated to elastic strains $\boldsymbol{\varepsilon}$; or $\overline{\boldsymbol{\sigma}} = \mathbf{D} : \boldsymbol{\varepsilon}$, where $\mathbf{D}$ is the elastic constitutive tensor. The tensor $\overline{\boldsymbol{\sigma}}$ is divided into a positive or tensile part $\overline{\boldsymbol{\sigma}}^{+}$ and a negative or compressive part $\overline{\boldsymbol{\sigma}}^{-}$, in the following way:

$$\overline{\boldsymbol{\sigma}}^{+} = \sum_{i=1}^{3} \left\langle \overline{\sigma}_i \right\rangle \mathbf{p}_i \otimes \mathbf{p}_i \qquad \overline{\boldsymbol{\sigma}}^{-} = \overline{\boldsymbol{\sigma}} - \overline{\boldsymbol{\sigma}}^{+} \tag{2.8}$$

where $\overline{\sigma}_i$ is the i-th principal stress of $\overline{\boldsymbol{\sigma}}$; $\mathbf{p}_i$ represents the unit vector associated with the principal direction i and $\langle \bullet \rangle$ are the Macaulay brackets.

Two internal variables of damage, each one associated with a sign of the stresses are also defined: d^{+} for tensile damage and d^{-} for compressive damage. Under these considerations, the constitutive equation is written as:

$$\boldsymbol{\sigma} = \left(1 - d^{+}\right)\overline{\boldsymbol{\sigma}}^{+} + \left(1 - d^{-}\right)\overline{\boldsymbol{\sigma}}^{-} \tag{2.9}$$

These variables state the level of damage reached at each integration point, in such a way that $d^{\pm} = 0$ means that the material is intact and $d^{\pm} = 1$ indicates the total material failure. The use of a different variable for each sign of the stresses implies that, for example, a material previously damaged to traction would recover its original behaviour if it is put under compression, and vice versa.

Next, the equivalent effective stress norm is defined. This is a scalar positive value that is used to compare different stress states in three dimensions, and it is useful to unify load, unload and reload concepts. The equivalent norms for tensile effective stress (τ^{+}) and for compressive effective stress (τ^{-}) have the form:

$$\tau^{\pm} = \left(\overline{\boldsymbol{\sigma}}^{\pm} : \mathbf{C}^{\pm} : \overline{\boldsymbol{\sigma}}^{\pm}\right)^{1/2} \tag{2.10}$$

where the two non-dimensional fourth order metric tensors $\mathbf{C}^{+}$ and $\mathbf{C}^{-}$ are identical and equal to the inverse of tensor $\left(\mathbf{D}/E\right)$, being E the Young's modulus of the material.

Starting from the previous definitions, two different criteria of damage can be introduced, namely, g^{+} and g^{-}, defined as

$$g^{\pm}\left(\tau^{\pm}, r^{\pm}\right) = \tau^{\pm} - r^{\pm} \leq 0 \tag{2.11}$$

where r^+ and r^- are internal variables that control the size of the damage surface in the stresses space in every time step. Their initial values are $r_0^{\pm} = f_e^{\pm}$, where f_e^+ and f_e^- are the strength of material—the stresses at which the material fails and damage appears. In this sense, the explicit definition of these internal variables has the form:

$$r^{\pm} = \max\left[r_0^{\pm}, \max\left(\tau^{\pm}\right)\right] \tag{2.12}$$

The criteria stated above imply that damage evolution occurs when condition (2.11) is not satisfied. In this case, $r^{\pm}$ is updated using (2.12) $r^{\pm} = \max\left[r_0^{\pm}, \max\left(\tau^{\pm}\right)\right]$ (2.12), until damage criterion is satisfied again. Finally, the damage variables d^+ and d^- are defined explicitly as a function of their respective internal variables $r^{\pm}$. They are monotonic increasing functions of the form $0 \le d^{\pm}\left(r^{\pm}\right) \le 1$. The post-peak behaviour is defined by means of the tensile and compressive fracture energy of the material $G_f^{\pm}$. This parameter is normalized respect to the characteristic length of the finite elements, to ensure objectivity respect to the mesh size.

2.4 Capacity spectrum method

Rehabilitation of old masonry structures in seismically vulnerable areas is a matter of growing concern. The main objective is to identify the masonry structures susceptible to damage and also determine the acceptable level of damage. Simplified linear static analyses are found to be inadequate to make such kind of assessment. A continual research by the structural engineering community has successfully developed a new generation of analysis procedure called performance based structural evaluation and thereby leading the analysis procedure from linear static towards the nonlinear (inelastic) analysis. An inelastic procedure commonly referred to as the pushover analysis is a viable method to assess damage vulnerability of existing buildings. Basically, a pushover analysis consists of a series of incremental static analysis carried out to develop a capacity curve for the building. Based on the capacity curve, a target displacement which is an estimate of the displacement that the design earthquake will produce on the building is determined. The extent of damage experienced by the structure at this target displacement is considered representative of the damage experienced by the building when subjected to design level ground shaking. Many methods were presented to apply the nonlinear static pushover (NSP) to structures.

These methods can be listed as: (1) the capacity spectrum method (CSM) (2) displacement coefficient method (DCM) (3) modal pushover analysis (MPA).

The capacity spectrum method was developed by Freeman (1975). By means of a graphical procedure, it compares the capacity of a structure with the demands of earthquake ground motion on the structure (Figure 2.1). The graphical presentation makes possible a visual evaluation of how the structure will perform when subjected to earthquake ground motion. The method is easy to understand. The capacity of the structure is represented by a force-displacement curve, obtained by non-linear static (pushover) analysis. The base shear forces and roof displacements are converted to the spectral accelerations and spectral displacements of an equivalent Single- Degree-Of-Freedom (SDOF) system, respectively. These spectral values define the capacity spectrum. The demands of the earthquake ground motion are defined by highly damped elastic spectra. The Acceleration-Displacement Response Spectrum (ADRS) format is used, in which spectral accelerations are plotted against spectral displacements, with the periods represented by radial lines. The intersection of the capacity spectrum and the demand spectrum provides an estimate of the inelastic acceleration (strength) and displacement demand.

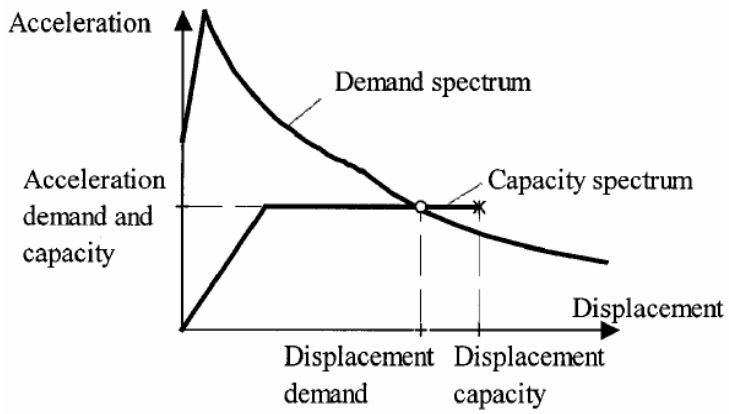

Figure 2.5: Capacity spectrum method.

2.4.1 Modelling of capacity curve and capacity spectrum

Capacity curve

A building capacity curve, termed also as 'pushover' curve is a function (plot) of a buildings' lateral load resistance (base shear, V) versus its characteristic lateral displacement (peak building roof

displacement, Δ_R). Building capacity model is an idealized building capacity curve defined by two characteristic control points (as in Figure 2.6): 1) Yield Capacity (YC), and 2) Ultimate Capacity (UC).

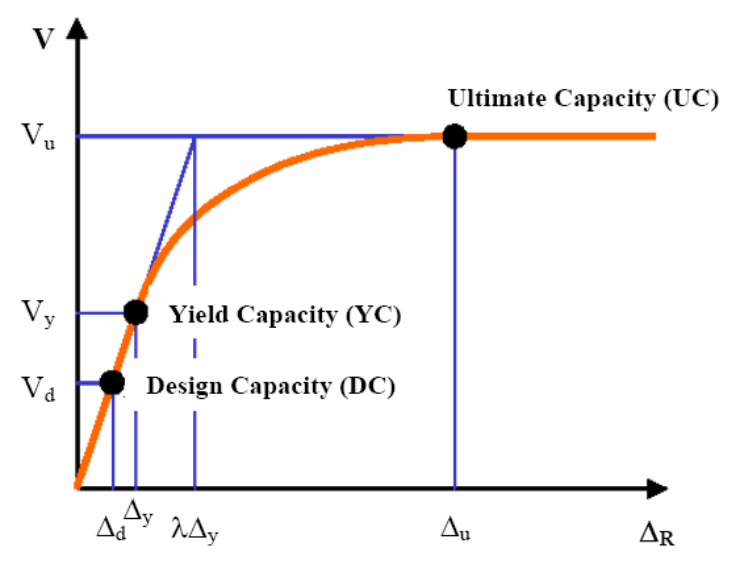

Figure 2.6: Building capacity model.

Yield capacity (YC) is the lateral load resistance strength of the building before structural system has developed nonlinear response (Figure 2.6).

Ultimate capacity (UC) is the maximum strength of the building when the global structural system has reached a fully plastic state (Figure 2.6). Beyond the ultimate point buildings are assumed capable of deforming without loss of stability, but their structural system provides no additional resistance to lateral earthquake force.

Both, YC and UC control points are defined as:

$$\begin{aligned} &\text{YC } (V_y, \Delta_y): && V_y = \gamma C_s && \Delta_y = \frac{V_y}{4\pi^2} T^2 \\ &\text{UC } (V_u, \Delta_u): && V_u = \lambda V_y = \lambda \gamma C_s && \Delta_u = \lambda \mu \Delta_y = \lambda \mu \gamma C_s \frac{T^2}{4\pi^2} \end{aligned} \qquad (2.13)$$

where:

C_s is design strength coefficient (fraction of building's weight),

T is true "elastic" fundamental-mode period of building (in seconds),

γ is "overstrength" factor relating design strength to "true" yield strength,

λ is "overstrength" factor relating ultimate strength to yield strength, and

μ is "ductility" factor relating ultimate (Δ_u) displacement to λ times the yield (Δ_y)

displacement (i.e., assumed point of significant yielding of the structure)

The overstrength (γ, λ) and ductility (μ) parameters are defined by the code requirements, based on experimental/empirical evidence and/or on an expert judgment.

Capacity spectrum

For assuring direct comparison of building capacity and the demand spectrum as well as to facilitate the determination of performance point, base shear (V) is converted to spectral acceleration (S_a) and the roof displacement (Δ_R) into spectral displacement (S_d). The capacity model of a model structure presented in AD format (Figure 2.7) is termed Capacity Spectrum (Freeman, 1975, 1998). Conversion of capacity model (V, Δ_R) to capacity spectrum shall be accomplished by knowing the dynamic characteristics of the structure in terms of its period (T), mode shape (φ_i) and lumped floor mass (m_i). For this, a single degree of freedom system (SDOF) is used to represent a translational vibration mode of the structure. Two typical control points, i.e., yield capacity and ultimate capacity, define the Capacity Spectrum (Figure 2.7):

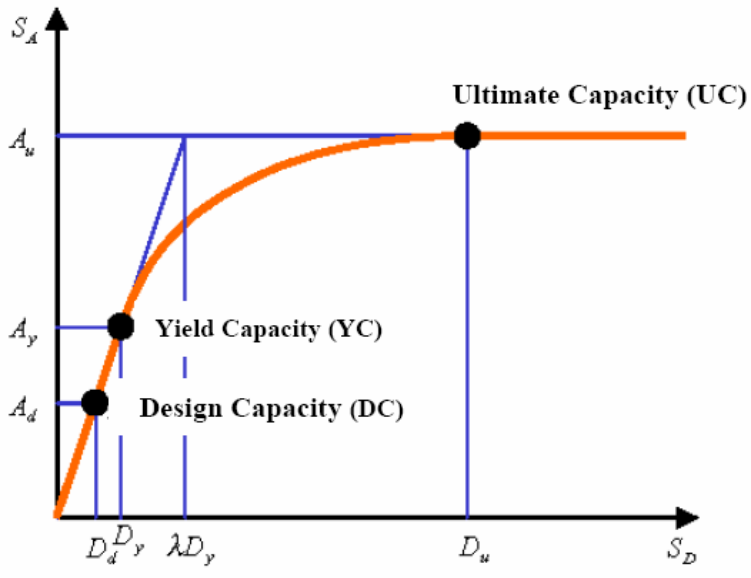

Figure 2.7: Building capacity spectrum.

$$\begin{aligned}
&\text{YC } (A_y, D_y): && A_y = S_{ay} = \frac{C_s \gamma}{\alpha_1} && D_y = S_{dy} = \frac{A_y}{4\pi^2} T^2 \\
&\text{UC } (A_u, D_u): && A_u = S_{au} = \lambda A_y = \lambda \frac{C_s \gamma}{\alpha_1} && \\
&D_u = S_{du} = \lambda \mu D_y = \lambda \mu \frac{C_s \gamma}{\alpha_1} \frac{T^2}{4\pi^2} &&
\end{aligned} \tag{2.14}$$

where α_1 is an effective mass coefficient (or fraction of building weight effective in push-over mode), defined with the buildings modal characteristics as follows

$$\alpha_1 = \frac{\left[\sum m_i \phi_i\right]^2}{\sum m_i \sum m_i \phi_i^2} \tag{2.15}$$

where:

m_i is i-th story masses, and φ_i is i-th story modal shape coefficient.

Based on first mode vibration properties of vast majority of structures, literature suggests even more simplified approaches. Each mode of an MDOF system can be represented by an equivalent SDOF system with effective mass (M_{eff}) equalling to

$$M_{eff} = \alpha_1 M \tag{2.16}$$

where M is the total mass of the structure. When the equivalent mass of SDOF moves for distance S_d, the roof of the multi-storey building will move for distance Δ_R. Considering that the first mode dominantly controls the response of the multi-storey buildings, the ratio of Δ_R/S_d = PF_{R1} is, by definition the modal participation for the fundamental (first) mode at a roof level of MDOF system:

$$PF_{R1} = (\sum m\phi_1 / \sum m\phi_1^2)\phi_{R1} \tag{2.17}$$

where φ_{R1} is the first mode shape at the roof level of MDOF system.

In RISK-UE for most multi-storey buildings α_1 ≈ 0.80 and $PF_{\varphi R}$ ≈ 1.4 (Freeman,1998).

Consequently, $S_a = \gamma\ [V/(\alpha_1 Mg)]$ and $S_d = \gamma\ (\Delta_R/PF_{\varphi R})$ can be estimated at

$$\begin{aligned}
S_a &= 1.25\ \gamma\ Cs \\
S_d &= \gamma\ \Delta_R/1.4
\end{aligned} \tag{2.18}$$

To define quantitatively the capacity model and the related AD spectrum, five parameters are to be known or estimated:

1) Design strength (C_s);

2) Overstrength factors γ and λ;

3) Ultimate point ductility (μ); and,

4) Typical elastic period of the structure T.

2.4.2 Modelling of demand spectrum

The level and frequency content of seismic excitation controls the peak building response. The elastic response spectrum (S_{ae}) is an extremely useful tool characterizing ground motions demand. It also provides convenient means to summarize the peak responses of all possible linear SDOF systems to a particular component of ground motion. It is usually computed for 5 percent damping being representative for a waist majority of structures.

General procedure

The application of the Capacity Spectrum technique requires that both, the structural capacity and the demand spectra (elastic spectra reduced for developed level of nonlinearity) be defined in AD (spectral acceleration vs. spectral displacement) coordinate system. General procedure for developing demand spectrum assumes:

STEP 1: Calculation of elastic, 5 percent damped, site-specific demand spectrum for selected period range or a set of discrete period values;

STEP 2: For buildings with elastic damping radically different than 5 percent, the 5 percent damped site-specific demand spectrum should either be modified, or a new elastic spectrum calculated by considering the proper damping ratio;

STEP 3: Conversion of elastic demand spectrum in AD format.

STEP 4: Reduction of elastic AD demand spectrum to account for developed nonlinearity.

Traditionally the elastic seismic demand is defined in the form of an elastic pseudo-acceleration spectrum (S_{ae}) in which ordinates [$S_{ae}(T)$] are directly linked to corresponding ordinates of elastic displacement spectra [$S_{de}(T)$] by factor ($T^2/4\pi^2$). While, for defining the elastic demand any

spectrum form can be used, the most convenient one is of Newmark-Hall type, i.e., a spectrum with constant acceleration, constant velocity and constant displacement regions.

AD Conversion of elastic demand spectrum

For an elastic SDOF system the following relation applies between the pseudo-acceleration (S_{ae}) and displacement (S_{de}) response spectra:

$$S_{de}(T) = \frac{S_{ae}(T)}{4\pi^2} T^2 \tag{2.19}$$

Thus, each spectral acceleration ordinate associated to period T is converted into corresponding spectral displacement ordinate by multiplying it with a factor $T^2/4\pi^2$. The S_{ae} vs. S_{de} plot is usually referred to as seismic demand in AD format.

Ductility strength reduction of AD demand spectrum

The acceleration spectrum [$S_a(T)$] and the displacement spectrum [$S_d(T)$] for an inelastic SDOF system of a bilinear force-deformation relationship are defined as (Vidic et al., 1994):

$$S_a(T) = \frac{S_{ae}(T)}{R_\mu} \tag{2.20}$$

$$S_d(T) = \frac{\mu}{R_\mu} S_{de}(T) = \mu \frac{T^2}{4\pi^2} S_a(T)$$

where;

μ is the ductility factor, defined as the ratio between the maximum displacement and the yield displacement; and,

R_μ is strength reduction factor due to ductility, counting for hysteretic energy dissipation of ductile structures.

For selected damping ratio and predefined ductility, the R_μ factor converts the elastic response spectrum [$S_{ae}(T)$] to the corresponding nonlinear one [$S_a(T)$]. Since $S_a(T)$ or $S_d(T)$ are defined for predefined value of μ, they are often referred as *constant ductility spectra*.

A bilinear representation of the strength reduction factor R_μ (Vidic et al, 1994; Fajfar, 2000 as referred in RISK-UE, 2003) can be:

$$\begin{cases} R_\mu = (\mu - 1)\dfrac{T}{T_C} + 1 & T < T_C \\ R_\mu = \mu & T \geq T_C \end{cases} \quad (2.21)$$

where T_C is a characteristic period of the ground motion, typically defined as the transition period where the constant acceleration segment of the response spectrum passes to the constant velocity segment (corner period at the beginning of constant velocity range). A typical value of T_C, as proposed by Faifar, 2000 is T_C = 0.6s, or T_C = 0.7s (Cosenza and Manfredi, 1997) (as referred in RISK-UE, 2003).

2.4.3 Obtaining performance point

The capacity spectrum method initially characterises seismic demand by an elastic response spectrum. Converted and plotted in AD format it shows the spectral accelerations as a function of spectral displacements. The AD format allows the demand spectrum to be "overlaid" on the buildings' capacity spectrum. The intersection of the demand and capacity spectra is seismic demand [from the structure]. It represents a point where demand and capacity are equal, and often is termed building 'performance' point, or simply *'Performance Point'*.

The location of the performance point must satisfy two conditions:

1. The point must lie on the capacity spectrum curve in order to represent the structure at the given displacement; and,
2. The point must lie on a spectral demand curve, reduced from the elastic 5 percent damped response spectrum that represents the nonlinear demand at the same structural displacement.

If the performance point is located in the linear range of the capacity, it defines the actual displacement of the structure. This is not normally the case as most structures experience inelastic (nonlinear) behaviour when exposed to strong seismic action. For seismic inputs being of interest for damage/loss assessment, the performance points will regularly be out of linear, i.e., in inelastic (nonlinear) capacity range.

When the performance point is located in the nonlinear range of the capacity, in the general case, determination of the performance point requires a trial and error search for satisfying the two criteria specified above. There are three different procedures in RISK-UE, 2003. All are based on the same concepts and mathematical relations, but vary in assumptions made in solution process and the dependence on graphical versus analytical techniques. Below is the procedure for bi-linear representation of the capacity curve.

Performance point for bi-linear representation of capacity spectrum

In the case the capacity spectrum is represented by bilinear shape, as it is the case with developments achieved under RISK-UE, a simplified and more direct approach can be used for defining the performance point (see Figure 2.8). It is based on the assumption that not only the initial slope of the bilinear representation of the capacity model remains constant, but also the yield point and the post-yield slope. This simplifying assumption allows a direct solution without drawing multiple demand spectra, i.e.:

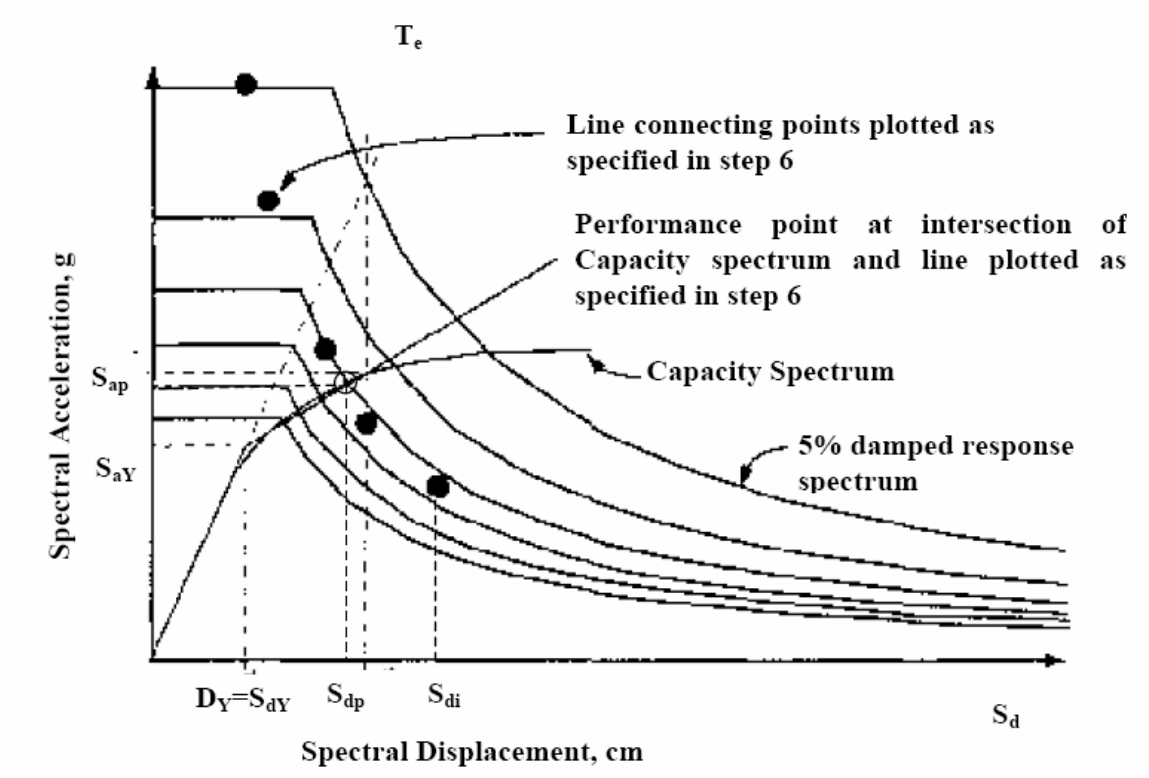

Figure 2.8: Capacity Spectrum Procedure for Bilinear Capacity Model

STEP 1: Plot the 5 percent damped elastic spectrum and the capacity spectrum on the same chart;

STEP 2: Chose several values of $S_{d,i}$, i=1, 2, 3, …, N, such as $S_{d,i} > S_{dy}$, $S_{d,i+1} > S_{d,i}$

STEP 3: For each chosen $S_{d,i}$ define ductilities $\mu_i = S_{d,i}/S_{dy,}$ spectral periods T_i, $T_i = 2\pi\sqrt{(S_{d,i}/S_{a,i})}$ and define the spectral range (acceleration $T_i < T_C$, or velocity $T_i \geq T_C$) where it falls

STEP 4: Calculate strength reduction factors $R_{\mu,i}$ using the appropriate expression of Eqs. (2.21.

STEP 5: Calculate reduced spectral accelerations ($S_{a,i}$) by reducing the corresponding 5% damped elastic spectral accelerations ($S_{ae,i}$) for adequate strength reduction factor $R_{\mu,i}$;

$$S_{a,i} = S_{ae,i} / R_{\mu,i} \tag{2.22}$$

STEP 6: Plot the calculated discrete acceleration/displacement spectral values ($S_{d,i}$, $S_{a,i}$) and draw a line connecting plotted points. The intersection of this piecewise linear line with the capacity spectrum is the demand spectral displacement, i.e., the performance point.

Although procedure requires plotting of multiple ($S_{d,i}$, $S_{a,i}$) points, the only ($S_{d,i}$, $S_{a,i}$) point that has any real significance is the one that lies on the capacity spectrum curve. This point defines the intersection point of the capacity spectrum with the adequate constant damping demand spectrum, and thus defines the demand displacement. It is evident from Figure 2.8 that the ($S_{d,i}$, $S_{a,i}$) piecewise line steadily slopes down until intersect with the capacity spectrum. This provides opportunity for the procedure to be fully coded and completely automated.

2.5 Conclusion

Structural analysis of historical masonry construction is a great challenge to the researchers. Due to high variation of material and geometrical irregularity a good judgement needs to be employed. Expert's pinion in this field suggests a simple geometrical idealization of a complex construction. If necessary, complexity should be incorporated depending on the goal of the study. The present chapter discussed different material and structural modelling strategies. A great deal of research is still needed for more accurate idealization of material. Especially study of behaviour at the interface of two different materials (such as stone/brick and mortar) will provide a new arena for micro-modelling issues. As considered for analysis of the present structure, basic idea as well as advantages of tension-compression damage model had been discussed. To ensure the safety against the seismic hazard, performance based analysis named capacity spectrum method had been introduced and the procedure to be followed for obtaining the performance point. Till date this method has found to be employed in several occasions to the reinforced concrete structures. Therefore application of this method to masonry structure would be relative new direction.

3

Mallorca cathedral

3.1 Introduction

Designed in a French-gothic style Mallorca Cathedral is one of the most legendary architectural attractions in Spain (Figure 3.1). The cathedral was build on the site of an existing Arab mosque. The legend has it that one night in 1229, as Jaime I was on his way to recapture Mallorca, his fleet was struck by a terrible storm. He vowed to the Virgin Mary that if he survived the storm, he would erect a church in her honour. And after the storm had blown over, finding himself safe and sound, he immediately undertook the project. It was a vow that was to take a long time to fulfil. Till date it has been an attraction to tourist as well as the researchers for its distinctive architectural characteristics which are typical compared to contemporary constructions. Existence of some structural elements puzzled the analysts greatly. So far concerning the safety, this cathedral had been under research for several occasions in different period of time. Passing through the following sections in this chapter the reader will find interest on the structural aspects, historical phases of repair and alterations, past seismicity in Mallorca island and damages in the cathedral. In addition to this a brief account on the present observations of different part of the structure has been presented. This will be kept in reference to discuss the behaviour of the structure from analytical point of view in the chapter 5.

Figure 3.1: Mallorca cathedral.

3.2 Description of the building

The Cathedral is made of limestone from the local quarries of Santanyi. Figure 3.2 shows the internal arrangement of the cathedral with eighteen chapels. A – J are different other functionaries of the cathedral. However, the historical process leading to its final lay-out and dimensions is not very well known. Two distinct part of the structure can be understood from the plan and the longitudinal sections (Figure 3.2 to Figure 3.5). The first was formed by the main nave at the west and a second composed by the choir and surrounding chapels. The first body of the cathedral comprises of the central nave and two lateral ones, these are well bordered by eight strong and heavy abutments in between the lateral chapels. The second body had been built in previous historical stage. This includes the Royal chapel (a single nave Gothic construction) and Trinity chapel (the first element built in the complex). There is no single opinion about the building was planned into this three-nave present arrangement or it is the result of decisions taken after completion of one part and then decided to extend to other parts. Remains of unused capitals and nervure springings at the end of the Royal Chapel suggest that the decision of building an imposing body of larger dimensions was actually taken after the completion of the eastern part of the building

(see *Detailed description of Mallorca cathedral under* EU-India economic cross cultural programme*, 2003*).

1 – 18. Chapels
A. Renaissance door.
B. Mirada portal, a Spanish gothic masterpiece (1389-1401).
C. Casa de l'Almoina (1529).
D. Puerta de l'Almoina (1498).
E. Sakrista de Vermells (Sacristy).
F. the Campanario (Bell Tower).
H. the Claustro (Cloister).
J. Capilla Real (Royal Chapel).
K. the Capilla Trinitad (Chapel of the Holy Trinity)

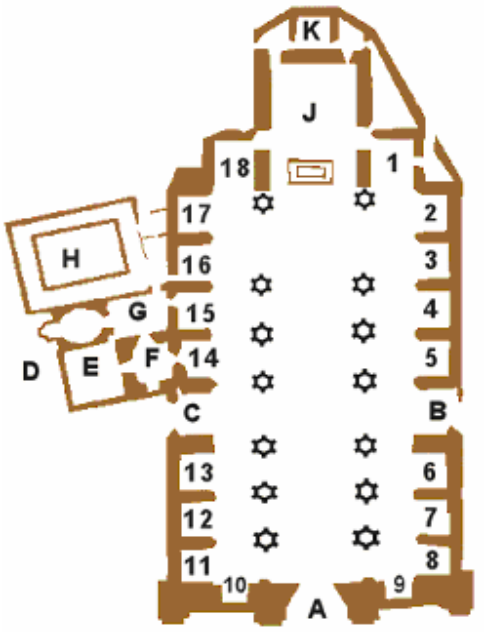

Figure 3.2: Plan describing the interior arrangement of Mallorca cathedral.

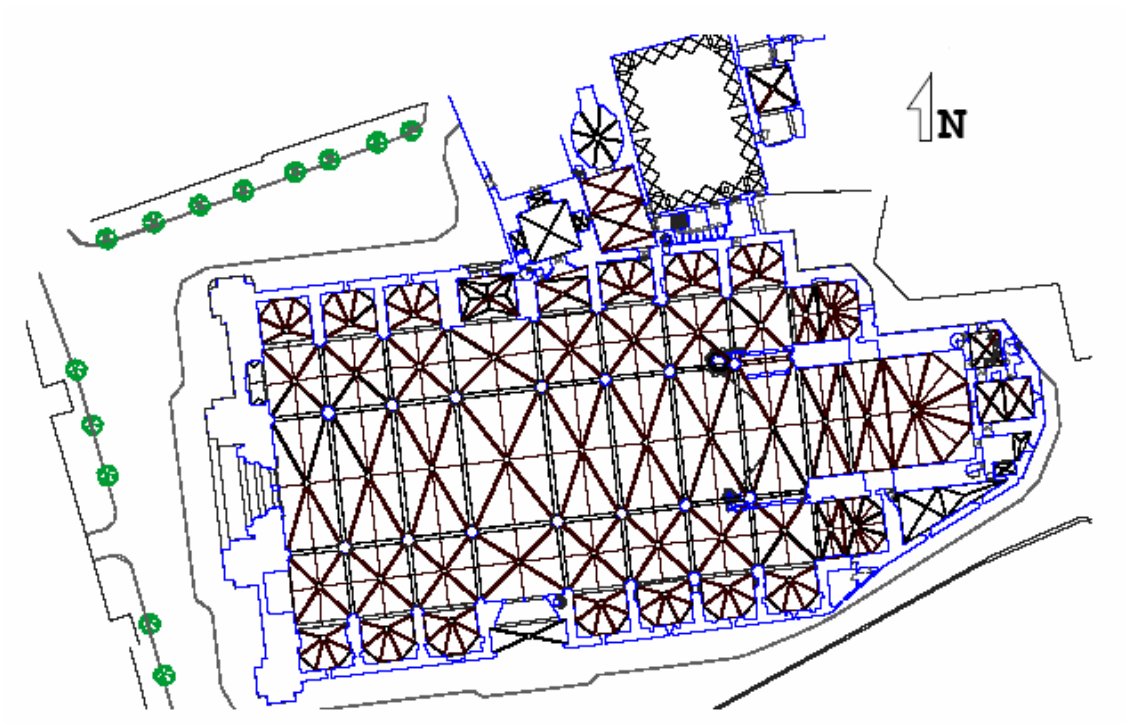

Figure 3.3: Plan at roof level showing structural arrangement.

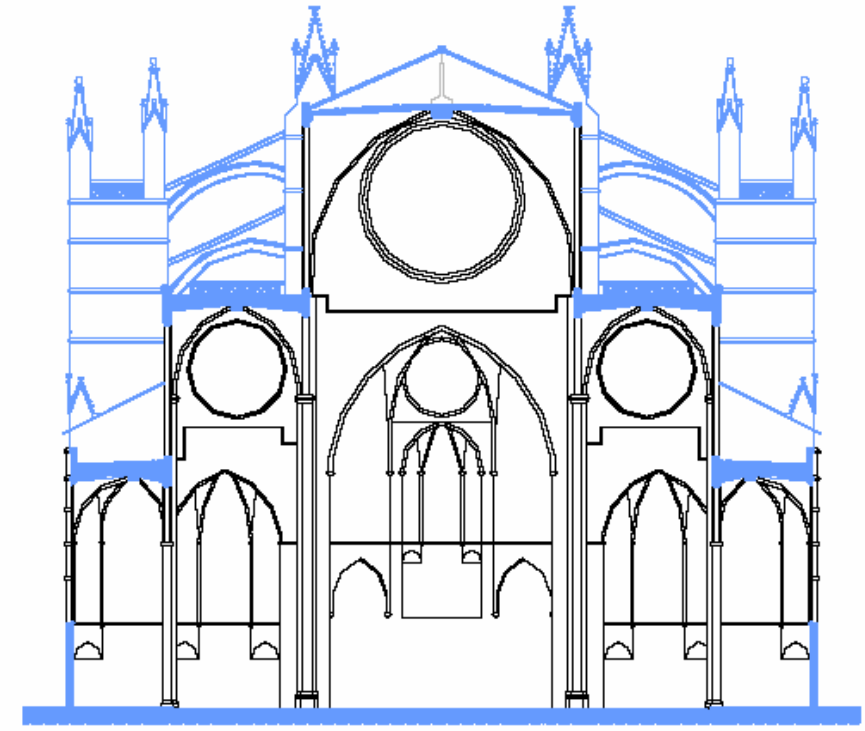

Figure 3.4: Transverse section of Mallorca cathedral.

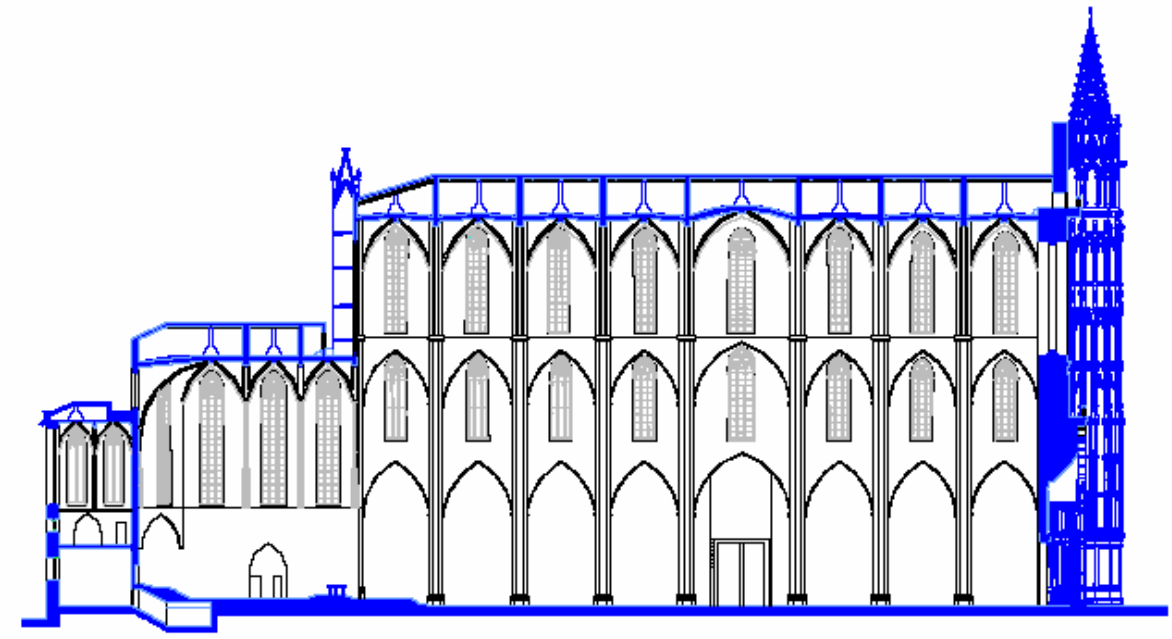

Figure 3.5: Longitudinal section of Mallorca cathedral.

3.3 Structural arrangement

The cathedral, having an over dimension of 120m in length and 55m in width, consists of three parts in the longitudinal direction from east side to the west side. These are a small apse (the Trinity chapel, K), a choir in the shape of single nave Gothic construction (the Royal chapel, J) and the main nave surrounded by the lateral chapels (Figure 3.2).

The main nave is the largest body consisting of the choir and limited by the west façade. This main nave is again composed of a central nave and two collateral naves surrounded by a series lateral chapel built in between the buttresses. The central nave spans 19.9 m and reaches 43.9 m at the vaults keystone. The two collateral naves span 8.72 m each and reach 29.4 m at their vaults keystone. The naves are sustained on octagonal piers with a circumscribing diameter of 1.6 or 1.7 m and a height of 22.7 m to the springing of the vaults.

Study on the Mallorca cathedral shows a very clever judgement on placing different structural elements. Figure 3.6a double battery of flying arches which were placed to transfer the lateral thrust offered by the central vault towards the buttresses. In a similar way the transverse arches of the central nave are also connected to the buttresses by means of the double battery of flying arches, creating diaphragmatic action. The overload in the form of pyramid with square base over the key of the central vault (Figure 3.6b) provides vertical stability so far the in conjunction with the upper battery of double flying arches. The octagonal shaped piers are very slender but composed of good quality of stone pieces. A false transept connects the main door in the north and south side of the building. The bell-tower and cloister are located next to the northern façade. The vaults are not filled or backed with rubble masonry, but just with a light structure composed of slender stone wallets and slabs.

The building has been subjected important repairs throughout its history; particularly, a significant number of vaults of the central nave were repaired or even reconstructed during the 18th and 19th centuries. The original western façade, build during 15th c., was taken down and rebuilt as a new neo-Gothic construction during the second half of 19th c. The demolition of was motivated by the significant out-of plumb (about 1.3 m) experienced by the façade (see *Detailed description of Mallorca cathedral under* EU-India economic cross cultural programme*, 2003*).

(a) (b)

Figure 3.6: (a) Double battery of flying arches. (b) Pyramid over the key of central vault.

3.4 Historical issues

The history of construction, alterations and significant events taken place in the history of Mallorca cathedral are not fully documented in the historical period. Several attempts have been made by the researchers in the present century to investigate the historical aspects and related events for understanding the structure. A more comprehensive information regarding the construction process, historical repairs had been presented by Gonzalez and Roca (2003-2004) as referred in *Detailed description of Mallorca cathedral under* EU-India economic cross cultural programme*, 2003*. The study points out five different periods in the history of Mallorca cathedral. These are as follows:

First stage: The royal construction (1300-1368)

The construction started in about year 1300 during the first reign of insular dynasty when king Jaume II (1276-1311) declared (1306) to support the cost of building the Trinity Chapel. So the work began with lodging the tombs of the Royal family. Following this, started the construction of the Royal chapel in 1311 and concluded in 1370.

Second phase: The naves (1368-1601)

In the year 1368 the architect Jaume Mates chose the quarries of Santanyí (Mallorca) to be used in the construction of the seven pairs of octagonal piers. By the year of 1400 the works were mainly in construction of the door of the Mirador and by 1601 the main façade in the west was finished accumulating a noticeable Renaissance style. Keeping reference to the article of Llompart (1995), Domenge (1997) revealed that during this phase of construction an arc of the central nave fell in April of 1490 causing serious deterioration.

Third period: 1601-1851

Within this period a significant alterations had been proposed and implemented due to occurrence of numerous problems and damages. In 1639 the major vault close to the façade was recommended for complete dismantlement to avoid future disgraceful situation, might result from the wide spread cracks. The greater arc of the main nave and the first northern flying buttress were considered necessary for remake in 1655. In 1659 an arc fell down, although it was not specified the location of the arc. At the end of the year 1960, Palma de Mallorca underwent an earthquake of degree VII and suffered the failure of two arcs near the façade and possibly this caused the out of plumb of the façade. After the reconstruction due the collapse in 1698, the second bay collapsed again in 1699. Finally the recommendation of the architects to rebuild the set of vaults of the nave was implemented in the nineteenth century along with the reconstruction of the north lateral vault. After this proposals had been made in several occasions made to prop up six flying buttresses and also to demolish the out-of-plumb façade. In the nineteenth century (1851) the Palma de Mallorca was struck by an earthquake of intensity between VII and VIII. This enhanced the possible destruction of the main façade, which already had some problem of deterioration. The other part of the building was practically unaffected.

Fourth Period: The reconstruction (1851-1888)

After the earthquake of 1851 reconstruction works of the cathedral started. Initially the work started with the disassembling of the main façade under the supervision of Architect Antoni Sudera and lasted six months. Following him the work of design and reconstruction of the new façade started with architect Preyronet Baptist. In place of the old façade (Figure 3.7a) a neo-Gothic showy façade (Figure 3.7b) came out altering the originality of construction. Sections of the buttresses of the new façade were significantly increased. The reformation finished in 1888.

Fifth Period: Reforms 1888-2002

In the previous century between 1904 to 1914 Antoni Gaudi in association with ther architects carried out a series of interventions. Resources from the Gaudiclub presents that Gaudi made several architectural alterations to the cathedral to give a stylistic view. His works includes removal of the gothic choir stalls from the centre of the nave, and its relocation in the presbytery, around the high altar, removal and recycling of the mudejar wooden candle gallery from the walls of the Capilla Real, decoration of the presbytery with ceramic tiling, representing the crests of the bishops of Mallorca, surrounded by olive-tree branches, with inscriptions in Latin on the wall that surround the episcopal throne, removal the baroque retablo (high altar) from the presbytery, that was moved the to the Church of Santa Catalina, removal of the gothic retablo and reinstalled it at the Puerta del Mirador etc etc. Another important alteration of him was using a new method for giving colour to the stained-glass windows, consisting of superimposing three glass sections in the primary colors

(yellow, blue and red). Gaudí abandoned his work on the Cathedral of Palma de Mallorca in 1914 after an argument with the contractor over the pinnacles of the Puerta del Mirador. In time, the project was definitively cancelled upon the death of Bishop Campins in 1915. Throughout the last decades there had been continuous repair and maintenance of Palma de Mallorca. A recent restoration work has been done on the western façade and in the towers.

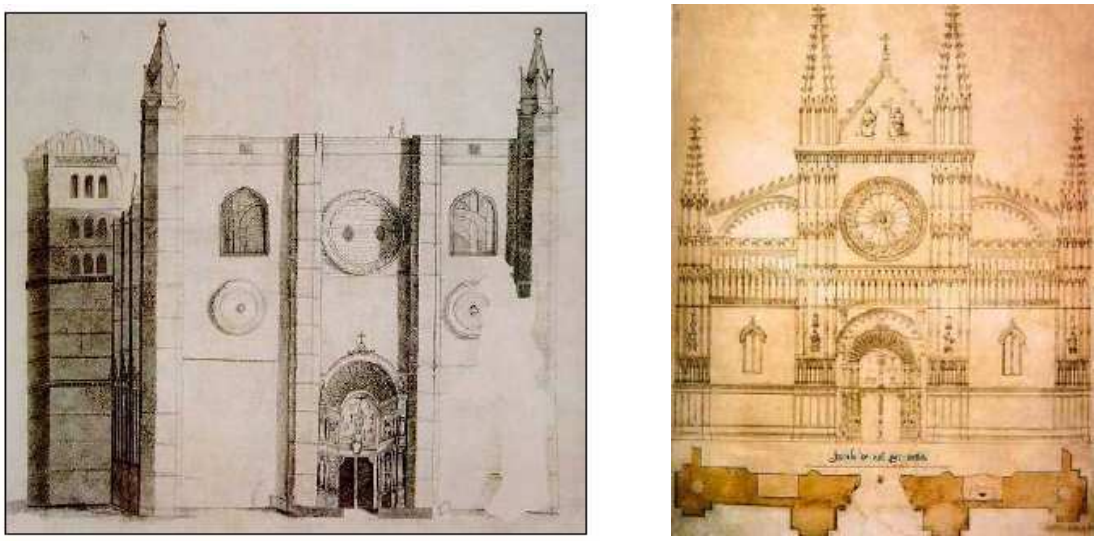

(a) (b)

Figure 3.7: Western façade. (a) Original view before. (b) New façade after reconstruction.

3.5 Past seismicity in Mallorca

According to the studies of researchers (Giménez and Gilbert, 2002; Silva et al. 2001) the island of Mallorca is subject to low seismicity. The Instituto Geografico Nacional (IGN) of Spain seismic catalogue accounts three I(intensity) > VI earthquakes since 1660 out of which two were well considered to be tectonic earthquakes. The first, felt with an intensity VII in the southern part of the island, took place in 1660 and was followed by three I = III to I = IV aftershocks. The second one occurred in 15th May,1851 at an intensity of VIII at Palma de Mallorca city and the surrounding localities. This was followed by 18 aftershocks, ranging between the intensities I = III and I = V, and extending for more than seven months (Silva et al. 2001) causing severe damage and collapse of buildings. Seismic activity during the 20th century was lower than that of the 19th century. Discrete events occurred in two well defined periods: (A) 1919-1923 and (B) 1995-1996. The first period (A), 68 years after the 1851 event, was initiated by I = V and terminated with I = III event. During the second period (B) only I = II - III intensities were produced by 3.3 to 2.6 mb shallow earthquakes. No earthquake with mb>3.5 were recorded (Giménez and Gilbert, 2002).

As it has been discussed earlier section 3.4, the historical events regarding the damage and historical changes of the cathedral due to earthquakes are in deep conformity of the studies done

by the modern researchers on the natural calamity suffered by the Mallorca island. The damage suffered by the cathedral in two earthquake event (1660 and 1851) were well documented and are the proof of the earthquake studies done in present. There had been a low intensity earthquake in 1721. No structural damage of the cathedral was documented, meaning that the earthquake left no impact on the island. More over there are no documentations of restoration for any seismic event in the twentieth century. But in any case the safety of the cathedral should be checked for any probable future occurrence of seismic hazard with low value of seismic parameters according to Spanish Seismic Code (NCS-94 as referred by Silva et al. 2001).

3.6 Existing damages

Study on the building revealed that the building has a certain structural problems in terms of large deformations and structural cracks that demand for more structural studies to understand the cause and future consequences. Very recently some of the minor damages have been repaired. Therefore now it is not possible to find all those minor damages behind the repairments. Following are the observations on the structural problems:

(i) Piers found to have undergone significant deformation showing remarkable curvature and lateral displacement in both the longitudinal and transverse directions of the nave.

(ii) Vertical cracks exist at the bottom of the piers (Figure 3.8). But these cracks seem to be restricted in the outer surface of the piers as these expel the material of the core in the form of surface wedges.

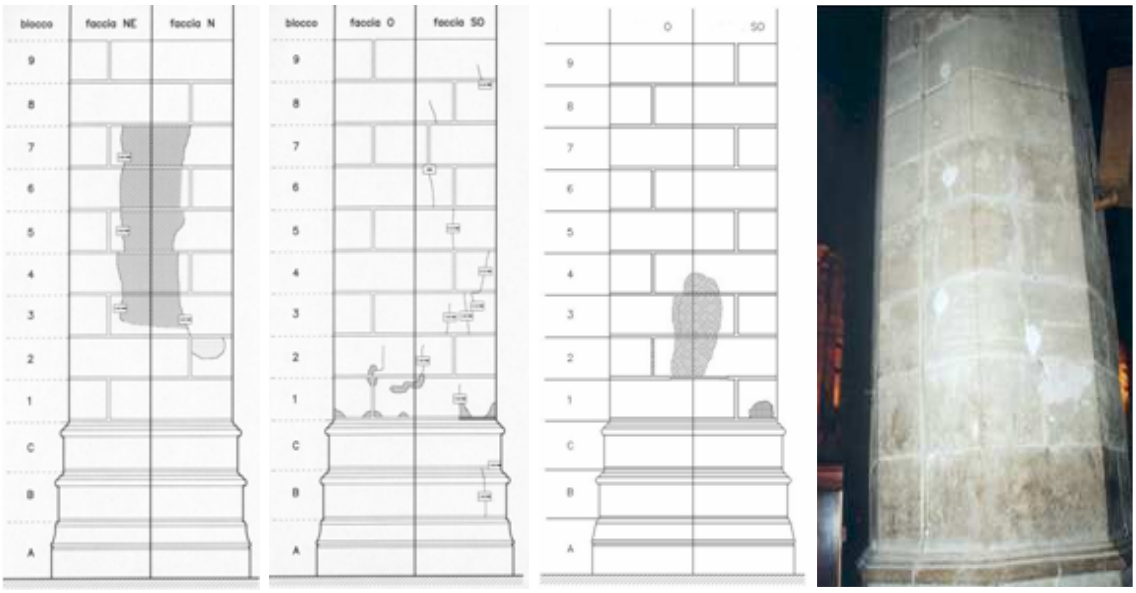

(a) (b) (c) (d)

Figure 3.8: (a),(b),(c) Example of cracking of piers documented. (d) Photograph corresponds to the wedge developed at the pier face sketched left.

(iii) Significant deformation has been observed in the flying arches, particularly the upper battery of the flying arches.

(iv) The vaults of the central nave and the main transverse arches are separated by wide cracks developed throughout their contact lines (Figure 3.9b).

(v) The western façade has been found to experience excessive out-of-plumb and thereby causing cracks in the panels of the clerestory wall close to it (Figure 3.9a). Also cracks were found abundantly in the walls that configures the transept.

(a) (b)

Figure 3.9: (a) Cracking in the clerestory wall. (b) Cracking by separation at the junction of central vault and the transverse arch.

(vi) Cracking has been observed in the central vault itself near the key and the ribs as can be seen from Figure 3.10.

Figure 3.10: Cracking in the central vault.

(vii) Cracking is also observed in other structural components (as in buttresses, caused by existing openings or false windows between lateral chapels, and also in lateral vaults).

Because of the concern caused by these observed anomalies – and, in particular, by the cracks and deformations affecting the piers of the central nave - a detailed assessment has been lay-out devising comprehensive historical investigation, inspection, monitoring and structural analysis (González and Roca, 2000, 2003-2004). Most recent studies done by Clemente (2007) as presented in chapter 4 features simulating construction process and creep deformations to investigate if the present problems were consequenes of long term existence of the building. The present study will be based on similar kind of study but simulating the constuction material in a more realistic way.

3.7 Conclusion

Mallorca cathedral is one of the well known cathedrals in Spain for its architecture. In comparison to other cathedrals like Santa Maria del Mar, built within 53 years (González et. al) Mallorca cathedral was built over a large period, spanning over two hundred years. Major features of the Mallorca cathedral can be inferred from the structural characterization are the spaciousness, the high lateral naves (although not so high as to take the role of flying arches), the lateral chapels between buttresses and the extremely slender, solid octagonal piers. From the starting of construction in fourteenth century to present century the cathedral has been altered in several occasions. As discussed earlier, the present out look of the main western façade was not originally built in this way. After the 1851 earthquake the western façade was repaired and came out in a showy renaissance style. Several internal alterations including change of the colour of the window glasses had been incorporated by famous architect Gaudi from 1904 to 1914. Understanding from the past events and present state of the building has still demand for future analysis, as several cracks has been documented (recently repaired) in the buttresses, clerestory walls, central vaults, separation of the transverse arch from the central vault etc. Although there had been no earthquake since 1851 in the island, but a safety check considering the minimum earthquake intensity according to Spanish guideline will put more confidence to the structure.

4

Previous analysis on Mallorca cathedral

4.1 Introduction

Compared to its long duration construction period, the history of analysis performed on Mallorca Cathedral is relatively new. Till date it has analysed in several occasions to understand the structural behaviour and to assess the safety that became questionable to the researchers time to time in its history of analysis. In the present chapter one will find the previous researches done earlier using from rigorous hand calculation (static graphic method) to modern computer codes. Mostly the structure has been analysed for real vertical load. In order to get a psychological assurance of the safety under vertical load, analyses had been carried out by applying the gravity load fictitiously beyond the actual. Some researches comprised of response of the structure under the lateral load (i.e. wind and seismic load). A group of alternative configuration were assumed by the authors to understand the suitability of some structural components which were initially believed to be extra elements having no particular contribution towards the safety. Also recent researches had been intensive in the sense that the material had been represented by most sophisticated computer codes (thanks to International Center for Numerical Methods in Engineering (CIMNE)) that introduced material parameter more precisely. Finally different parametric studies had been made (particularly by Clemente, 2007) to know the effects of the same on the global behaviour of the whole structure. Following are the records of some important analysis taken place from the starting of the twentieth century.

4.1.1 Rubio (1912)

A comprehensive study based on thrust line analysis in two dimensions was performed by Rubio for Mallorca Cathedral. As acknowledged by the author, the analysis of this kind of structure being complex in nature is very difficult. After laborious iterations he could find a solution for which the thrust line was contained within the thickness of the elements. The thrust line of the equilibrium solution appeared almost tangential to the perimeter of the pillar at the junction of the springing of the lateral vault (see Figure 4.1).

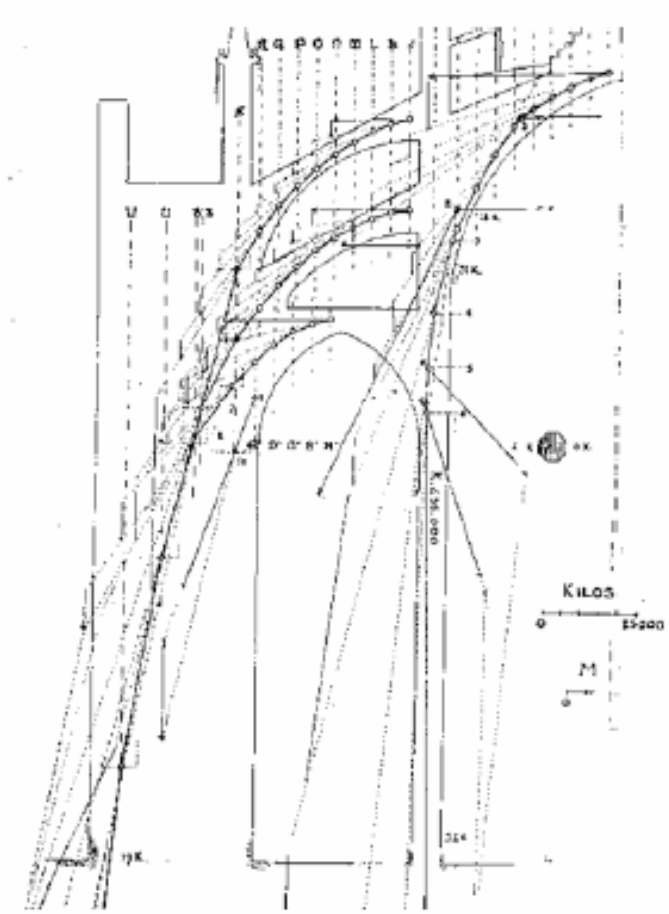

Figure 4.1: Static-graphic analysis by Rubio, 1912

Through his clever observations, he noticed the solution was commensurate to the curvature of the pillar. His conclusions pointed to the necessity of the inclusions of extra dead load over the vault and main arches. He justified that it would have been better if the superior battery of the flying arches did not exist as these generate pushes towards the central vault. Safety was ascertained in terms of material strength. At the point of maximum pressure in the principal arches a compression of 3.1 MPa was reached, whereas in the pillars the maximum compression reached to 4.5 MPa.

Both the values are smaller but nearer to the resistance of the material. The kind of calculation and effort to justify of the safety embodies the adequacy of knowledge present at that period.

4.1.2 Mark (1982, 1998)

In 70's Clemente Mark, a dedicated engineer, made a study of old structures utilizing the method of photo-elasticity, which was initially introduced for complex mechanical analysis of components of airplanes and reinforced concrete structural elements.

Flat model describing the section of the structure was implemented on epoxy plastic plate. Scaled load equivalent to gravity and wind load were applied to the model. Simultaneously the model was heated (at 50^{o}C). The material started to deformation which remained even after removal of load. Then the model was observed through polar scope. The pattern of light interprets the qualitative distribution of internal forces. Figure 4.2 below shows the distribution of internal forces within the photo elastic model of Mallorca Cathedral.

Figure 4.2: Photo-elastic analysis showing distribution of internal forces. Mark (1982)

Like Rubio he was also of the same opinion of placing only one battery of flying arch with more inclination towards the buttress to transfer the load effectively to it. However, it is interesting to mention that some of the remarks made by Mark contradicted that of made by Rubio. According to Mark, the photo-elastic study encompass uniform state of compression (differs from Rubio) in the piers under gravity load (2.2 MPa) which means that the amount of bending is negligible.

4.1.3 Maynou (2001)

A more recent analysis to study the thrust lines was done by Maynou in 2001 by means of computer programming. The analysis was carried out using a 2D model of the section of the structure and the result displayed a certain number of thrust line within the geometry of the section the structure (a good agreement with the results obtained by Rubio, 2001) which can be observed from Figure 4.3. In his careful examination he agreed that placing of extra weight over the key of the principal arches were justified to provide stability of the structure. According to his study it was possible to obtain thrust lines without taking into account the collapse of the pillars. Also the result obtained from the computer program specifies that the optimal horizontal displacement of the top of the pillar could be 31 mm before collapse (contrasting 45 mm as calculated by Rubio, 1912).

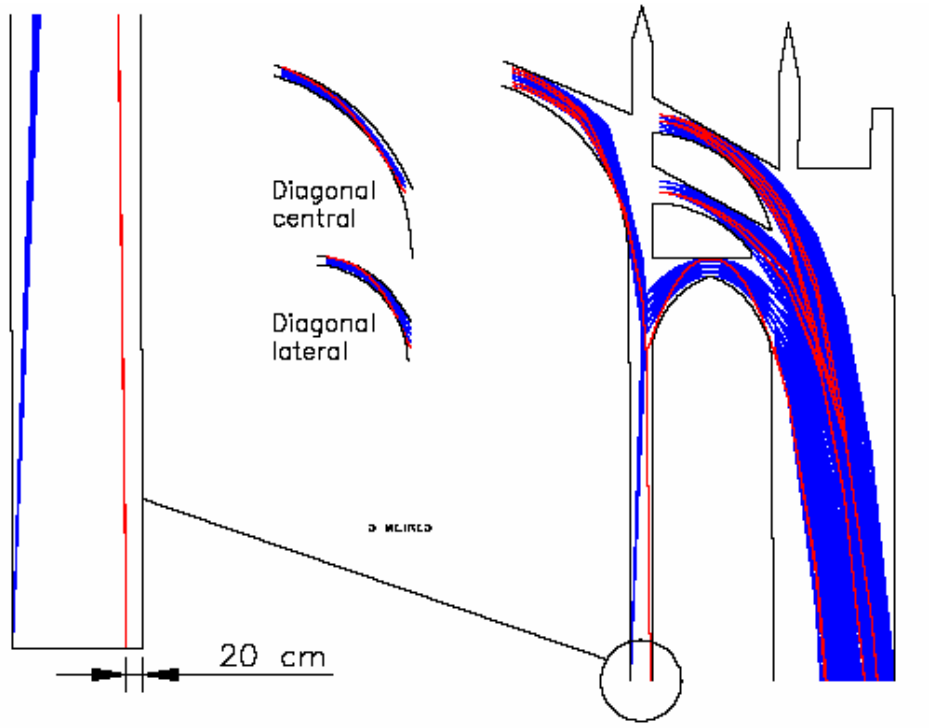

Figure 4.3: Thrust line analysis of Mallorca Cathedral by Maynou (2001).

4.1.4 Salas (2002)

A more detailed structural analysis of Mallorca cathedral was carried out by Salas (2002). In his study he used two different methods and made comparison of the results obtained from them. Like other authors he also verified the functional requirements of some element of the structure. In the first method, analysis was performed by Finite Element Methods with isotropic damage model and

in the second a generalized matrix formulation was prepared. Following are the studies and the principal observations made by him.

Using both the methods gravity load, beyond the actual, had been applied in both the models and interestingly similar results were obtained in terms of factor of actual gravity load (nearly 1.7) that lead the structure to collapse. Figure 4.4 below shows the collapse mechanism of the structure in this load condition.

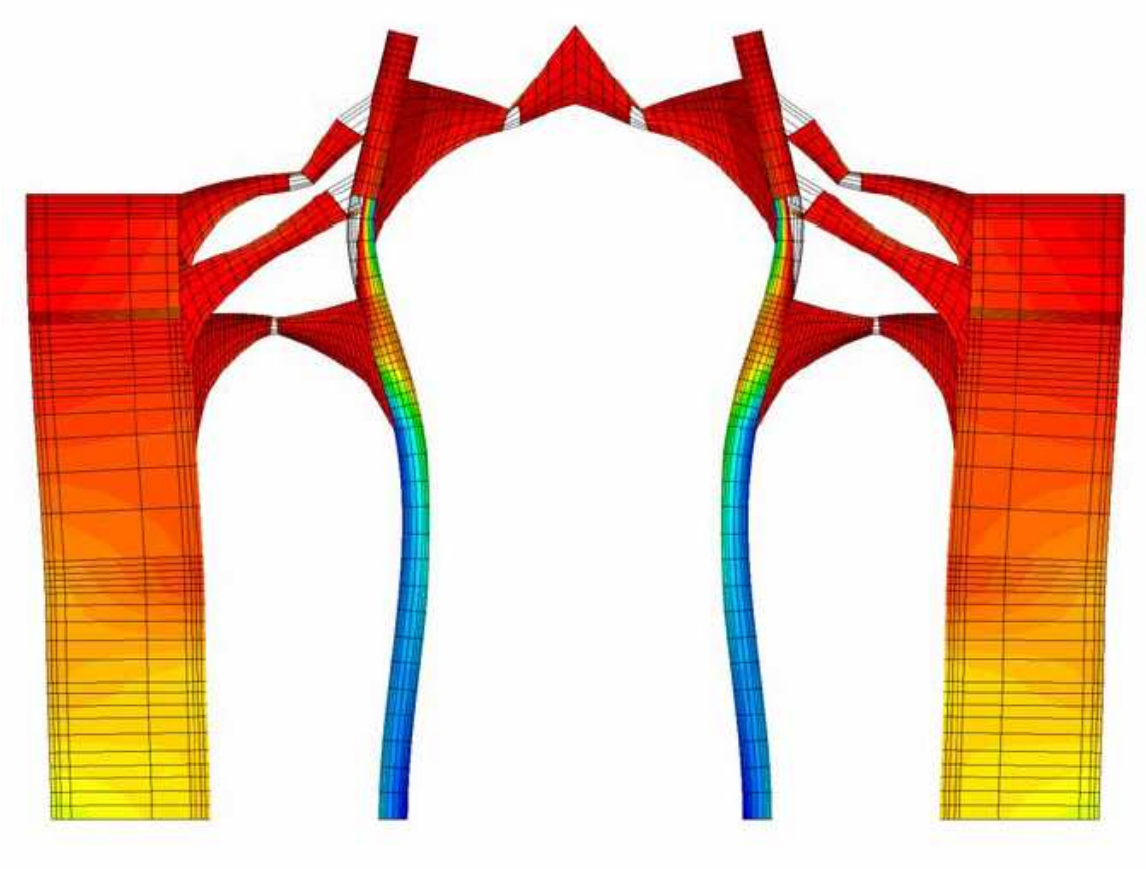

Figure 4.4: Collapse mechanism with a gravity load factor of 1.7. Salas (2002).

Three different studies had been made considering alternative configurations for the purpose of analysing the validity of some components in the original design that includes the overweight in the key of the main arch and the superior battery of flying arches. Conclusions made by him are as follows:

Through the examination of the structure he understood the justification of the extra weight over the principal arch (similar to the opinion made by Rubio, 1912) as it assures the stability of the structure. Otherwise the structure could fail after reaching 90% of the gravity load. Figure 4.5 shows the collapse mechanism in this particular condition.

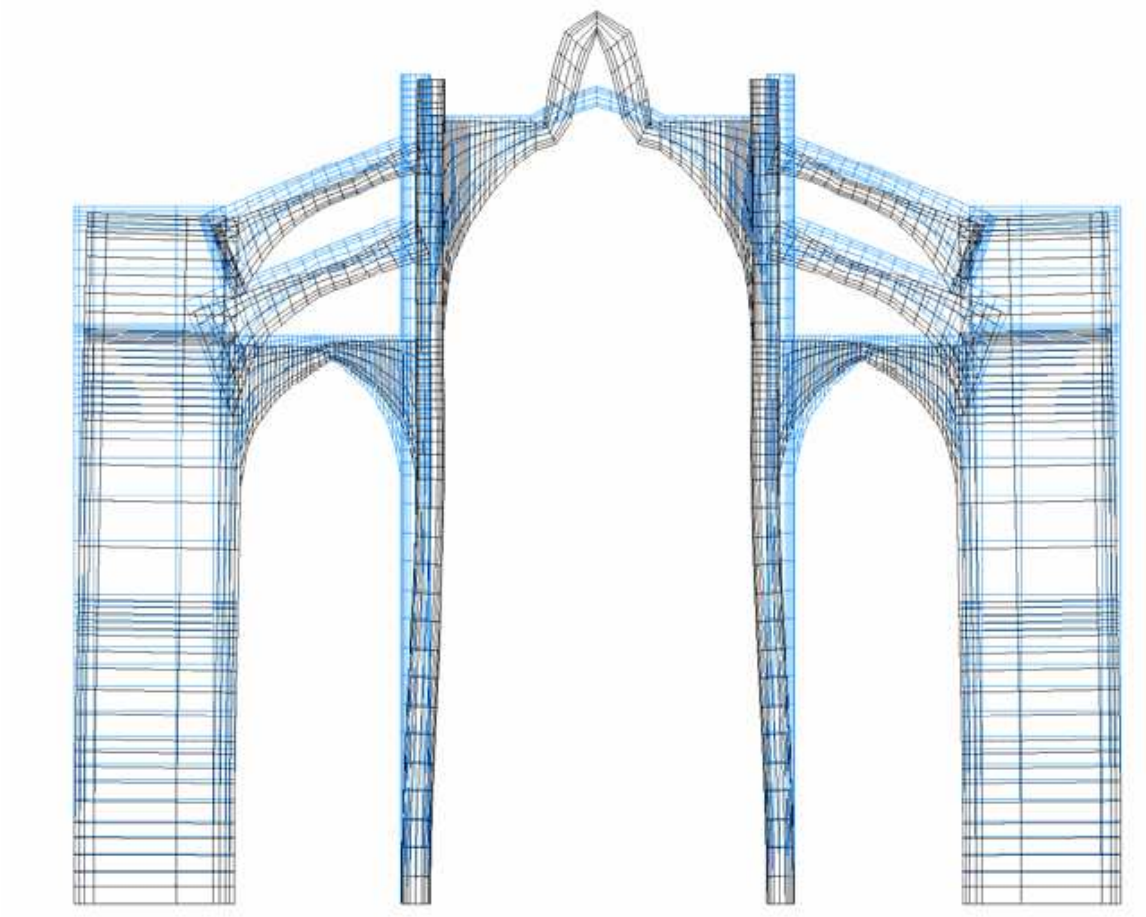

Figure 4.5: Collapse mechanism of the structure with a gravity load factor of 0.9 without considering the extra weight over the key stone of the principal arch. Salas (2002)

Analysis carried out neglecting the effect (both weight and stiffness) of the superior battery of the flying arch shows the structure would have collapsed after attaining a load factor of 0.7. Therefore the superior battery of the flying arches had been introduced out of careful understanding of its contribution towards the stability of the structure that can be understood from the collapse mechanism in Figure 4.6 below.

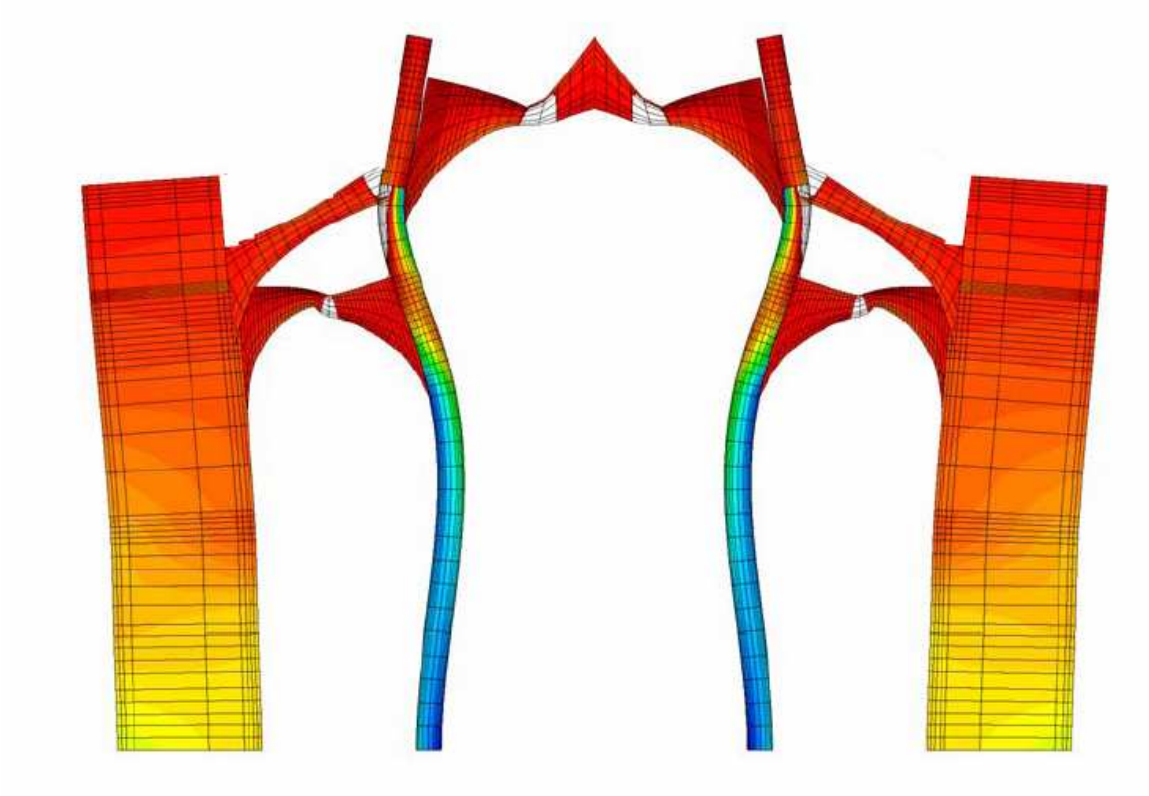

Figure 4.6: Analysis without considering the effect of superior flying arch. Mechanism of collapse with gravity load factor of 0.7. Salas (2002)

Another interesting study of him concluded that the structure would be safe if both the extra weight over the principal arc and the upper battery of the flying arch were not taken into consideration. The failure load at gravity reached at factor of 1.6.

Wind and earthquake load corresponding to 1000 years return period were applied on the structure by means of simplified equivalent static load procedure. Lateral loads were estimated conforming to Spanish guidelines (NBE-AE-88 for wind load and NCSR-94 for seismic load). The analysis showed that the structure could resist wind pressure of 1.45 kN/sq. m and earthquake of $a_c/g=0.12$. But the resulting condition of the structure is very severe and seems to be near the collapse. Also both these lateral loads resulted formation of cracks and collapse mechanism at failure in a similar fashion (see Figure 4.7). An improved lateral analysis can be seen in the analysis performed by Clemente (2007) where pushover analysis of the structure was done to ultimate lateral load carrying capacity.

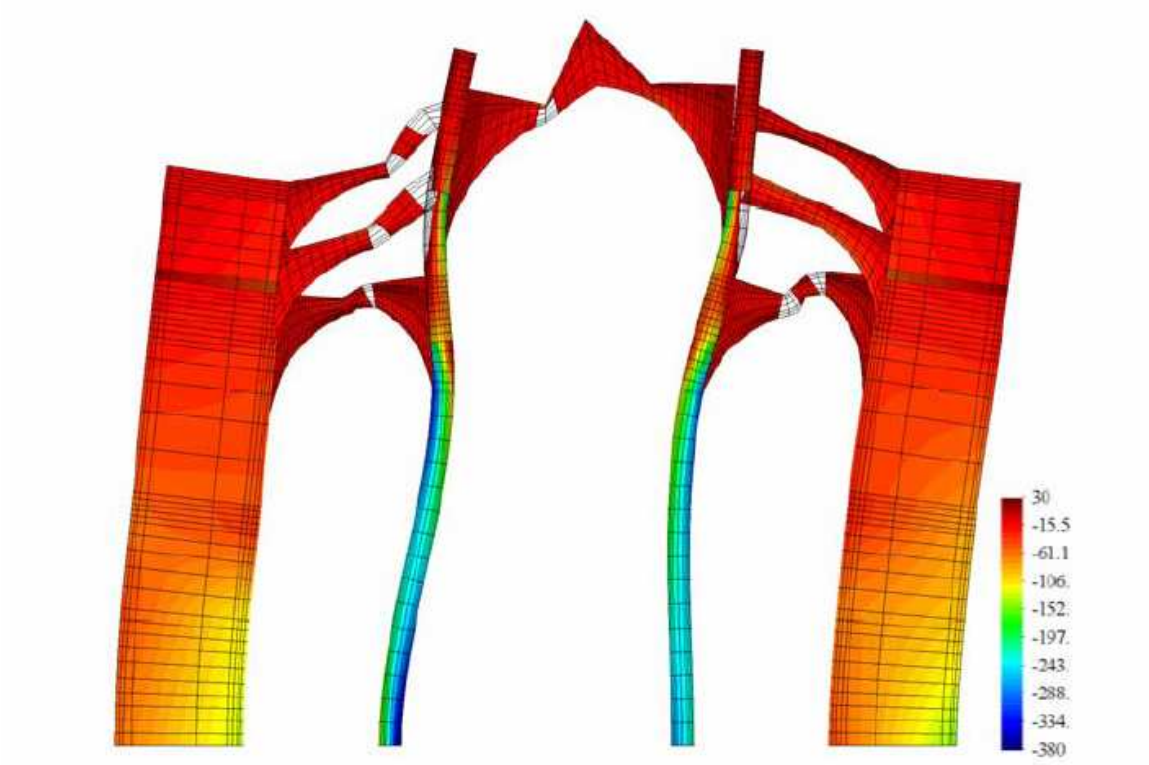

Figure 4.7: Distribution of normal stresses (100xMPa), cracking and deformation x 1000 for the structure subjected to a wind pressure corresponding to a return period of 1000 years. Salas (2002).

4.1.5 Clemente (2007)

Most recently a detailed analysis using intelligent computer code has been done by Clemente (2007). A more detailed 3D geometry of a bay was prepared in GID (ver. 7) with refined mesh in the zone of potential stress concentration and the analysis was carried out in COMET. In his analysis he used tension compression damage model (also referred as distributed damage model, see section 2.3.1) to represent the material. Within the frame work of his research he also applied crack tracking algorithm (also referred as localized damage model), which was developed by the author in 2006 (see Clemente Clemente et al. 2006), to the structure to reproduce the localized individual cracks under tension. Table 4.1 summarises the material parameters used in his study. Young's modulus of elasticity was considered thousand times the compressive strength and tensile strength was considered 5% of the compressive strength. Another important material parameter i.e. fracture energy was considered infinite (according to Eurocode EC-6), but this may overestimate the results as in case of masonry, softening of material is most important phenomenon. This problem would be eliminated by considering very low fracture energy in current analysis in chapter 5.

Type of material	Structural element	Young's modulus (MPa)	Compressive strength (MPa)	Tensile strength (MPa)
1	Buttresses, vaults, clerestory and walls.	2000	2	0.1
2	Pillars and flying arches	8000	8	0.4
3	Filling over the cental vault	1000	1	0.05

Table 4.1: Material parameters used by Clemente, 2007.

The first model was analyzed under instantaneous loading taking into account the nonlinearity of material as mentioned in the previous paragraph. Next the same analysis was performed but simulating the construction process in two phases and observation was made to understand the effect of sequence of loading. The same model was analyzed then considering the creep of material due to long term loading.

In the second phase a two dimensional model equivalent to the earlier three dimensional model was prepared. Comparative analyses were performed for both the models (2D and 3D) using distributed damage model. Later only the two dimensional model with localized damage was considered for sensitivity analysis using diverse parameter of the material. In all cases gravitational load increased in a fictitious way until reaching the collapse of the structure.

In the third phase of analysis, gravitational load was applied in the horizontal direction to simulate the seismic force. Condition of symmetry of the structure about the axis passing through the key of the central vault was eliminated and a two dimensional model was created. The seismic load analysis was done considering both localized and distributed damage models and finally comparison was made to understand the effect of these damage models in the collapse condition.

(i) Instantaneous gravity load analysis with non-linear material

An instantaneous gravity load was applied with 10% load increment as the material was modelled for nonlinear behaviour by means of tension-compression distributed damage model. The deformed shape obtained showed displacement of the pillar towards the central part of the building whereas the abutment displaced toward the part exterior of the structure (see Figure 4.8). Both tendencies coincide qualitatively with real condition observed in the structure. But the maximum displacement of the pillar (0.76cm) obtained did not agree with the real state of the structure (as the displacement of the pillar varied 4 to 16cm). As can been seen from Figure 4.8b model reproduced the damage in the large windows (already repaired) of the buttresses. The analysis again showed damage due to

tension in lateral vault and in the wall on the central vault. Apart from these the results were in good agreement with the undamaged part of the structure in other locations.

After reaching 100% of the self weight, further analysis was carried out by increasing the gravity load in a fictitious way (although this conditions are little realistic) to determine the load necessary to arrive at the collapse and the mechanism it forms. The load factor reached to 2.0 at collapse. The state of stress and collapse shows that the structure fails mainly because of the fracture that happened in the abutment (at the base of the large window, see Figure 4.9) due to concentration of tension and compression next to each other. Severe tension damage occurred in lateral vault and also in the flying buttresses and in the central vault.

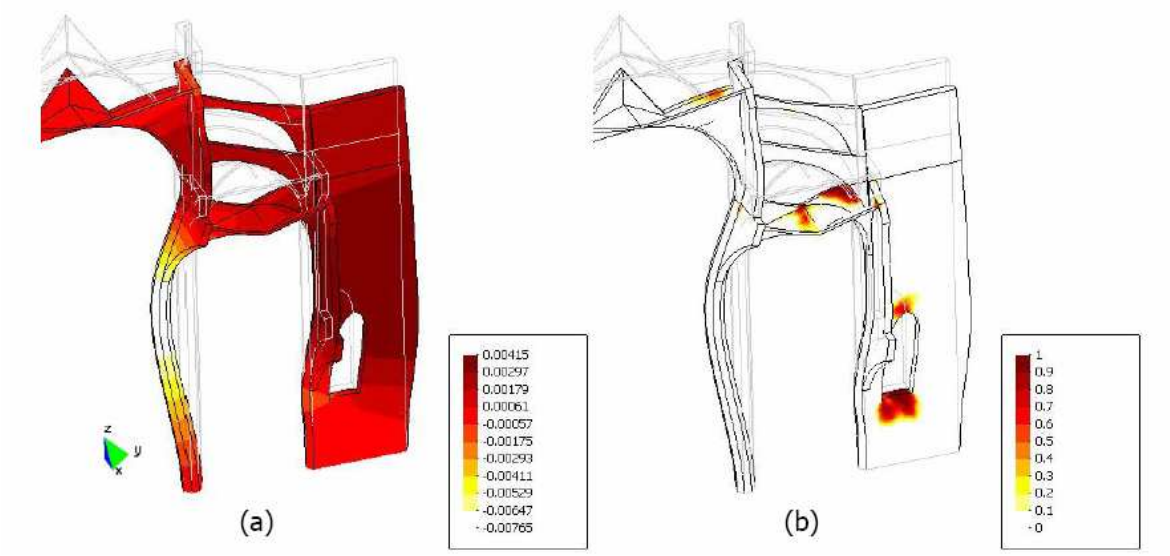

Figure 4.8: 300 x (a) Deformed shape, (b) Damage due to tension. Clemente (2007).

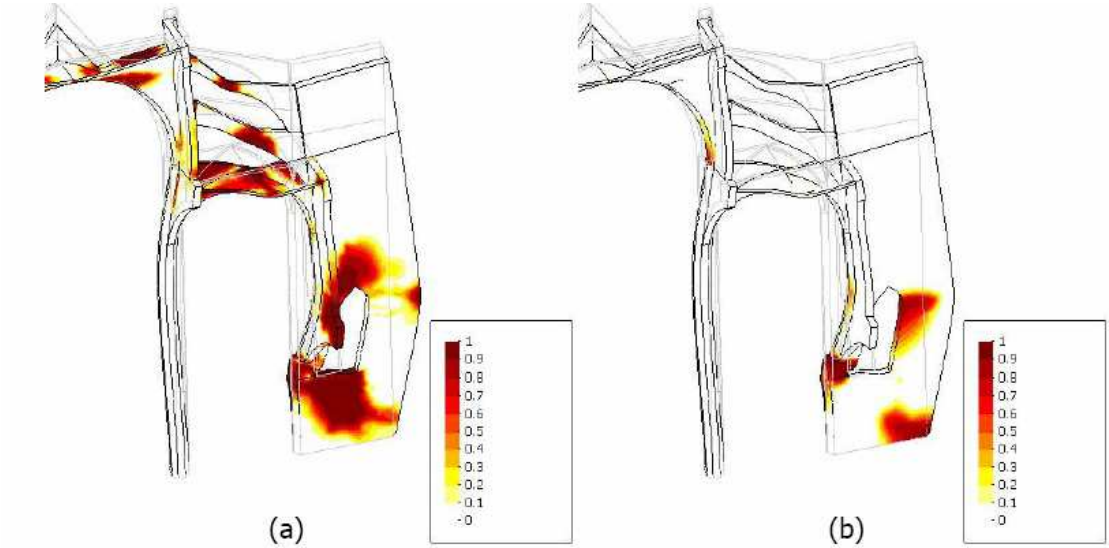

Figure 4.9: Collapse mechanism. (a) Damage due to tension; (b) Damage due to compression. Clemente (2007).

(ii) Sequential analysis for the simulation of the construction process with nonlinear material

To examine possibility of damage in the pillar during construction phase of the cathedral, sequential analysis was performed. The construction process (see Gongalez and Roca, 2003) had been simulated by dividing the structure into two parts by cutting the structure over the lateral vault as can be observed in Figure 4.10. Thus analysis was performed first in the inferior part and then in the whole part.

Analysis of the first phase shows that horizontal displacement of the superior part of the pillar (see Figure 4.11a) reached to 3 cm (four times that obtained in the case analysed in single phase) which confirmed the deformation of the pillar during the construction of the structure. As observed in Figure 4.11b more area of material in the inner face of the pillar and in the wall located on the lateral vault found to be affected, which was not observed in the first case.

Second phase analysis depicted that the horizontal displacement (see Figure 4.12a) of the superior part of the pillar decreased with respect to that in first phase. The final value obtained was 1.84 cm, which continued to be more that double of 0.76 cm obtained in the case without simulating the construction process. Compared to the previous analysis (gravity load simulated in one phase), there were no significant increase of stress level in the phase analysis.

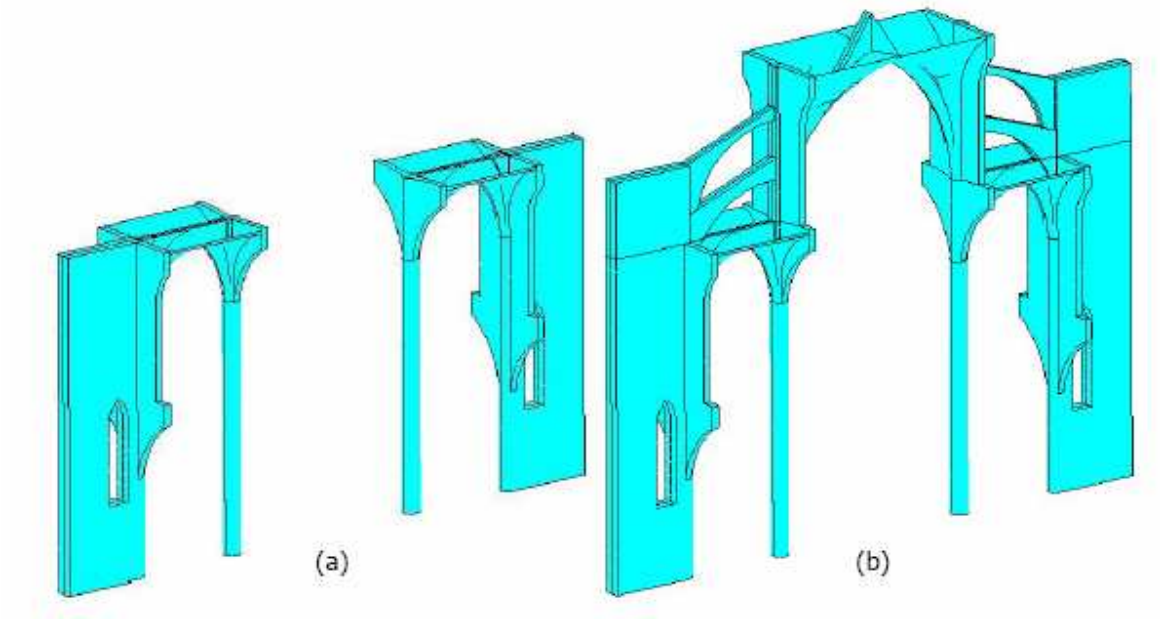

Figure 4.10: Simulation of construction process. (a) First phase of construction, (b) Second phase of construction. Clemente (2007).

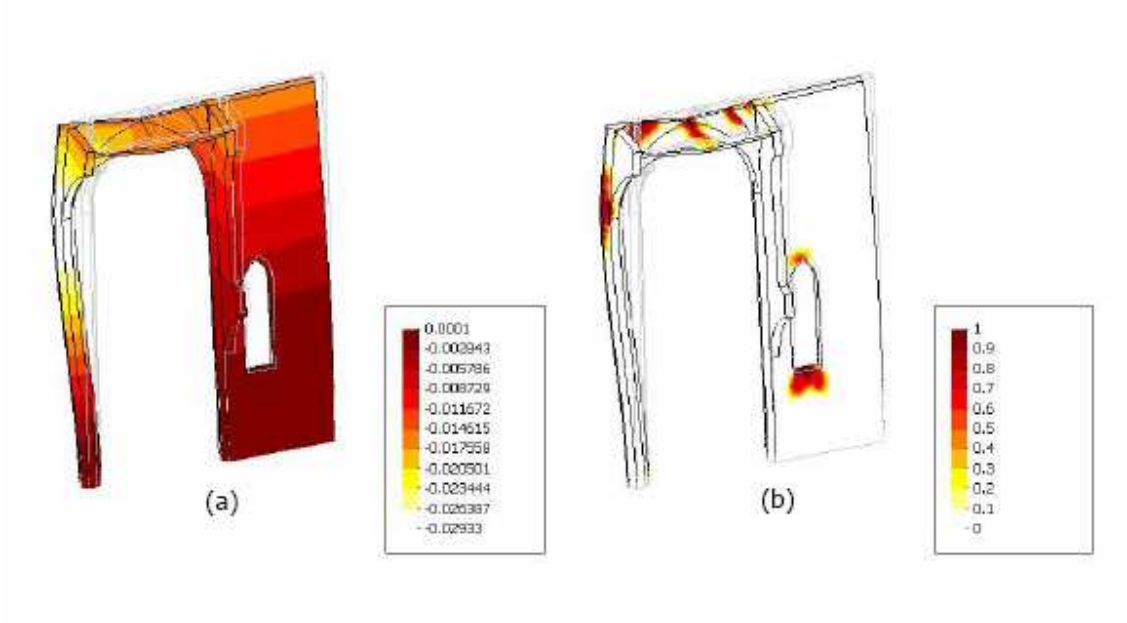

Figure 4.11: First phase of construction. (a) Horizontal displacement x 50, (b) Damage due to tension. Clemente (2007).

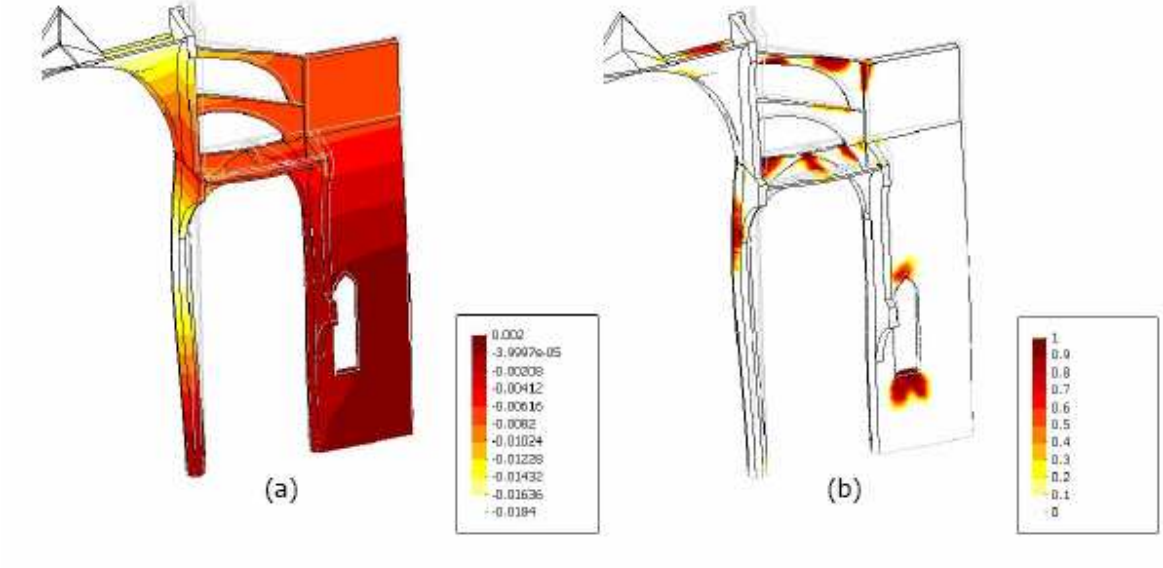

Figure 4.12: Second phase of construction. (a) Horizontal displacement x 50, (b) Damage due to tension. Clemente (2007).

(iii) Sequential analysis with nonlinear material to account the effect of creep

A study considering the effect of creep was carried out to clarify whether the existing deformation due to the creep of material and also to justify if the continual progress of damage resulting from the effect of creep would cause collapse of the structure in future.
A three step sequential analysis was performed in this case – the first two were for simulating the construction process like the previous model and the third one was for just passing the time to observe the increase of deformation as a result of creep of material. To take into account the creep of material two relatively higher values of $\xi^i (= E^i / E)$ (where *i* = 1) were considered. The adopted values were 0.875 and 0.975 which means the rigidity can descend unto 87.5% in the first case and in the second case unto 97.5%. In both the cases the retardation time for damage was considered $\tau = 50$ time units and the gravity load after the second phase was present constantly for 2000 units of pseudo-time.

The horizontal displacement of the pillar towards the central vault had been found to be 4 cm for $\xi^1 = 0.875$ and 14.5 cm (300% higher) for $\xi^1 = 0.975$. Also for smaller value of ξ^1 the stabilization time is less (1000 unit) than that (2000 unit) for higher value of ξ^1. The quantitative value of the horizontal displacement (between 6 to 18 cm) for the case of $\xi^1 = 0.975$ was observed to be in good agreement with horizontal displacement in the real structure (between 4 to 16 cm). But there had been no significant change in the state of stress.

(iv) Sequential analysis with nonlinear material and geometry to account the effect of creep

The same was analysed with large displacement formulation instead of small displacement formulation as in the previous analysis to observe the effect of creep deformation in the damage of the structure.

In comparison to material nonlinear model greater displacement at the top of the pillar had been observed in case of geometrical and material nonlinear model. Another important difference was that for $\xi^1 = 0.875$, the structure tend to stabilize after 3000 units of time. But for $\xi^1 = 0.975$, the structure collapse before 2000 units of time with more distributed damage.
The author showed that due to the effect of creep ($\xi^1 = 0{,}975$), damage progress gradually in the lateral vault, inner face of pillar and in the clerestory towards the collapse with passage of time. This is demonstrated in Figure 4.13.

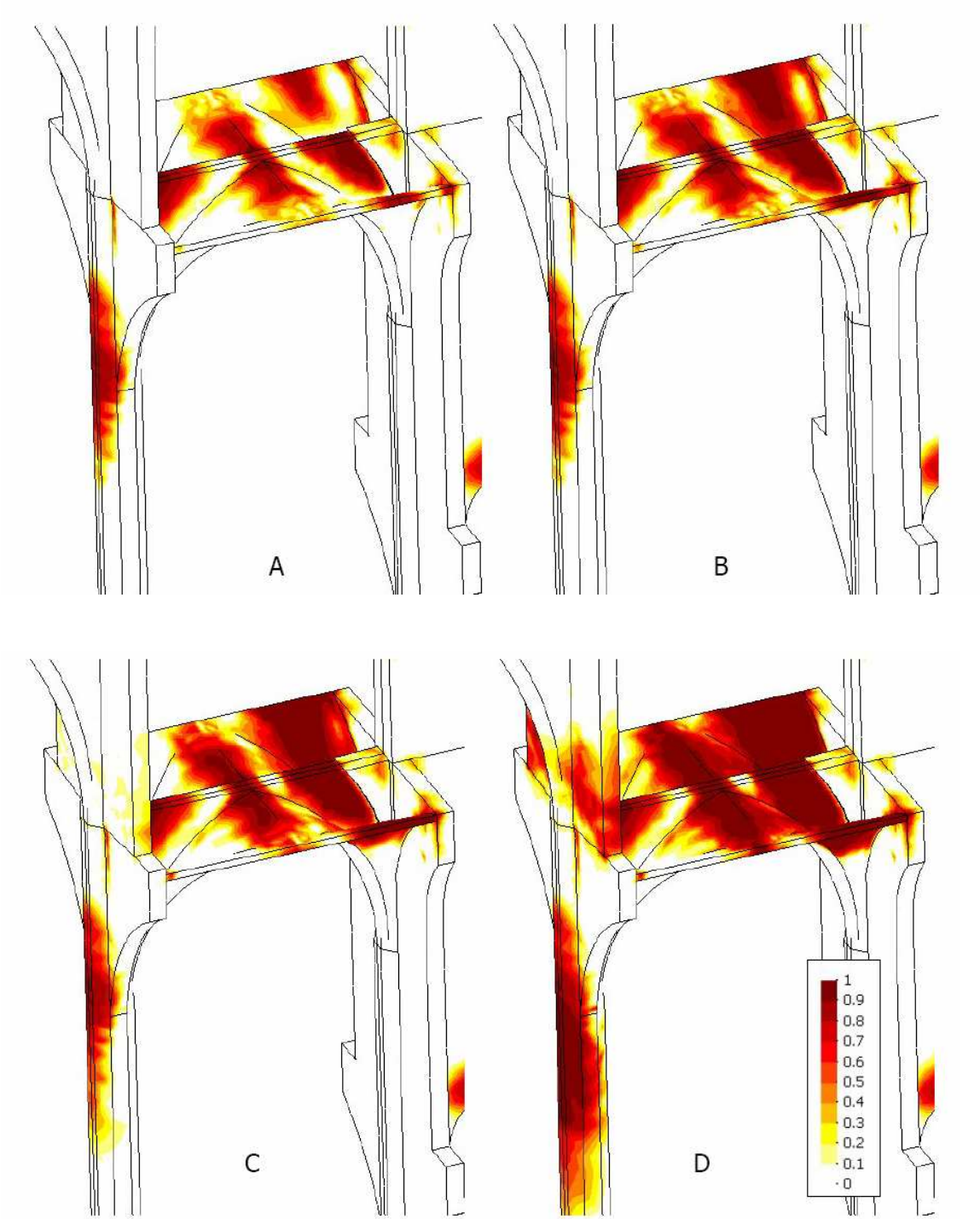

Figure 4.13: Distribution of damage due to tension in the lateral vault and the pillar during the passage of time. (a), (b), (c) and (d) are for pseudo-time of 500, 1000, 1500 and at time of collapse respectively. Clemente (2007).

(v) Analysis under gravitational loads under localized damage

To examine the applicability of the discrete crack model algorithm a two dimensional plane stress model equivalent to the original three dimensional model of the bay had been prepared by maintaining the weights of different structural elements (by varying the thickness and unit weight of different components). Then the 2D geometry was confirmed by comparing the deformed shape of 2D and the 3D model after a linear elastic analysis. Final configuration and thicknesses of different components are as in Figure 4.14.

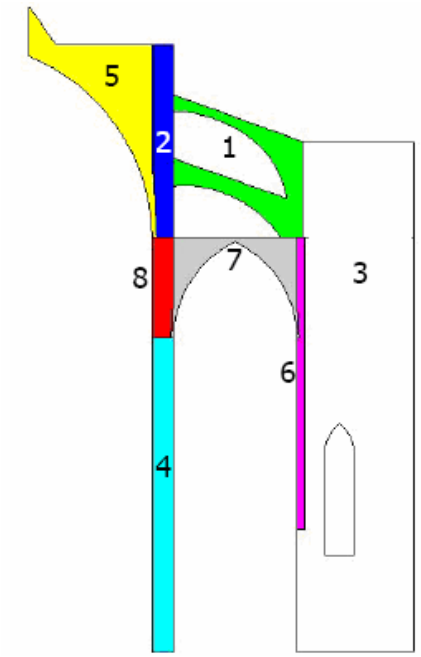

Flying arches (**1**) : 0.90 m;
Clerestory wall (**2**) : 3.44 m;
Buttress (**3**) : 1.55 m;
Pier (**4**) : 1.24 m;
Central vault (**5**) : 1.53 m;
Lateral clerestory wall (**6**) : 2.71 m;
Lateral vault (**7**) : 0.97 m;
Pier/clerestory wall (**8**) : 2.80 m.

Figure 4.14: 2D configuration of the model and thickness of different elements. Clemente (2007).

Gravity load analysis of the 2D model till collapse considering distributed damage model confirmed the same kind of mechanism obtained in case of 3D model. Also these results were in good agreement with that of Salas (2002) but in addition the 2D model could reproduce the damage at the top and bottom of the large window.

Diverse analysis using the localized damage model was performed with three different initial radii of exclusion namely 1, 2, 3 metre. These three models were analysed for two different load increment for the gravity (factor increase of load 0.01 and 0.02) thereby yielding a total of six analyses.

Force-displacement diagram obtained showed that in case of localized damage model, collapse gravity load was independent of the load factor increment. The last load of the 3D model corresponds approximately to a load factor of 2, whereas for 2D model is 2.05, which is 2.5% higher. When using the algorithm of localized damage the resistance of the structure increases nearly 5% with respect to that of distributed damage and the failure load factor was 2.15. Interestingly the three initial radius of exclusion of localized damage model yielded nearly the same final collapse load.

Another important observation was the difference in displacement at the collapse load. According to the author the 2D model was simplified into the 3D model hence not the exact representation. But if the 2D model was calibrated in better approximation it would have result the same displacement as the 3D model at collapse load.

The mechanism of failure in the model with localized damage were similar to one obtained for model with distributed damage. It is important to emphasize that the initial radius of exclusion (that is an arbitrary parameter) only affects the number of cracks that form, and that this does neither influence the last load nor in the mechanism of collapse. In Figure 4.15 explains the mechanisms of collapse and the cracks in the structure with the three initial radius of exclusion for load factor increment of 0.01.

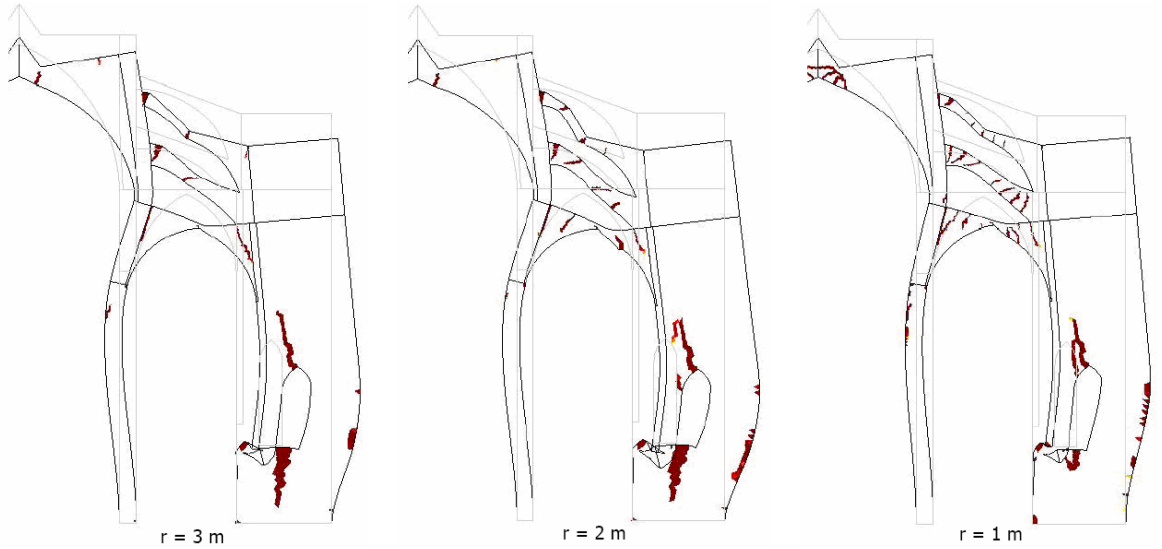

Figure 4.15: Localized damage model. Damage and collapse mechanism for three initial radii of exclusion(r). Clemente (2007).

(vi) Sensibility analysis

The sensibility analysis comprised of analyses by changing three important material parameters namely tension resistance, compression resistance and the fracture energy. In each case the gravity load was increased fictitiously until collapse.

Tensile strength

The tensile strength were considered full, one-half, one-fourth and one-tenth of the original keeping other parameters unaltered. And the analyses were performed for both the distributed and localized damage model. Result shows that in case of distributed damage model collapse load has direct relationship with tension resistance of the material. On the other hand in the case of localized crack model the structural resistance is practically remains the same. All the curves corresponding to different tensile strength tend to converge to a value that is 5% less than the initial. Therefore it is very clear that the model of localized damage is less sensitive to the resistance to tension of the material (see Figure 4.16).

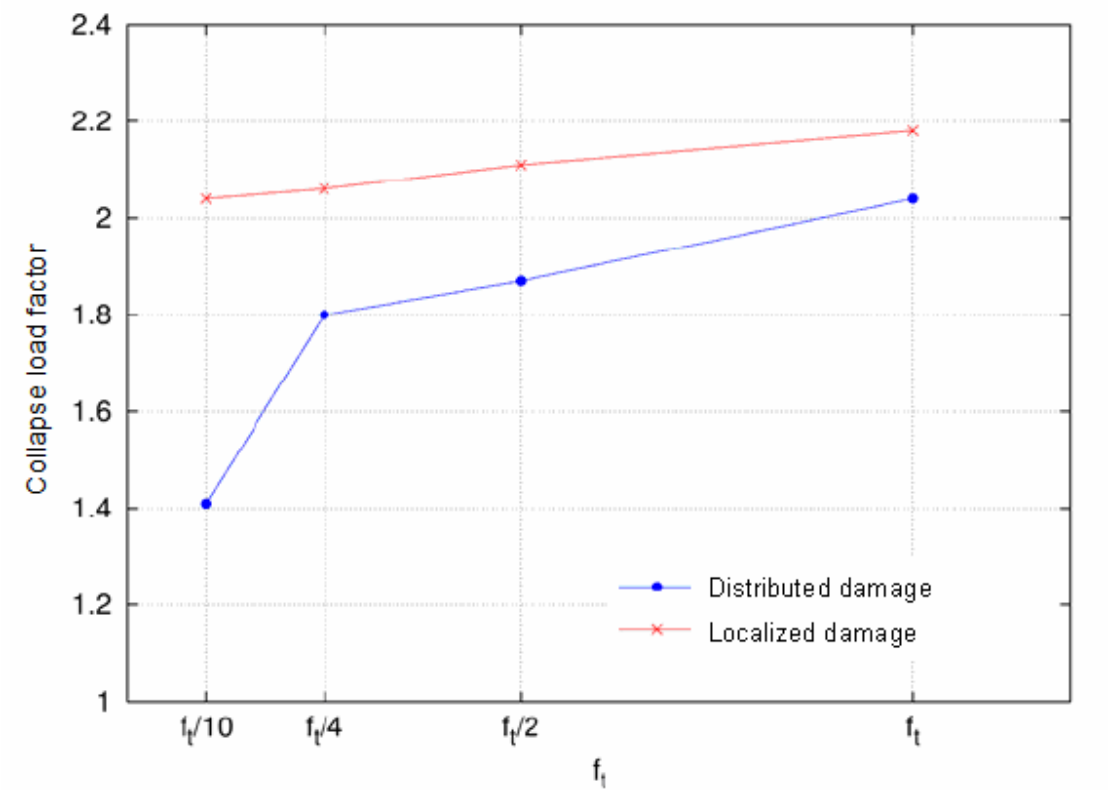

Figure 4.16: Relation between the tension resistance and the collapse load factor. Clemente (2007).

Tensile fracture energy

From the plot of collapse load factor vs. tensile fracture energy (see Figure 4.17), it can be noticed that this relation is very similar for both the distributed and localized damage models. The final load resistance capacity of the structure significantly diminishes with the fragility of the material. In particular, in the case of G_f=1 J/m^2 (fragile material) the structure fails after attaining 35% of the collapse load obtained in case $G_f = \infty$ (ductile material). It is natural that the model with smaller energy of fracture collapse before, since in these cases there exists a faster dissipation of energy and therefore the damaged elements transfer tension to the neighbor more quickly and thereby accelerating the process of structural deterioration. This type of behavior of numerical model used for historical buildings creates complexity when it is desired to find the collapse load, since there are no enough information to determine the energy of fracture of the historical materials.

Also it has been observed that in the case of fragile material with distributed damage model, some numerical problem appeared, for example the occurrence of total loosening of one or more nodes. In some cases premature damage in some elements was also observed, even though the structure did not reach to collapse.

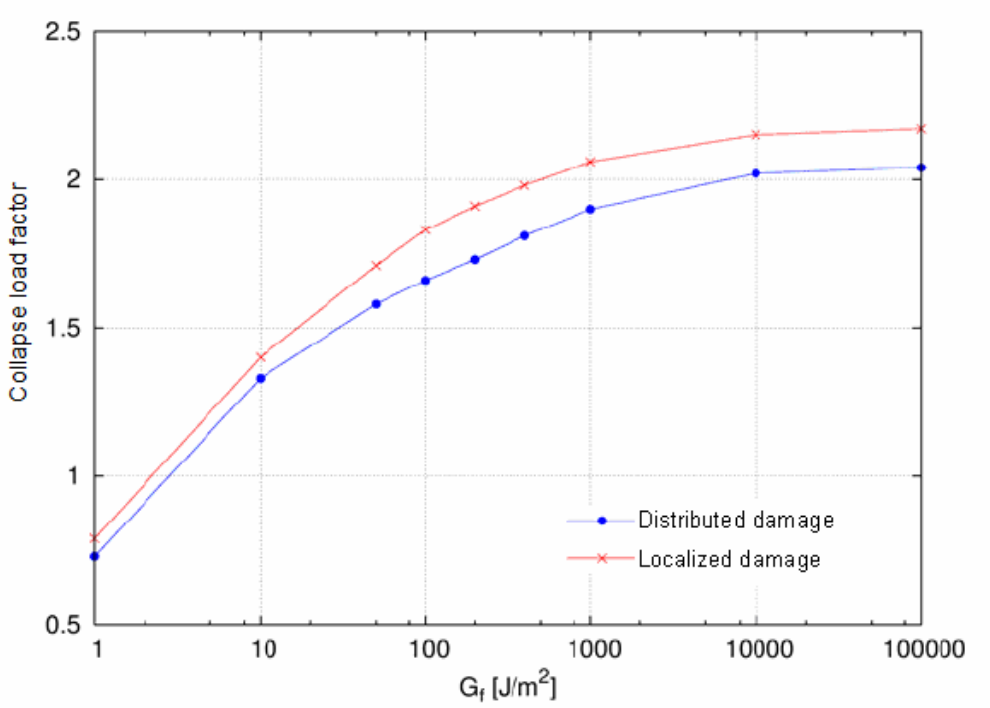

Figure 4.17: Relation between the fracture of energy due to tension and the final load factor. Clemente (2007).

Compressive strength

Existence of linear relationship between collapse load factor and compressive strength, f_c (see Figure 4.18) proved that the collapse mechanism was formed not only due to tensile damage of material but also due to compressive damage. For instance, collapse of the structure took place due to complete failure of abutment under compression at the height of the base of the large window.

This is worth mentioning that the collapses obtained are similar for both the models, with crushing of the material at the base large window (see Figure 4.19). Finally, it can be emphasized that the relationship of the compressive strength and the collapse load is practically independent of the model of damage used, being lightly more stressed in case of the localized damage model.

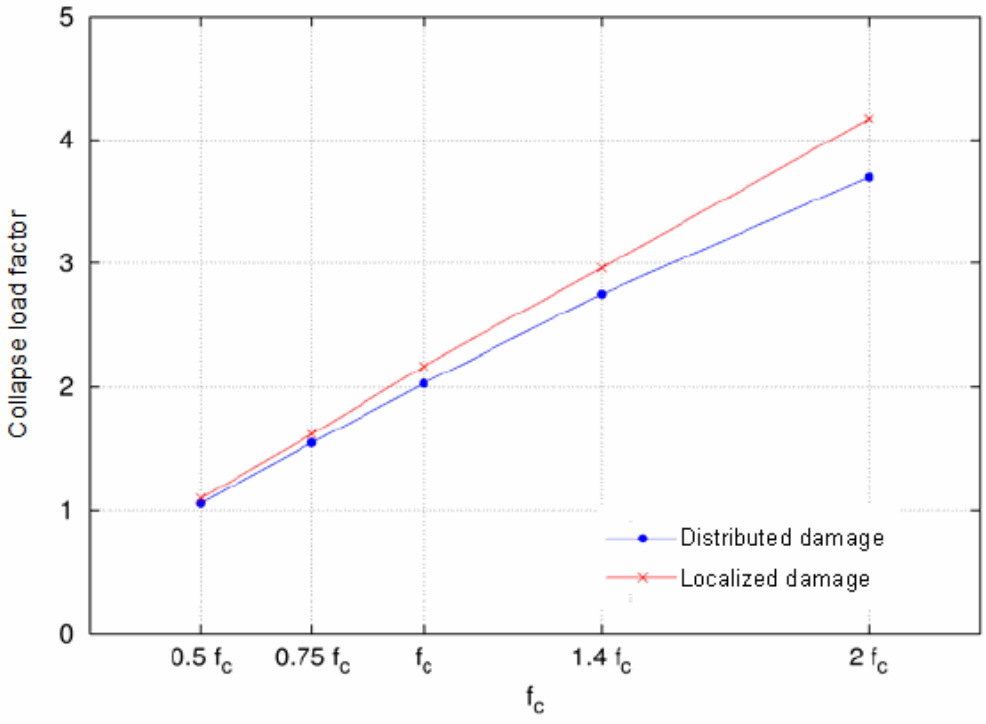

Figure 4.18: Relation between the compressive strength and the collapse load factor. Clemente (2007).

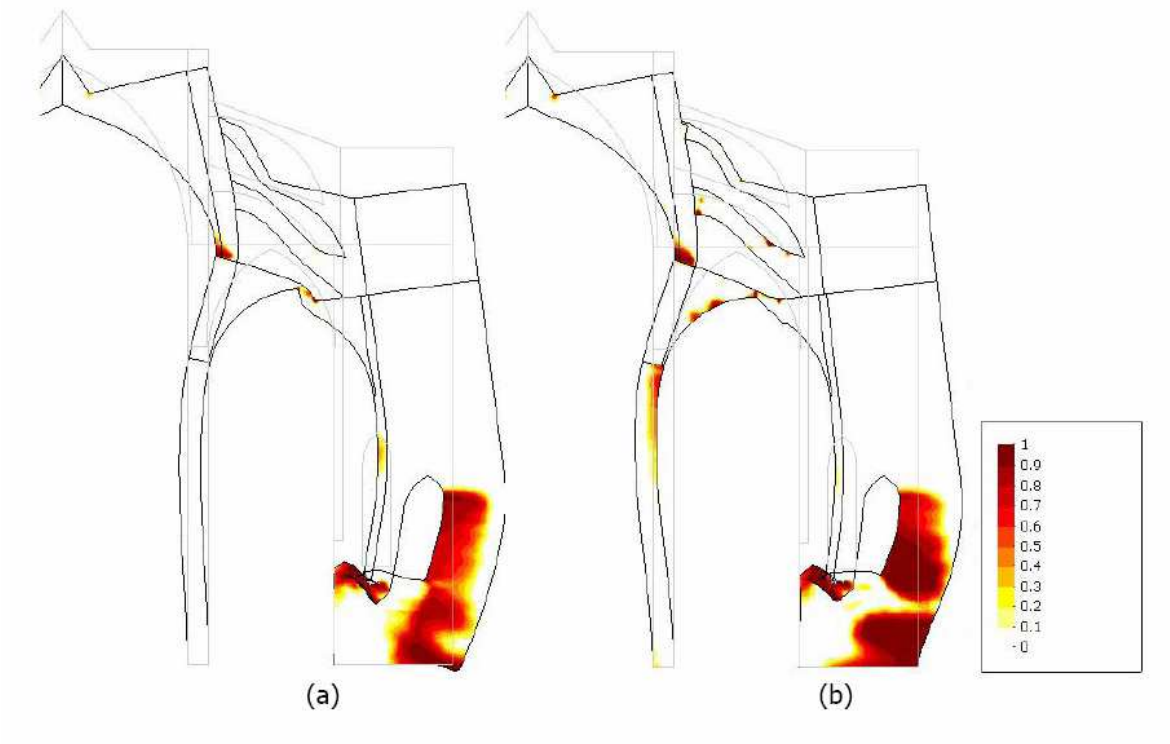

Figure 4.19: Damage due to compression at the moment of collapse. (a) Model of distributed damage (b) Model of localized damage. Clemente (2007).

(vii) Seismic load analysis

Complete 2D and 3D model were prepared considering both distributed damage and localized damage model. In this case condition of symmetry of the bay about the longitudinal axis passing through the central vault had been eliminated had been eliminated. Two phase load namely gravity and horizontal seismic load in the terms of gravity were applied in consecutive phases.

As can be seen in Figure 4.20 the models with distributed damage yielded coincident seismic collapse load (factor of 0.1) in terms of gravity, whereas models with localized damage generated higher collapse load. Choice of the initial radius of exclusion was found to have significant impact on the collapse load. Higher radius (r = 3m) produced collapse load factor of 0.14 (40% higher than that of distributed damage model). But radius r = 2m and 1m resulted in collapse load factor of 0.12 (20% higher than the distributed damage).

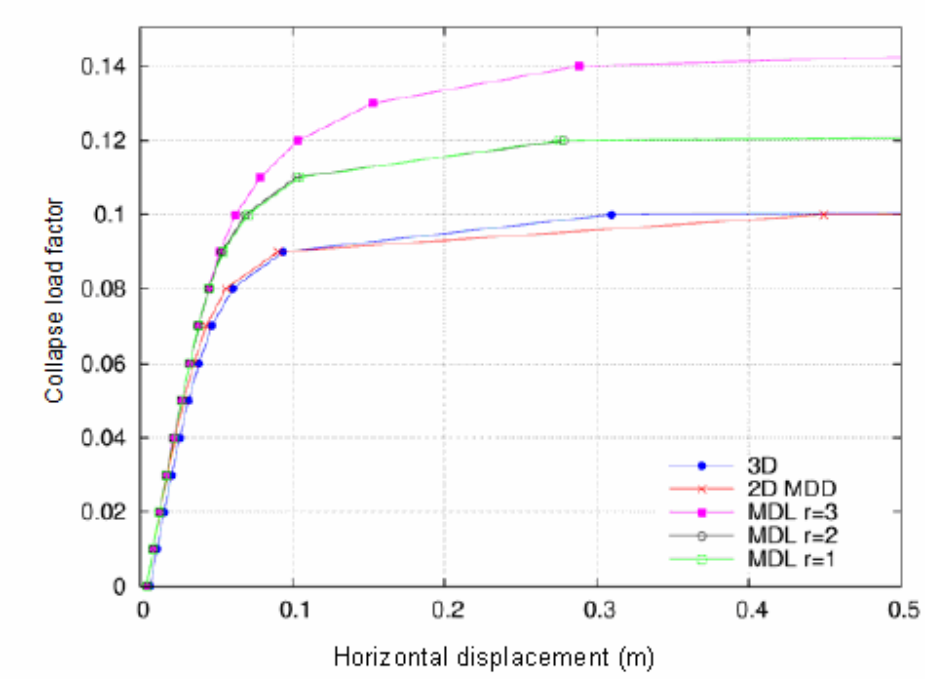

Figure 4.20: Comparison of collapse seismic load (MDD: Model of Distributed Damage; MDL: Model of Localized Damage). Clemente (2007).

Deformation and collapse mechanism for the models (2D and 3D with distributed damage) were similar except a couple of difference. Buttress in the 2D model was more affected, whereas the central vault in the 3D model underwent severe damage (see Figure 4.21).

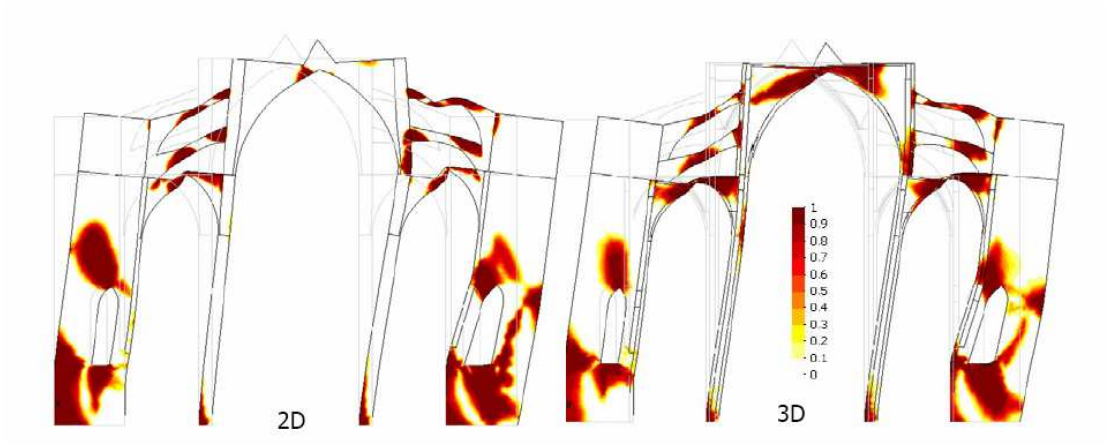

Figure 4.21: Seismic analyses with distributed damage. Collapse mechanism and tension damage. Clemente (2007).

In case of 2D localized damage model with r = 3m yielded higher collapse load but less damage compared to the models with r = 1 and 2 m. Another important observation was that the model with lesser initial radius of exclusion caused similar damage pattern as by 2D distributed damage model.

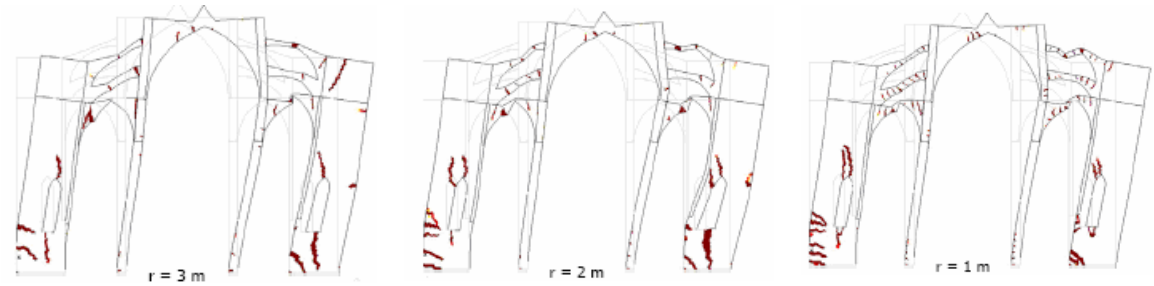

Figure 4.22: Seismic analysis of localized damage model. Mechanism of collapse and damage for three initial radii of exclusion. Clemente (2007).

(viii) Simulation of seismic reinforcement

Two dimensional analyses considering four steel braces (c/s area of 2 sq. cm each) were connecting the base of the lateral vault. But the result did not come out to be of meaningful. In one hand 2D localized damage model with r = 3m the structural model could attain the load factor of 0.135 (3.6% smaller than previous) at collapse. On the other hand the same model with r = 1m and 2m yielded collapse load nearly the same as previous (load factor = 0.12). Little smaller collapse load (factor = 0.098) was observed for 2D distributed damage model. There no change in the mechanisms that the models produced at collapse.

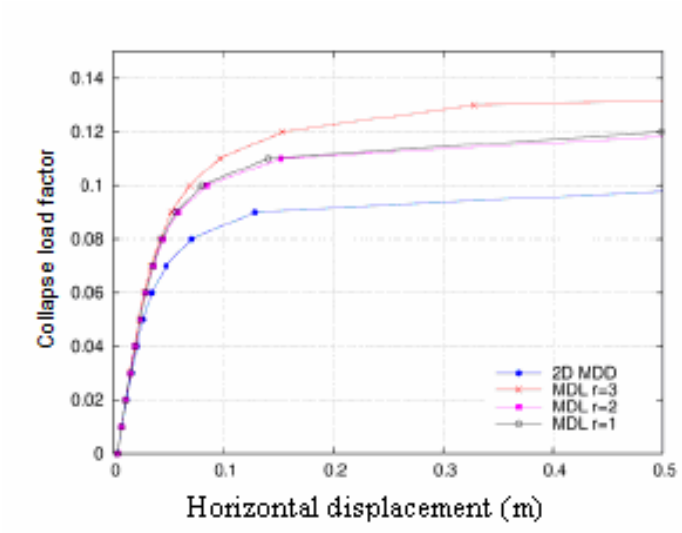

Figure 4.23: Load-displacement diagram for 2D model with steel bracing. Clemente (2007).

One possible reason could be that the area of reinforcement provided was not adequate to influence the structural behaviour. Also depending on the damage pattern and location of cracks placing of steel bracing is utmost important to cause the structure to collapse in higher load factor.

4.1.6 Conclusion

Previous analysis of Mallorca cathedral has been presented. The authors analyses show a careful investigation of the heritage building considering different alternatives. Those were implemented to explain the structural behaviour and also to judge suitability of some structural elements. Analysis done by Rubio, Mark, Maynou mainly concentrated in the gravity load analysis and the results agreed except few differences. Whereas a comprehensive study has been attempted by Salas, possibly put an inspiration to the study of Clemente, 2007. In a clever examination Clemente could find a possible cause of the large deformation of the top of pillar considering the effect of creep. Seismic analysis done by the same author showed a good resistance of the structure but at the cost of huge damage. An attempt to strengthen the structure for a seismic action was made by introducing tie rods connecting the bases of the lateral vault, but unfortunately the result did not prove the effectiveness of the attempt. In any case, Clemente's analysis is a good direction to the researchers to carry forward the analysis with different material parameters. The author was able to show that the variation of collapse load factor has a good dependence on the tensile strength, compressive strength and fracture energy of the material. Especially in case of heritage masonry building a good understanding of the material is necessary and can accomplished by performing experimental analysis side by side to the numerical analysis.

5

Present analysis of Mallorca cathedral

5.1 Introduction

In the present chapter structural analysis of a single bay of Mallorca Cathedral has been performed with the help of the numerical tools as discussed in section 2.2.1. The numerical analysis is based on macro modelling and tension-compression damage model (synonymous with the term distributed damage model) for the material. The main aim of the analysis is to verify the applicability of the tools to represent the behaviour of large historical masonry complex under gravitational and seismic loading and thereby assessing the strength capacity of the structure before collapse in either case. Through the proceeding sections a brief enlightenment has been made regarding preparation of numerical model, consideration of different material parameters that are utmost important to characterize material properties. Finally, results of the analyses performed are presented. Where ever applicable, comparison has been made with the analyses done by authors previously to understand and sustain interest on the applicability of the present analysis.

5.2 Preparation of model

Geometrical configuration

The numerical model is constructed in three dimensions using the program GiD (version 8), on a geometry as considered by Casarin and Magagna (2001), Salas (2002) and Clemente (2007). In

fact in the present case the model used by Clemente has been extended to the other side of the longitudinal plane of symmetry i.e. longitudinal plane of symmetry has not been considered but transverse plane of symmetry has been kept under consideration. This is due to the fact that the condition of longitudinal symmetry of the bay cannot work for the case of lateral load (perpendicular to that plane) as the deformation of one side of the plane of symmetry affects the deformation on the other side. Figure 5.1 below shows the geometry of the bay considered for numerical modelling.

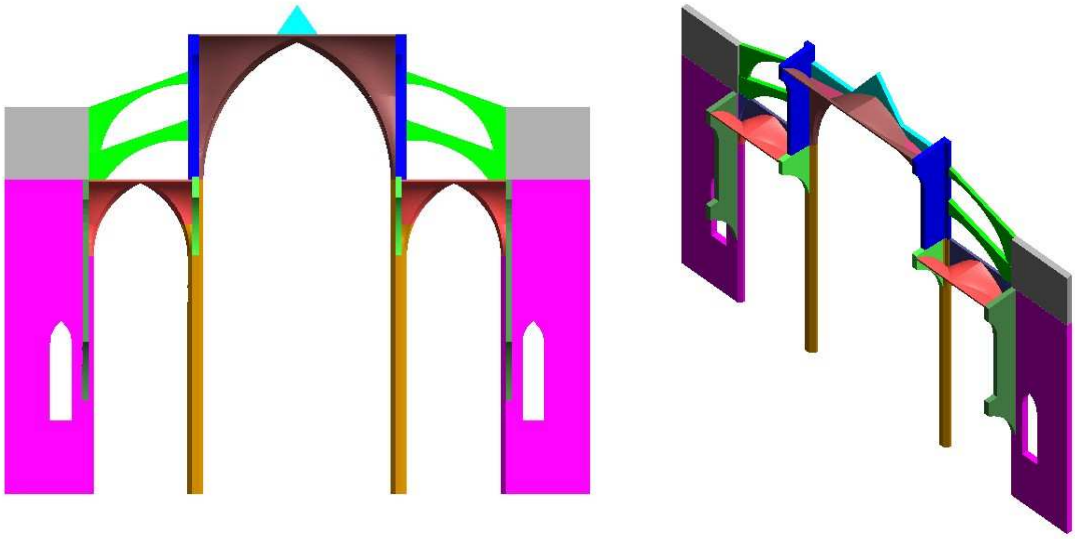

(a) (b)

Figure 5.1: Geometry of the bay of Mallorca Cathedral. (a) Sectional elevation (b) Isometric view.

Finite Element Meshing

The bay considered for analysis had been implemented into a three dimensional finite element meshing. The meshing has been done keeping in view the same considerations as used by Clemente, 2007. During the generation of the mesh it is very important to consider the proper size of the element to optimize the computational time and to have better accuracy of results. Figure 5.2a below demonstrates the mesh of the structural bay composed of 29304 nodes oriented to form 99958 elements. All the elements are four nodded tetrahedral elements. As can be seen from the same figure concentration of element is higher in some important locations susceptible to damage. On the other way it can be said that the mesh has been refined in those locations to identify specific zone of damage caused due to tension or crushing and also to obtain the continuity of stress and strain. For instance a size of order 0.3m has been defined in the junction of flying buttresses and claristory wall. Also from small to lager tetrahedron a smooth transition has been implemented (see Figure 5.2a & b).

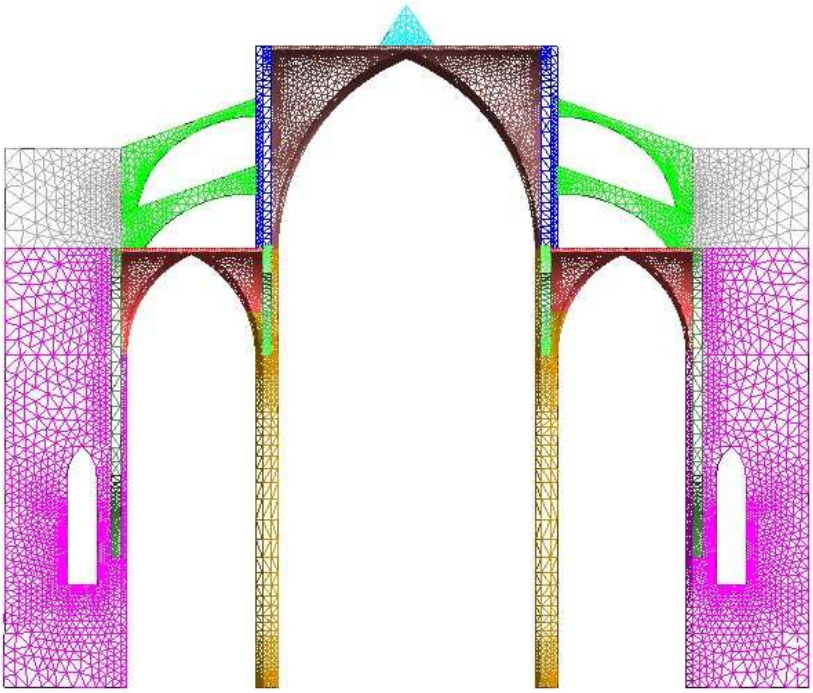

(a)

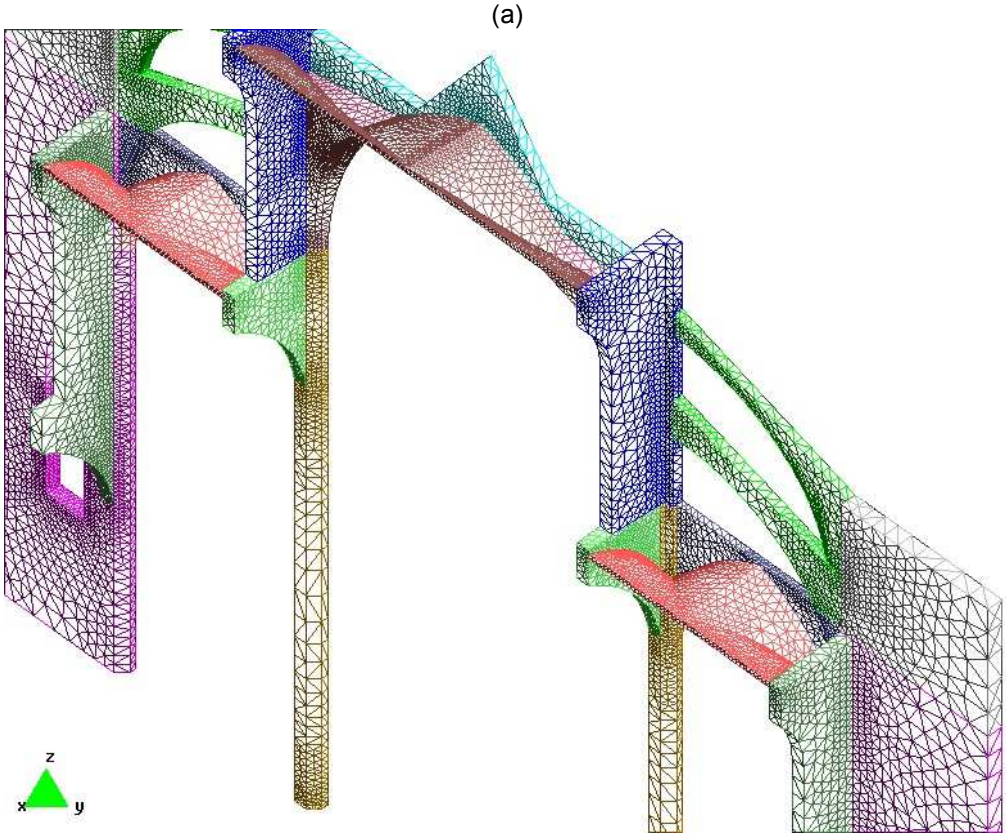

(b)

Figure 5.2: Finite element meshing of the bay. (a) Sectional view (b) Enlarged isometric view.

Loads

Some elements not being structural elements like the pinnacles and the pyramids on the keys of the vaults are not included in the model. Instead the excess weight of those elements is placed in corresponding positions. In both the cases the values taken were as adopted by Rubio (1912).For the pinnacle located on the top part of the cloister (on the axis of the column), a weight of 283.5kN has been placed in the form of distributed load. Distributing this load on the surface of the support gives 2.70MPa. The weight of the pyramid on the top of the keys of the vaults is 44.1kN. Applying the condition of symmetry, the concentrated load at the key of the vault appears to be 22.05kN for part of the structure under consideration. Finally, filling on side vaults is also omitted in the geometry. This was taken into consideration by placing an equivalent distributed load of 3600Pa.

Material

The constitutive model for the material has been characterized by adopting necessary material parameters. Tensile strength has been very low (5% of compressive strength). Young's modulus of elasticity of different materials has been considered as the same as considered by Martinez, 2008. In all the cases Poisson's ratio has been assumed to be 0.2. Table 5.1 below summarizes the material parameters used for materials for different structural components of the bay of the cathedral.

Type of material	Structural element	Young's modulus (MPa)	Compressive strength (MPa)	Tensile strength (MPa)
1	Buttresses, vaults, claristory and walls.	3816	2	0.1
2	Pillars and flying arches	15264	8	0.4
3	Filling over the cental vault	1906	1	0.05

Table 5.1: Parameters considered for material characterization

Fracture Energy

Fracture energy is another very important parameter for tension-compression damage model. This regulates the behaviour of the material after reaching the peak strength. So fracture energy has significant impact on the behaviour and load resistance capacity of the structure. Within the scope the current analysis softening behaviour of the material has been defined by adopting a value of 100 N.m/m for tensile fracture energy (G_{ft}) keeping in conformance with similar analysis done by

Ramos (2002); Lourenco et al. (2005); Senthivel et al (2006). And the compressive fracture has been considered based on the relationship $G_{fc} = 400*G_{ft}^2$ (see COMET data input manual ver. 5).

5.3 Plan of structural analysis

Dynamic identification

To check the suitability of the model prepared in GID, dynamic identification technique has been employed. Updated model has been analysed for the following analyses:

Gravity load analysis

Firstly a preliminary understanding of the structural behaviour a linear elastic analysis has been performed under gravity load. The same analysis has been repeated, but this time with non-linear material model called tension-compression distributed damage model and applying the gravity load step by step. The second model was checked against the first as the second will be used for other analyses.

Secondly the gravitational load was applied in a fictitious way until collapse using the non-linear model.

Seismic load analysis

Firstly seismic load analysis has been performed using the non-linear model. Distributed lateral load, in proportion to the mass, has been applied step by step until collapse.

Secondly a set of distributed force, according to the first mode, has been applied in small steps. The final load attained in the case has been compared with former.

Thirdly a parametric analysis has been performed to find the effect of a parameter in the final lateral load carrying capacity of the structure.

Fourthly capacity spectrum method has been implemented to assess the seismic load carrying capacity satisfying demand spectrum for the particular site.

5.3.1 Dynamic identification

Dynamic identification is necessary to validate the numerical model by comparing the dynamic parameters, which is in turn, depends on material properties (e.g. density, modulus of elasticity). A model, similar to that prepared in GID, has been implemented in computer code DIANA 9.2. Modal analysis has been performed to find the frequency, mode shape, mass participation factors. Table

5.2 shows the modal parameters for first five modes. It can be noticed that the first mode analytical frequency is 14.84% away from the measured frequency while other frequencies are not even comparable with the measured frequencies. Concerning the mass participation factors first made gives the most significant mass contribution of 80.09% (Table 5.2 and Figure 5.3). In contrast, other modes have almost nil mass contribution and so, these modes can be considered as associated with the local modes. They are not representative of the global mode shape of the structure. In an earlier occasion (Martinez, 2008) a global model with same elastic material parameters reproduced modal parameters that were in good agreement with the measured. Figure 5.4 shows similarity of mode numerical shapes of the structure as a whole and a single bay used in the present study. Therefore, in spite of a bit higher difference in the frequency (14.84%) of first mode, the model has been considered acceptable with the elastic material parameters as mentioned in Table 5.1

Mode	Analytical frequency	Analytical mass participation factor	Measured frequency	% Difference of frequencies
1	1.09	80.09	1.28	14.84
2	2.31	0.00	1.47	57.1
3	3.661	0.04	1.63	124
4	3.663	0.00	1.84	99
5	4.25	0.13	2.03	109

Table 5.2: Numerical and measured modal parameters.

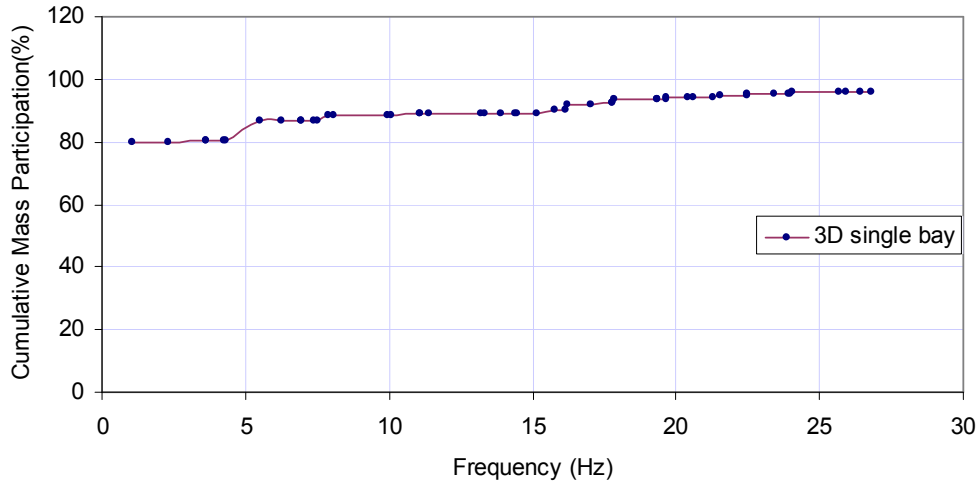

Figure 5.3: Cumulative mass participation factor vs. frequency diagram.

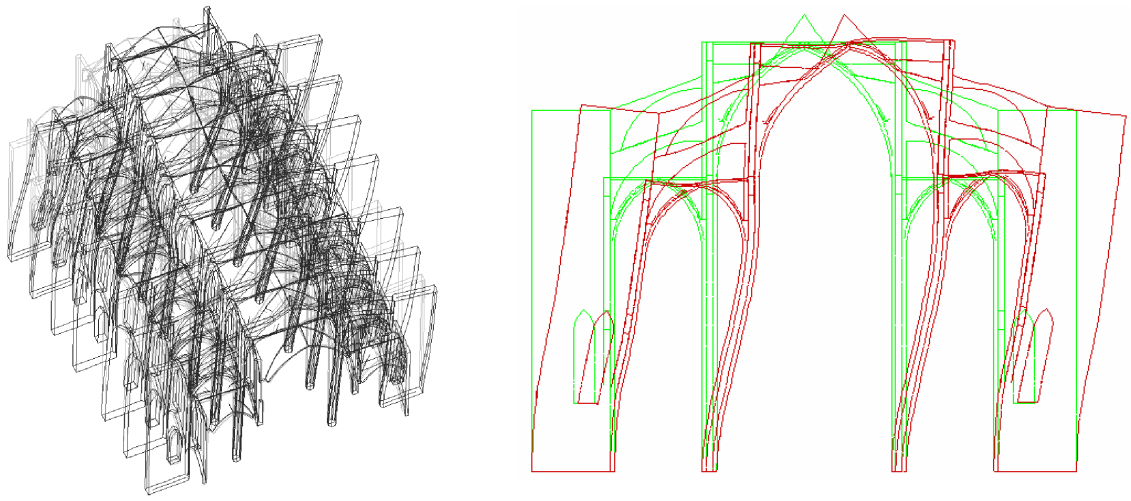

(a) (b)

Figure 5.4: (a) Numerical mode shape of the whole structure; (b) Numerical mode shape of 3D single bay.

5.3.2 Gravity load analysis using linear elastic material

Gravity load has been applied instantaneously at one step. The aim was to get an idea of the deformation of different parts of the structure. The deformed shape and stress level obtained will be used to compare in the next analysis.

Figure 5.5a shows the deformed shape of the structure and Figure 5.5b show the horizontal displacements. It can be noticed that maximum horizontal displacement occurs at the top region of the pillars (maximum displacement is 3.06 mm), which significantly lesser than the real value obtained from site measure measurement.

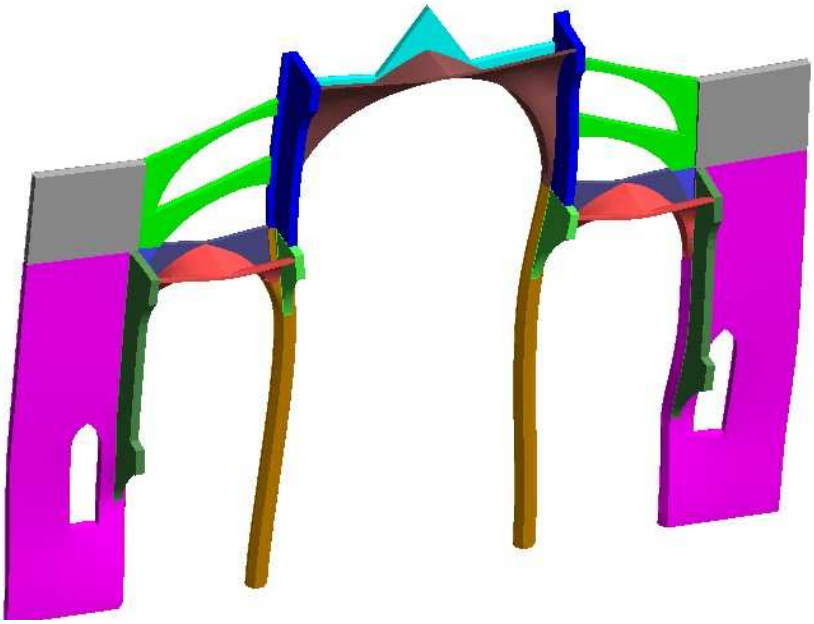

(a)

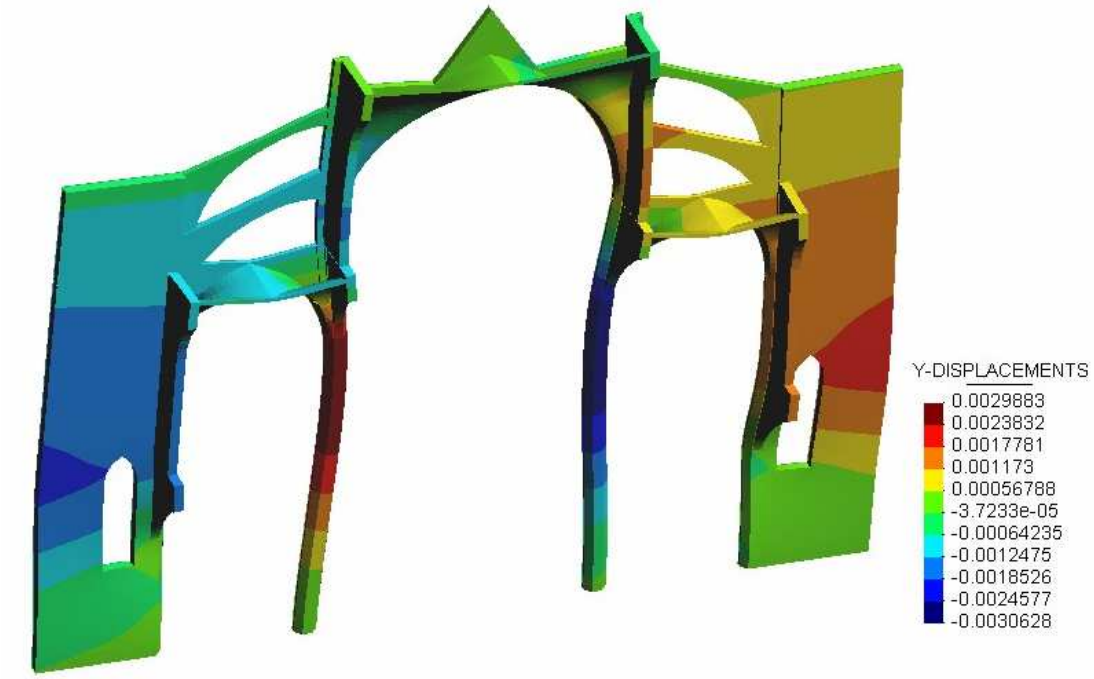

(b)

Figure 5.5: (a) 300 x Deformed shape. (b) Horizontal displacement.

5.3.3 Gravity load analysis using non-linear material

The same instantaneous gravity load analysis has been performed, but this time considering non-linearity (tension-compression distributed damage model, introduced earlier in section 2.3.1) of the

material, which, in turn, needs the load to be applied in step by step. Therefore full gravity load was applied giving 10% load increment at each step. The aim of this analysis was to find the effect of non-linearity of the material in the deformation of the structure. Also observation of the prevailing state of stresses existing in the structure is important.

The deformed shape in Figure 5.6 shows that maximum displacement near the top region of the structure increased from 3.06mm (in the earlier case) to 4.4 mm, whereas this value was 7.6 mm obtained by Clemente (2007). This increase of horizontal displacement signifies that the structure follows a nonlinear path within the range of gravitational load. But this comes to be less 7.6 mm is due to the fact that the present study utilizes the updated modulus of elasticity of the materials (see Table 5.1). Again none of these values are in the order of that found in the real observation in the structure (found to be 4 to 16cm). A non-linear analysis considering creep effect or a sequential analysis (similar to Clemente, 2007) may be employed to see if it comes closer to the real value.

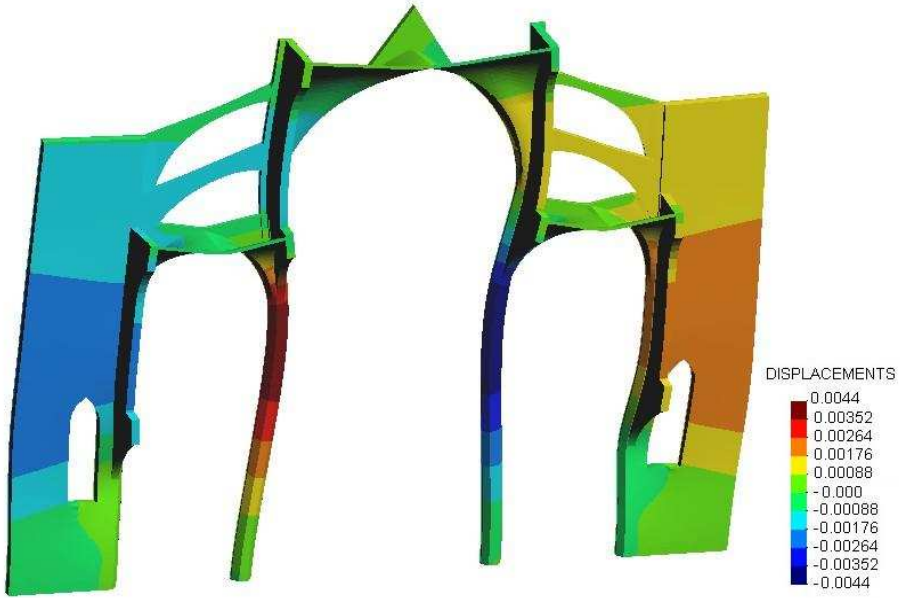

Figure 5.6: 300 x Deformed shape. Horizontal displacement of the bay.

Figure 5.7 shows the tensile damage in the bay at full gravity load. It can be noticed that the bay suffers tensile damage mainly at the base and at the top of the large window (which has already been repaired). The walls above the lateral vault and the bottom part of clerestory wall are also under tensile damage. Rest parts of the bay are unaffected. This result is with a good agreement with that carried out by Clemente (2007) as shown in Figure 4.8a.

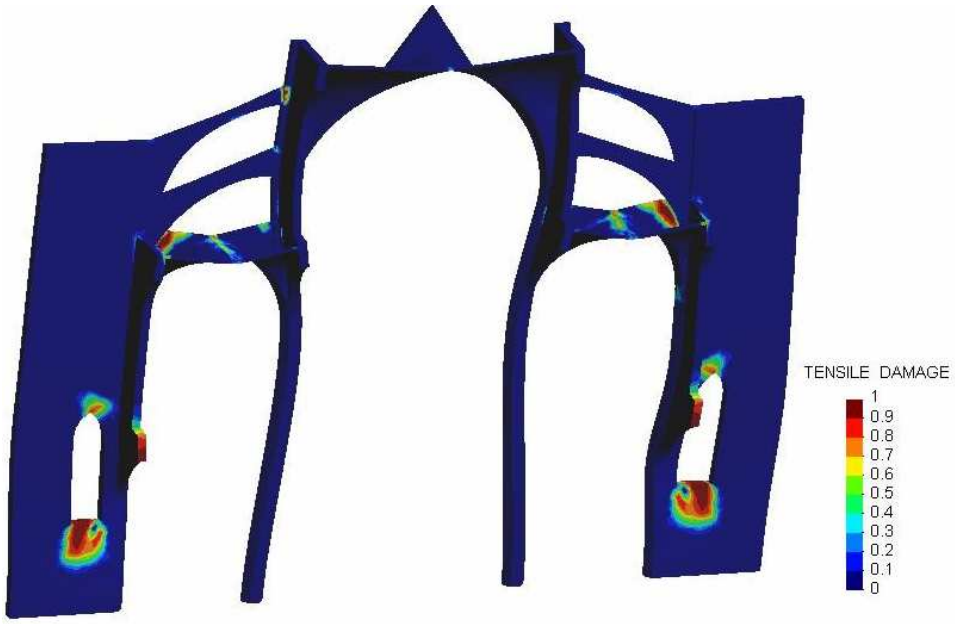

Figure 5.7: 300 x Deformed shape. Tension damage.

5.3.4 Collapse gravity load analysis using non-linear model

Gravity load, beyond the actual, has been applied on the bay with the non-linear material. The aim was to find the final vertical load carrying capacity of the bay before collapse. Although this analysis is little realistic, but this will give at least a sense of the present condition of the structure.

The analysis shows that the structure collapses at load factor of 1.62, which is 19% smaller than 2.0 (obtained by Clemente (2007)). The reason can be that the present case considers very low fracture energy (in contrast to infinite fracture energy used by Clemente) and high modulus of elasticity (almost doubled of that used by Clemente). Interestingly the current load factor is closer to that obtained by Salas (2002) (the value was 1.7, 4.9% higher).

Figure 5.8a, b, c shows the deformed shape, damage due to tension and damage due to compression respectively. Comparing Figure 5.6 and Figure 5.8a it can be noticed that the structure undergoes excessive vertical deformation at collapse load. The abutments undergoe out of plane bending, whereas the pillars undergoe a large deformation towards the central vault.

The collapse mechanism caused by tension damage shows (Figure 5.8b) that abutment at the base of the large window and bottom of the clerestory walls suffer a great amount of damage. Damage also increases at the top of the window and at the top of the lateral vaults and walls above it. Other parts like the central vault and the wall above it, the battery of flying arches suffer comparatively less damage. Compressive damage occurs at the bottom of the clerestory walls, corner of the windows (towards the central vault) and outer side of the bases of the abutments (Figure 5.8c). In comparison to Figure 4.9b (Clemente, 2007) compressive damage at the top outer face of the window is less as can be noticed in same Figure 5.8c. At an overall sense failure is mainly initiated

through the failure of the abutments (top and bottom area of the large window) due to occurrence of both tensile and compressive damage.

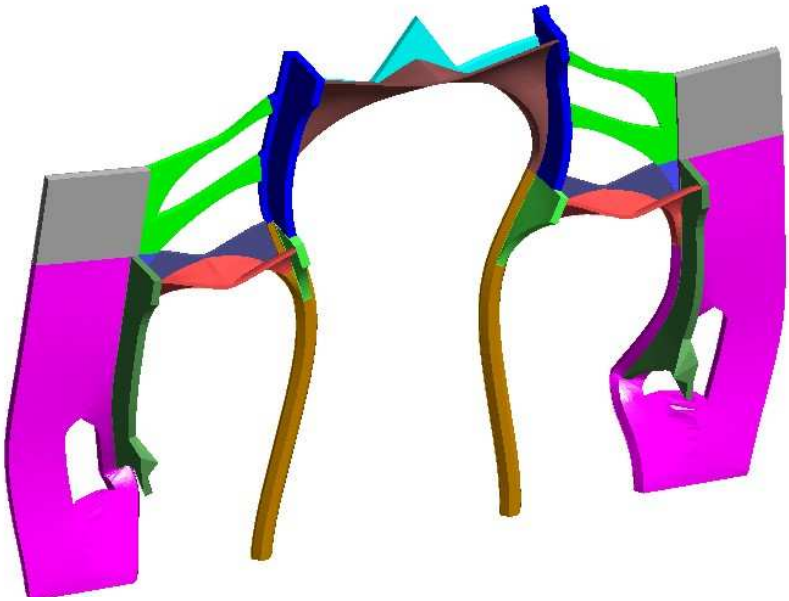

(a)

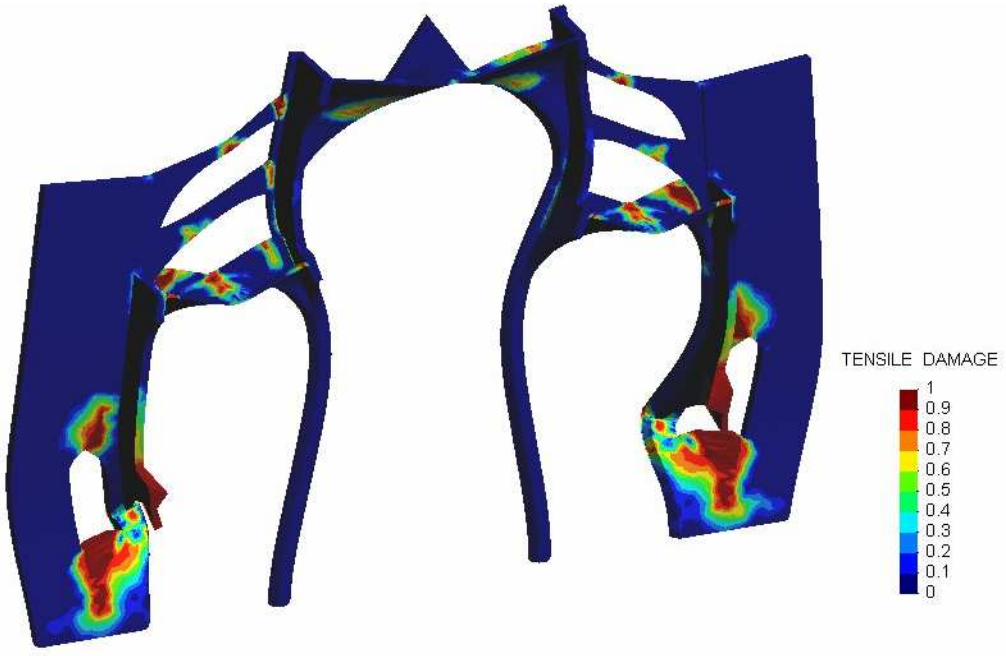

(b)

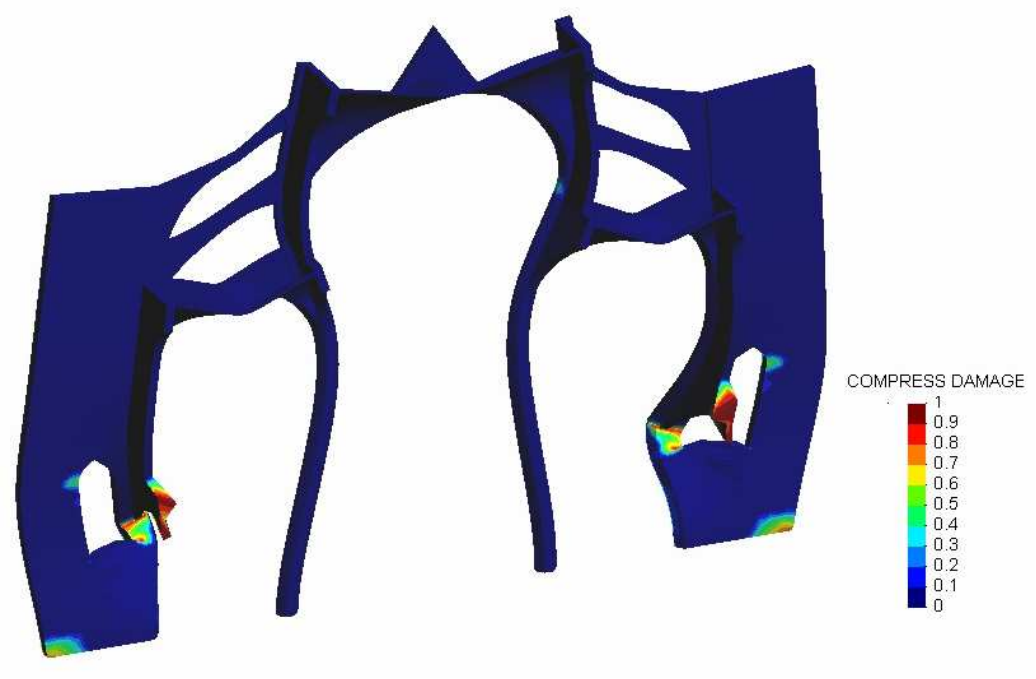

(c)

Figure 5.8: 300 x (a) Deformed shape; (b) Tension damage; (c) Compressive damage.

5.3.5 Seismic load analysis using non-linear material model

Seismic load analysis has been planned in two ways. In the first case a horizontal load proportional to the gravity has been applied in small increments (load-control method) until collapse. In the second case, instead of horizontal load, displacements according to the first mode shape have applied until collapse.

Distribution of force proportional to mass

The set of loading, which may act in case of seismic occurrence, has been considered as proportional to the mass of the structure. A step by step horizontal load increment has been applied in order to obtain a force-displacement diagram (pushover curve). Figure 5.9 shows the force-displacement diagram at the top of the pillar. It can be noticed that structure collapses after attaining a load-factor of 0.056 (e.g. 5.6% of the gravity load) and maximum displacement at collapse is 40mm (close to 45mm obtained by Rubio, 1912). The result again contradicts that obtained by Clemente, 2007. According to his calculations collapse-load factor was 0.1 (e.g. 10% of gravity load) and displacement at collapse was 500mm. The reason is again due to small value of fracture energy in the present analysis.

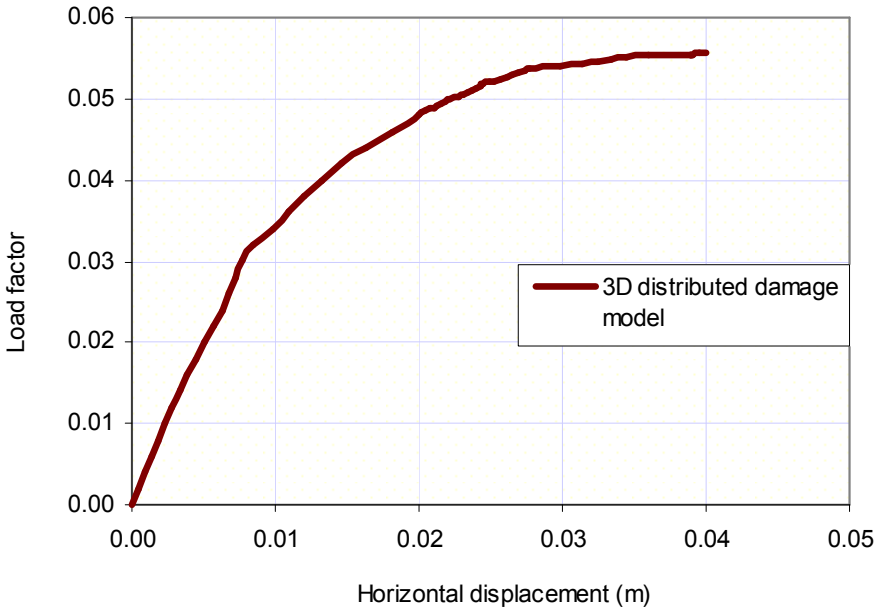

Figure 5.9: Force control method. Force - displacement diagram at the top of pillar.

Figure 5.10a, b, c show the horizontal displacement, tension damage and compressive damage in the structure at collapse load condition. The structure mainly collapses due to severe tensile damage at the base and top of the large windows, lateral vault and wall above it, central vault and battery of flying arches.

Compressive damage has been found to occur at the base of the abutments, and side of the large windows at bottom of the clerestory wall. But the compressive damage is limited to some areas.

Comparing the analyses of Clemente, 2007, it can be understood that the present state of tensile damage is almost similar to Clemente's models with both distributed damage (Figure 4.21) and localized damage (Figure 4.22) except that in his model tensile damage also occurs at the outer side of the abutments near the base and the damage occurs in a more distributed area. This may be due to the fact that Clemente's model allows more deformation at collapse, which is associated with inelastic parameter – the infinite value of fracture energy.


Y-DISPLACEMENTS
0.08
0.07175
0.0635
0.05525
0.047
0.03875
0.0305
0.02225
0.014
0.00575
-0.0025

(a)

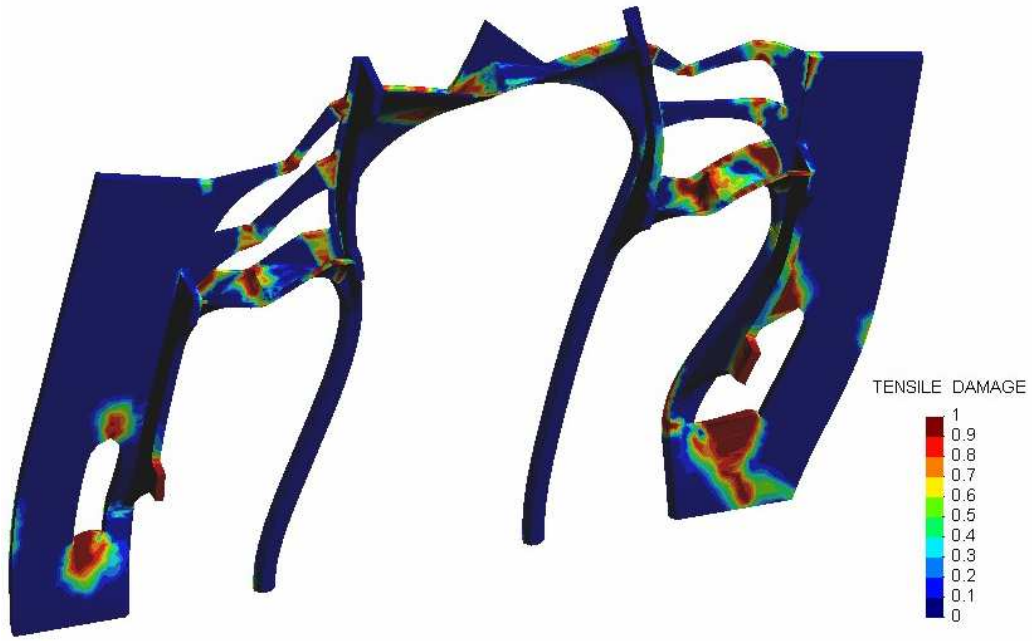
TENSILE DAMAGE
1
0.9
0.8
0.7
0.6
0.5
0.4
0.3
0.2
0.1
0

(b)

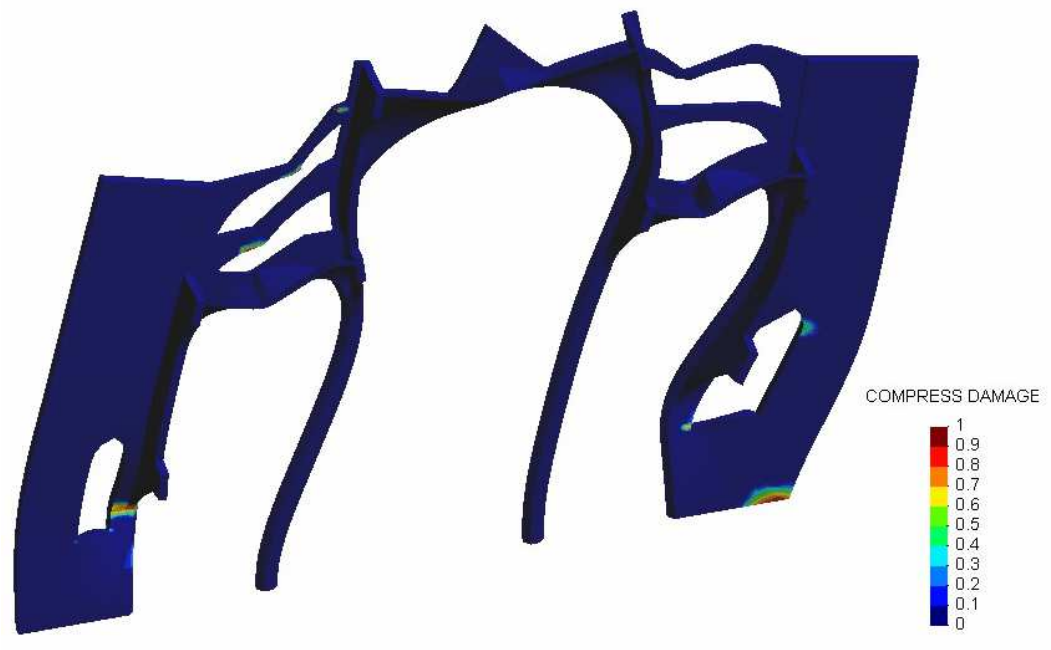

(b)

Figure 5.10: 300 x Deformed shape. (a) Horizontal displacement; (b) Tensile damage; (c) Compressive damage.

Distribution of force according to first mode

A explained earlier in sec. 5.3.1 that a model exactly similar to that of GID (ver. 8) has been prepared in DIANA for modal analysis. Frequencies, mode shapes and modal mass participation factors were obtained. Based on the mass participation factors the first mode has been found to be most significant one contributing 80.09% mass at the total response.

In opposite of application of force proportional to mass, the present analysis deals with application of force according to first mode shape (at some representative nodes). The concept is that the force increment is applied at those nodes in such a way that the first mode shape is always maintained. This has been accomplished by applying suitable boundary conditions at those points in the data file for COMET (introduced earlier). Reactions at the base of the structure and the displacement at the top of the pillar (as used for all other cases) were obtained for at each step. Then the reactions were divided by the total gravity load of the structure to get the corresponding load factor. Finally the load-factors have been plotted against the top displacement of the pillar to obtain force-displacement curve as shown in Figure 5.11 below. It can be noticed from the curve that the structure shows a linear elastic behaviour and then follows a non-linear path. The curve starts to

decline after reaching a load factor 0.07 (7% of gravity load). This means that the structure starts to soften after this peak load. Therefore the distribution of force (indirectly) according to first-mode shape reproduces the structural behaviour, which was initially assumed in the material by considering very low fracture energy.

Most importantly to mention that this peak load corresponds to first mode that contributes 80.09% of mass in the overall behaviour of the structure in case of any seismic occurrence. Therefore the peak load at full response of the structure should be obtained by dividing the peak load corresponding to the first mode by 0.8009 e.g (0.07/0.8009) equaling to 0.0874 (8.74% of gravity load). Displacement at the top of the pillar at this load is 47 mm (very close to 45mm obtained by Rubio, 1912).

Compared to the first method, the second procedure gives collapse load 56.3% higher than that in the former case (load-factor = 0.056). Also the displacement at peak load is 7.5% higher than the former case (that gave displacement at collapse = 40mm).

The reason can be that the structure was forced to deform according to two different set of loadings. The former case does not obey any shape, but applies a direct loading that is proportional to the existing gravity load. So the structure was forced to behave according to the load on it, but not giving any priority towards its tendency. The later case considers the intrinsic property of the structure (the mass and stiffness), which regulates the shape of different modes in which the structure vibrates during any earthquake action. Keeping priority on the structural behaviour, a set of loading has been applied indirectly to maintain the mode shape at each increment. Therefore the later case can provide more authenticity regarding the collapse mechanism at any event of dynamic action.

Based on the discussion, Figure 5.11 will be considered as the capacity curve that will be employed to evaluate the performance of the structure that would comply with the earthquake demand in the next section.

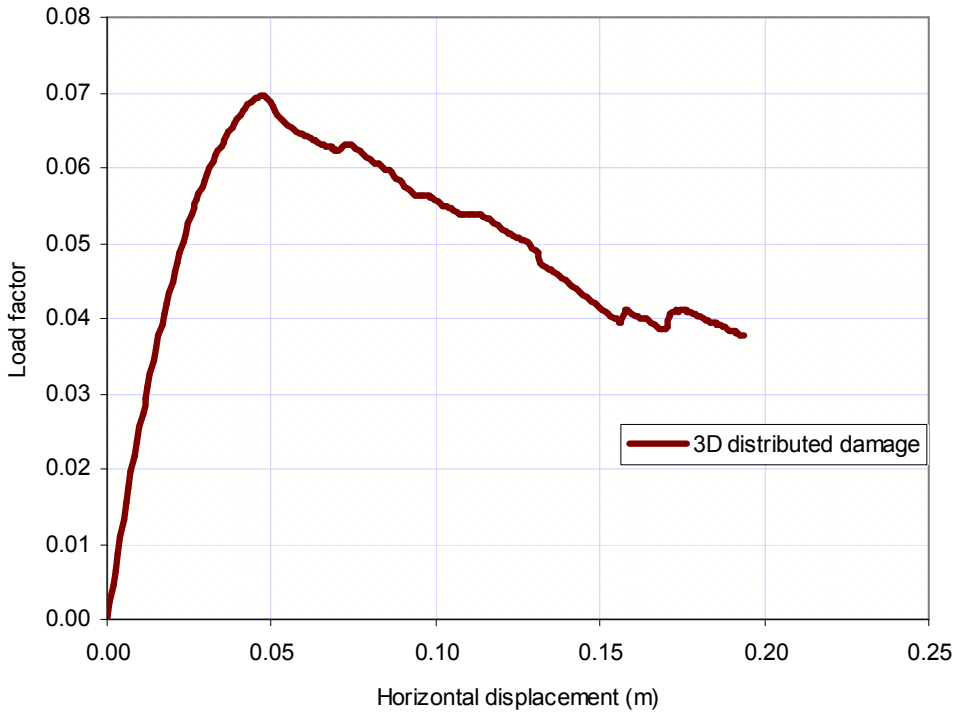

Figure 5.11: Displacement control method. Force-displacement diagram at the top of the pillar.

Figure 5.12 and Figure 5.13 below demonstrate the deformed shape, tension damage and compressive damage in the structure at peak load and at the final loading state. Some interesting phenomenons were observed during the process of the collapse of the structure.

Comparing the deformed shapes in Figure 5.12a and Figure 5.13a it can be inferred that the structure undergoes excessive deformation after the peak load. During the declining branch of the force-displacement diagram, some parts has been found to dislocate completely (e.g. upper battery of flying arch), which are not represented in the figure to avoid clumsiness.

The area of tensile damage at peak load (see Figure 5.12b) increases more and more and spread all over part of the structure to reach the final condition as in Figure 5.13b. Compressive damage, which is not much significant at peak load (see Figure 5.12c), has been found to occur at the base of the abutments, lateral vaults, battery of flying arches and at the corners of the large windows. Therefore the collapse occurs both due to occurrence of tensile and compressive damage (to a little extent).

(a)

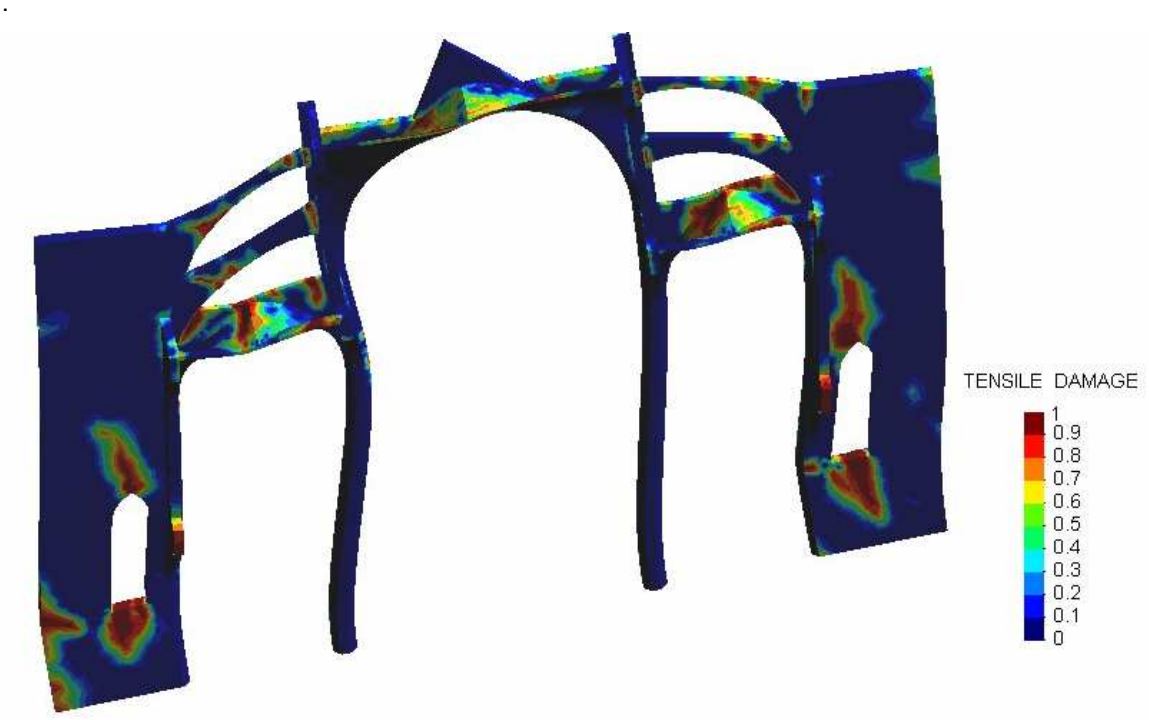

(b)

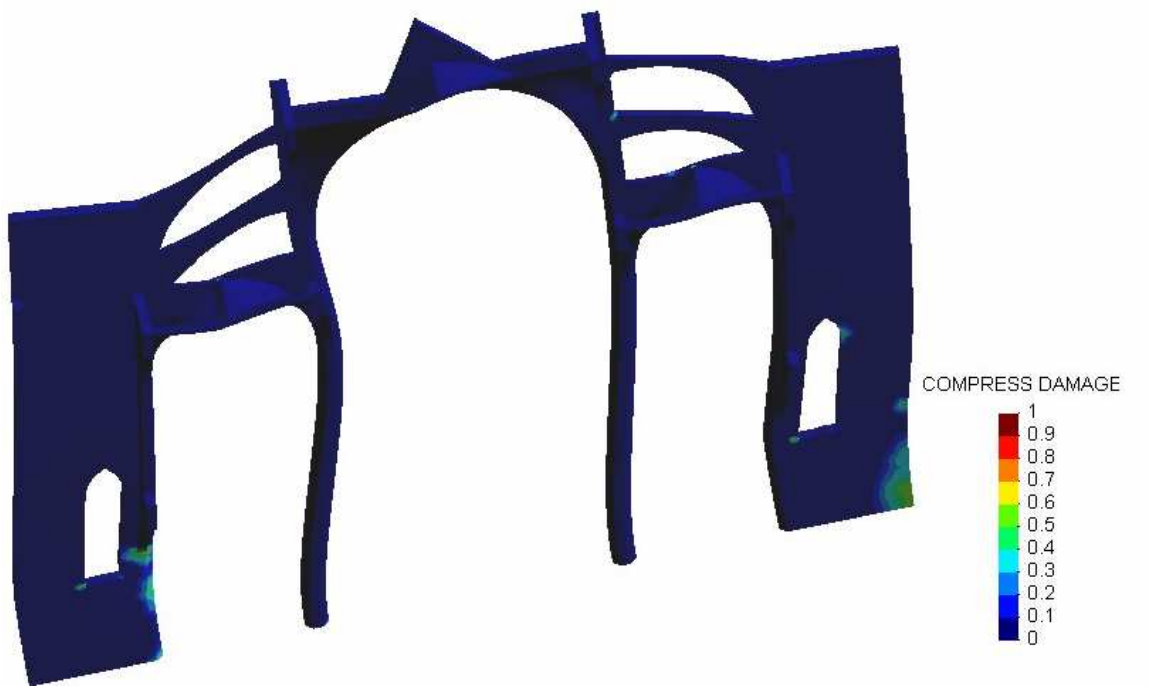

(c)

Figure 5.12: Peak load. 100 x (a) Deformed shape; (b) Tensile damage; (c) Compressive damage.

.

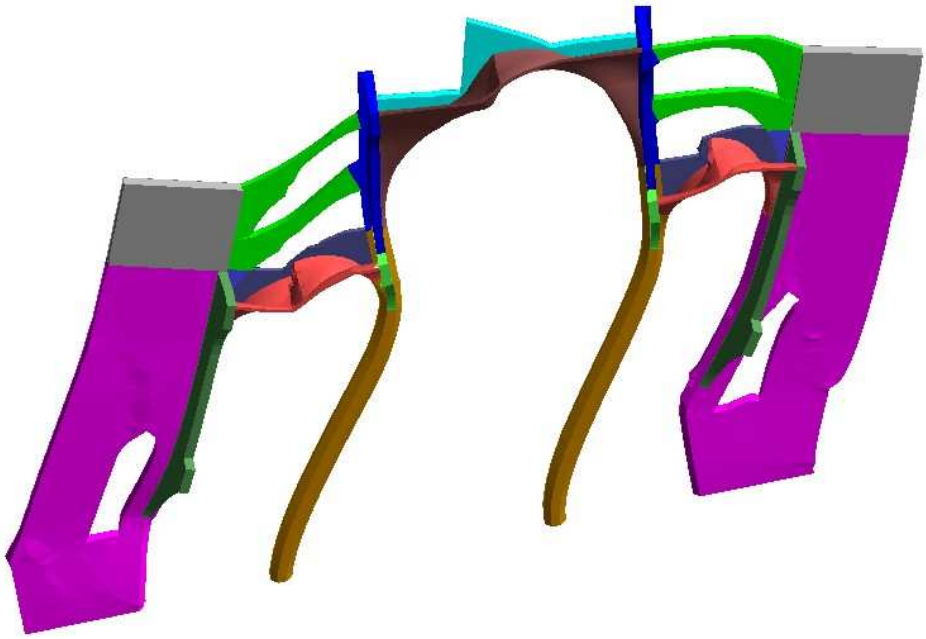

(a)

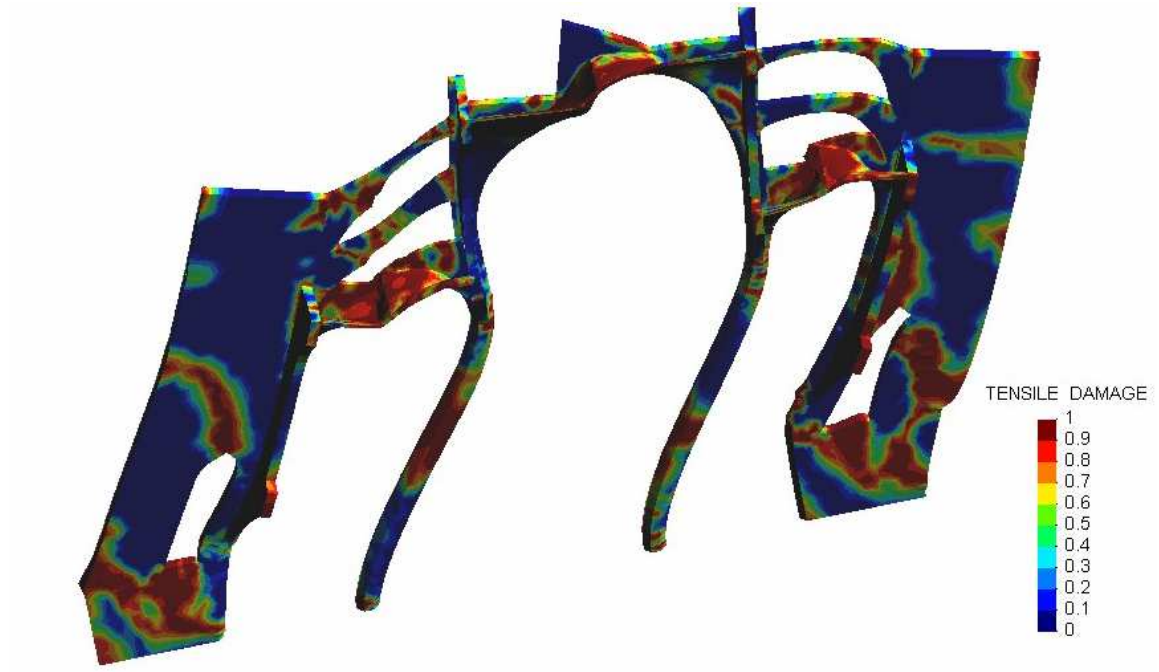

(b)

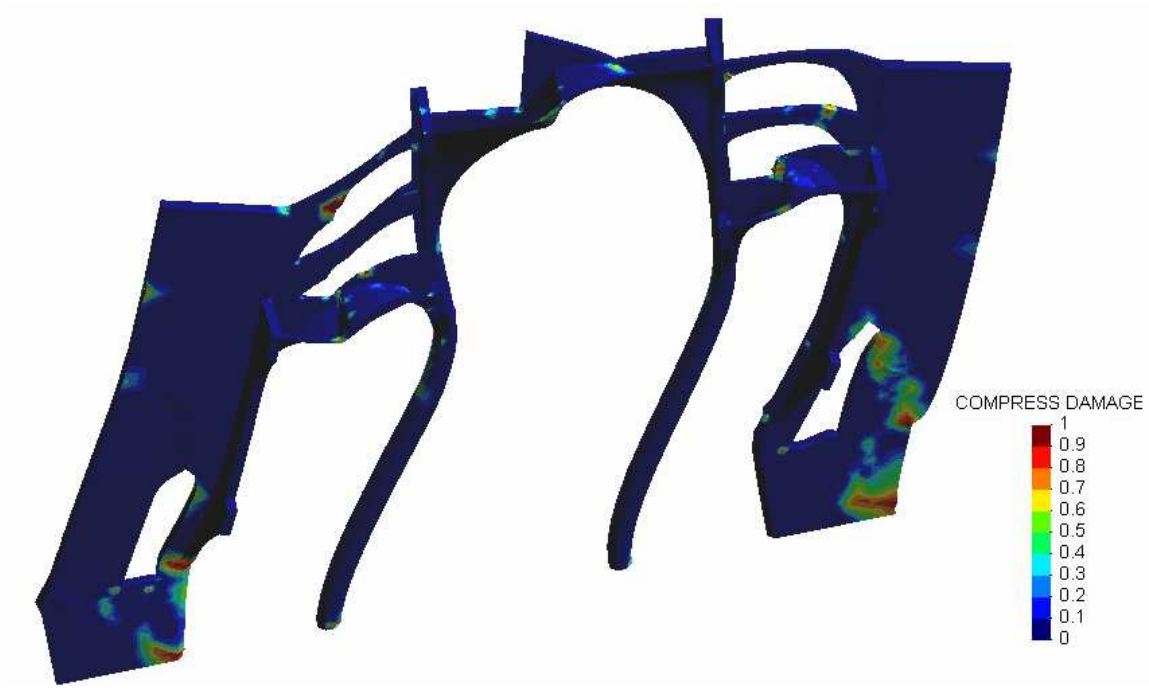

(c)

Figure 5.13: Final loading condition. 100 x (a) Deformed shape; (b) Tensile damage; (c) Compressive damage.

5.3.6 Parametric analysis

It has been noticed in the previous sections that the structural damage has been mainly associated with damage due to tension. Therefore it is interesting to find the influence of the tensile strength on the overall strength of the structure. Analyses has been planned to evaluate the variation of the collapse load factor upon variation of the tensile strength, the determination of which is a very challenging task for masonry.

In all the previous analyses, the tensile strength of material (t) has been considered to be 5% of the compressive strength. The present analyses consider values tensile strength as half, one-fourth, one-tenth together with the full value of that considered tensile strength i.e. t, t/2, t/4 and t/10. Other elastic and inelastic parameters of the material have been kept unaltered. In each case horizontal load proportional to the mass has been increased in step by step until collapse. Finally force-displacement diagrams at the top of the pillar have been plotted.

Figure 5.14 shows the variation of the horizontal collapse load factor for the considered values of the tensile strength. It's clear that the tensile strength has a good impact on the collapse load of the structure. The four values of collapse loads have been plotted against the four values of tensile strength factors in Figure 5.15. The curve turns out to be of bilinear nature. The initial rising branch shows that the collapse load varies steeply with the initial increment of the tensile strength. The second branch is not so steep as the first, showing that variation of tensile strength after a particular value does not does not affect so significantly the collapse load factor.

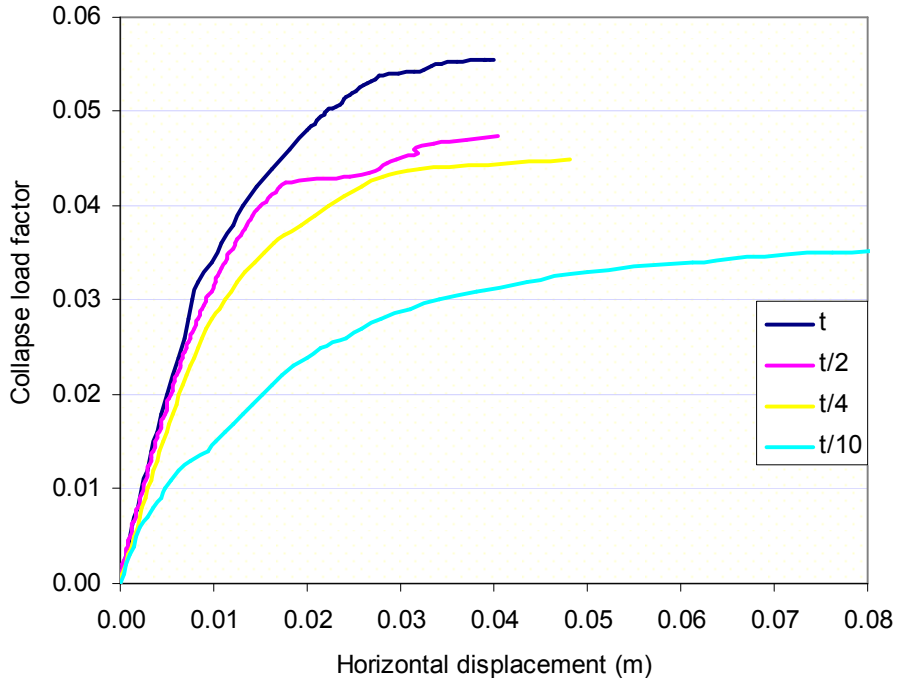

Figure 5.14: Force-displacement diagram for different tensile strength of material.

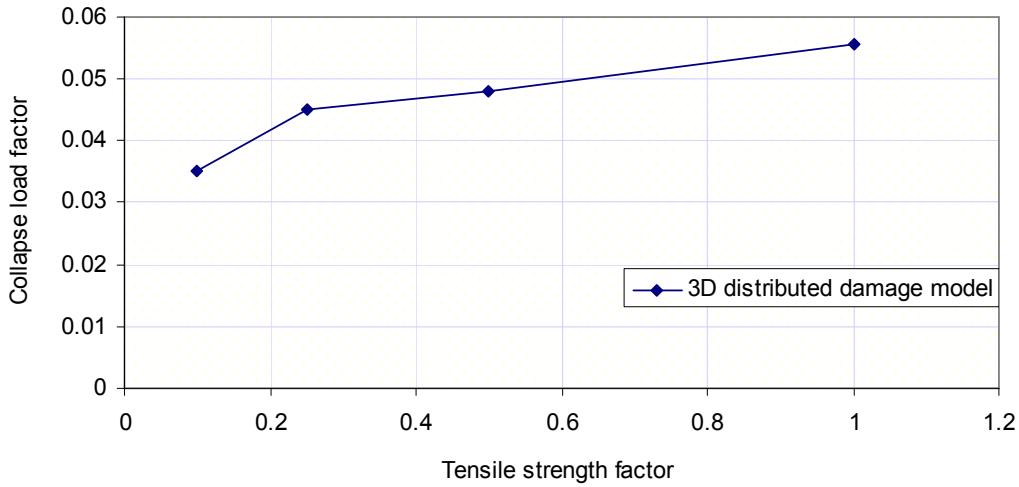

Figure 5.15: Collapse load factor vs. tensile load factor.

5.3.7 Application of capacity spectrum method

Capacity spectrum method has been applied to find the displacement corresponding to earthquake demand acceleration. The application of the Capacity Spectrum technique requires that both, the structural capacity and the demand spectra (elastic spectra reduced for developed level of nonlinearity) be defined in AD (spectral acceleration vs. spectral displacement) coordinate system.

Elastic demand spectrum

The demand spectrum utilized in the present study is the same used by Martinez, 2008, It had been developed conforming to the formulation in Eurocode EC-8 and NCSE-02 (details can be found in author's thesis), considering the following:

Seismic magnitude, M = 5.1,
Peak ground acceleration, a_g = 0.048g
Return period = 475 years.
Subsoil class = B
Damping = 5% of critical damping.

Figure 5.16 shows the elastic demand spectrum with a pseudo-acceleration (m/s^2) vs. period (sec) plot for Mallorca cathedral for return period of 475 years.

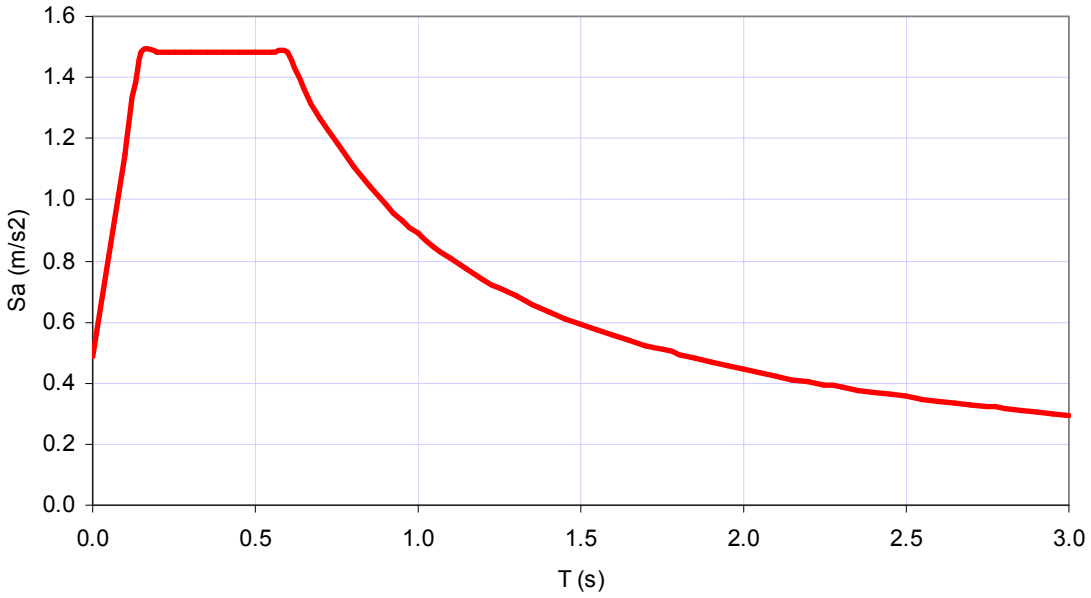

Figure 5.16: Elastic demand spectrum for Mallorca cathedral for 475 years return period.

AD conversion of elastic demand spectrum

Thus, each spectral acceleration ordinate associated to period T is converted into corresponding spectral displacement ordinate by multiplying it with a factor $T^2/4\pi^2$. The S_{ae} vs. S_{de} plot is usually referred to as seismic demand in AD format.

Therefore,

$$S_{de}(T) = \frac{S_{ae}(T)}{4\pi^2} T^2$$

Figure 5.17 below shows the plot of pseudo-acceleration, S_a (g) vs. pseudo-displacement, S_d (m) for Mallorca cathedral. This is called the acceleration-displacement format of elastic demand spectrum.

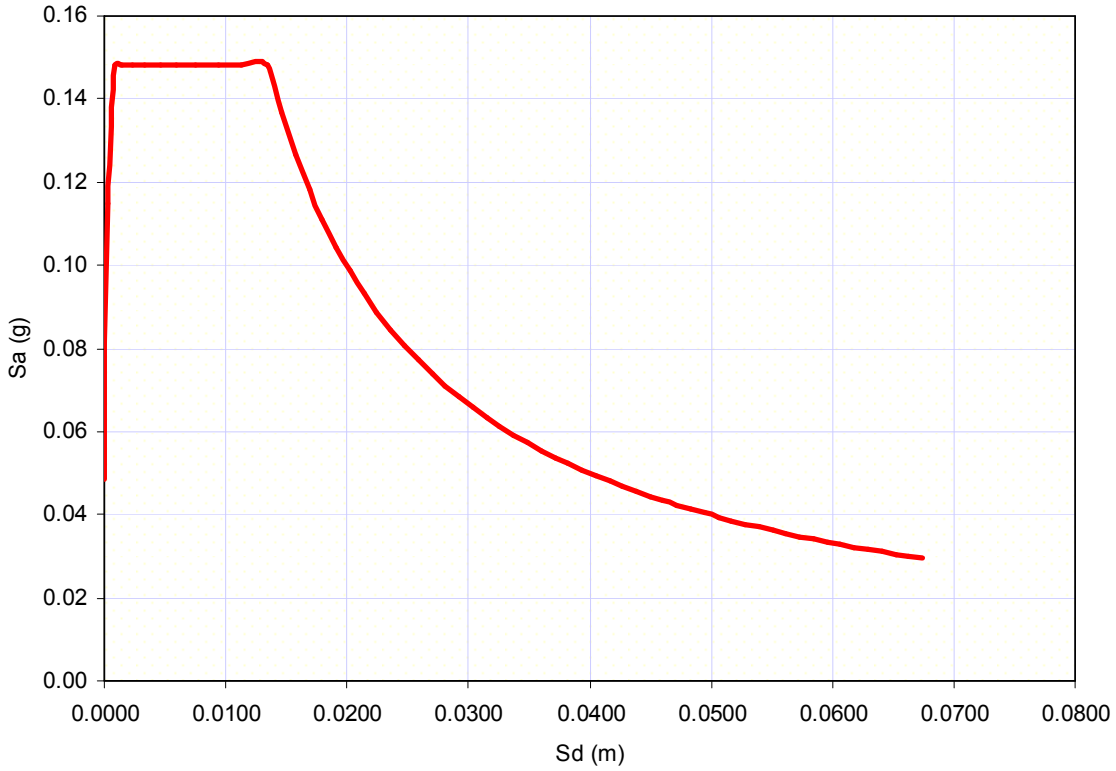

Figure 5.17: AD conversion of elastic demand spectrum for Mallorca cathedral for 475 years return period.

Capacity curve

It has been discussed earlier that two different capacity curves has been obtained depending on the methodology (application of horizontal load proportional to gravity and application of horizontal load according to first mode of vibration). These can be viewed, once again, from Figure 5.9 and Figure 5.11. Recalling the same reason as stated earlier that vibration mode shape is related to the intrinsic property of the structure. So the deformation of the structure during any earthquake action will be most closely to the mode shape associated with the highest mass contribution. The deformed shape obtained by gradual increase of horizontal load proportional to the gravity may not be the same as this mode shape. Therefore the capacity curve in Figure 5.11 has been considered for obtaining the capacity spectrum. In Figure 5.11 the base shear has been plotted as the load factor (i.e. function of gravity load). The capacity spectrum has been obtained by converting the base shear (V) is converted to spectral acceleration (S_a) and the control displacement (Δ) into spectral displacement (S_d) using the following formulation (see section 2.4.1):

$$S_a(g) = \frac{\gamma * V}{\alpha_1 M_g} = \frac{\gamma * Load \quad factor}{\alpha_1}$$

and,

$$S_d = \frac{\gamma * \Delta}{PF_\phi}$$

where, $\gamma = 1.0,$ $\alpha_1 = 0.79$ and $PF_{\phi 1} = 1.05$ (calculated for first mode shape, ϕ_1)

Figure 5.18 below shows the capacity spectrum of Mallorca cathedral. The curve in purple colour has been obtained by converting Figure 5.11 using the above formulations. Then this curve has been simplified to obtain the bi-linear representation (shown in blue colour) keeping in view that the area below and above the bi-linear curve are the same. In next section, this bi-linear curve will be utilized to find the performance point.

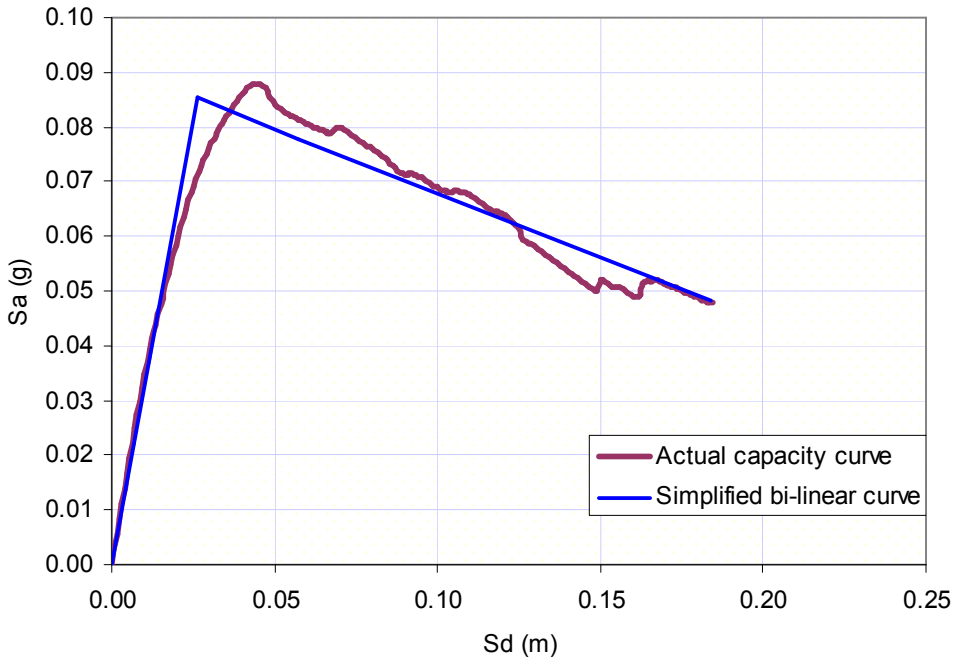

Figure 5.18: Capacity spectrum of Mallorca cathedral.

Obtaining performance point

It represents a point where demand and capacity are equal. Therefore the performance point is obtained by intersecting the demand and capacity spectra. If both the curves intersect at the elastic

range of the capacity curve it gives the actual displacement, but the intersection at the inelastic range of the capacity curve needs trial and error to find the performance point.

Figure 5.19 shows the intersection of the demand spectrum and the capacity spectrum. Fortunately, the demand curve intersects the capacity curve in the linear region. Therefore there is no need for trial and error. The displacement demand of the structure is S_d = 0.0245 m i.e. 24.5 mm at an acceleration of S_a = 0.081g i.e. 0.81 m/s^2. The intersection at the simplified linear range of the capacity curve suggests that the cathedral will have a good resistance with a safety factor of 1.079 during this kind of earthquake action.

Deformation and the damage induced at this displacement demand can be obtained from the numerical analysis of the model. Figure 5.20a, b, c shows the deformed shape, tensile damage and compressive damage in the structure at demand displacement for the seismic action. The structure should have tension damage mainly at the top and bottom of the large window with minor damage at the top of the lateral vault and the wall on the lateral vault as the performance point is in the linear range (see Figure 5.7) i.e. similar kind of damage like after application of full gravity load. But, these damaged parts widen and other parts like battery of the flying arches, central vault, outer side of the abutments and bottom of the clerestory wall have been found to undergo tension damage (Figure 5.20b) at the considered earthquake intensity. Compressive damage in the structure is very insignificant. This is due to the fact that although the structure shows a linear behaviour according to the bi-linear curve, it is actually in the non-linear range. To know the whether the damage at demand displacement really affects the structure, a load-unload cycle corresponding to the demand displacement should be carried out.

To accomplish this, a set of force according to the first mode, again, has been applied to the representative points till the top of the pillar reaches the demand displacement (calculated from the spectral displacement). Then the set of force at those points has been removed slowly in step by step. A force displacement curve has been plotted for the top of the pillar (Figure 5.21). The declining branch of the curve shows that the structure retains 3.8% deformation at the control point even upon removal of the set of force, which means that the applied demand displacement caused the structure to enter into non-linear phase and cause the damage as shown in Figure 5.20b. Comparing damage pattern in Figure 5.20b and Figure 5.22, it is again confirmed that the structure undergoes some damage but that is not so significant to affect the global behaviour. This means the damage is permanent at demand displacement but they are not so severe to change the structural behaviour significantly.

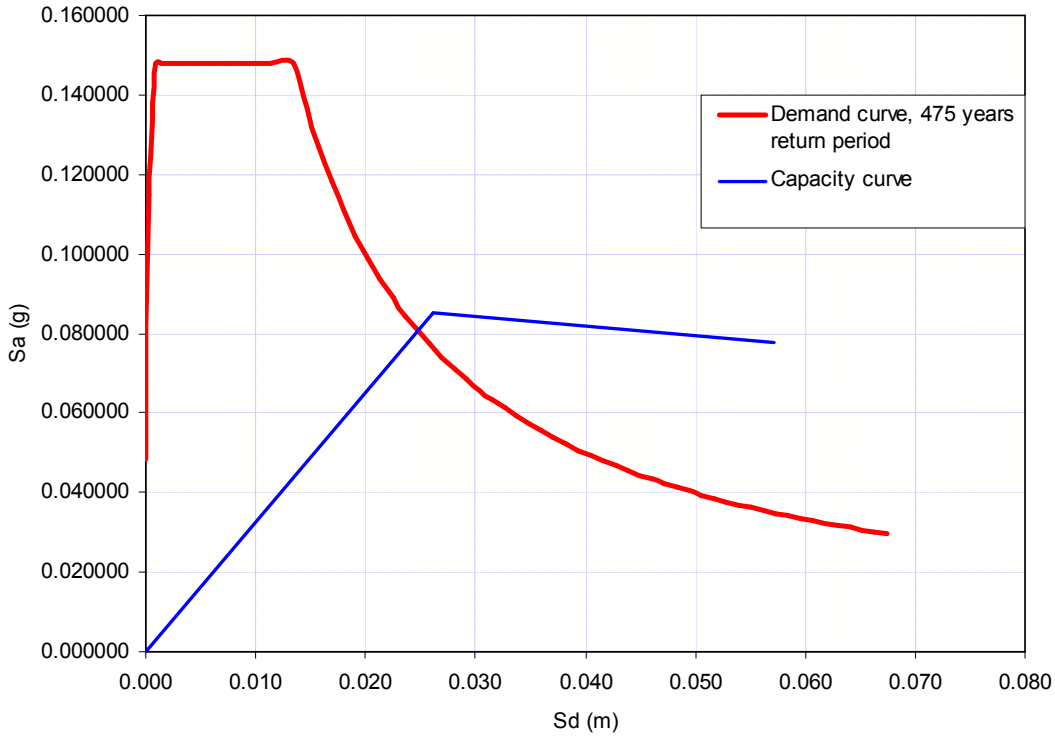

Figure 5.19: Intersection of demand spectra and capacity spectra. Performance point (S_a = 0.081g, S_d = 0.0245)

(a)

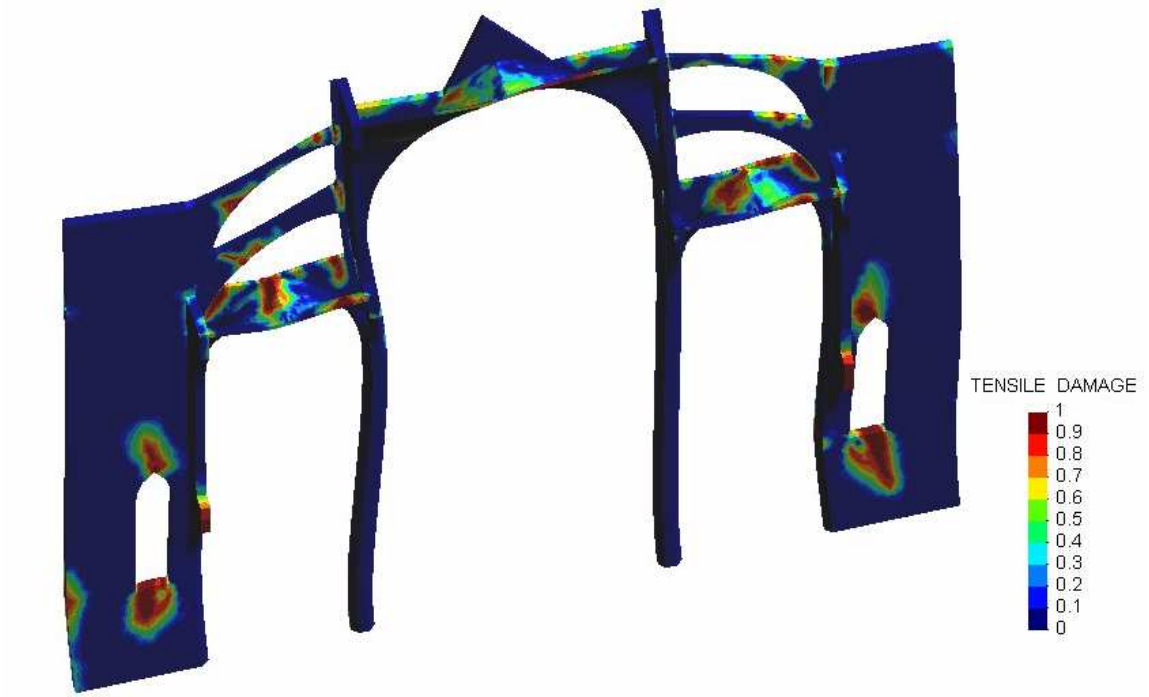

(b)

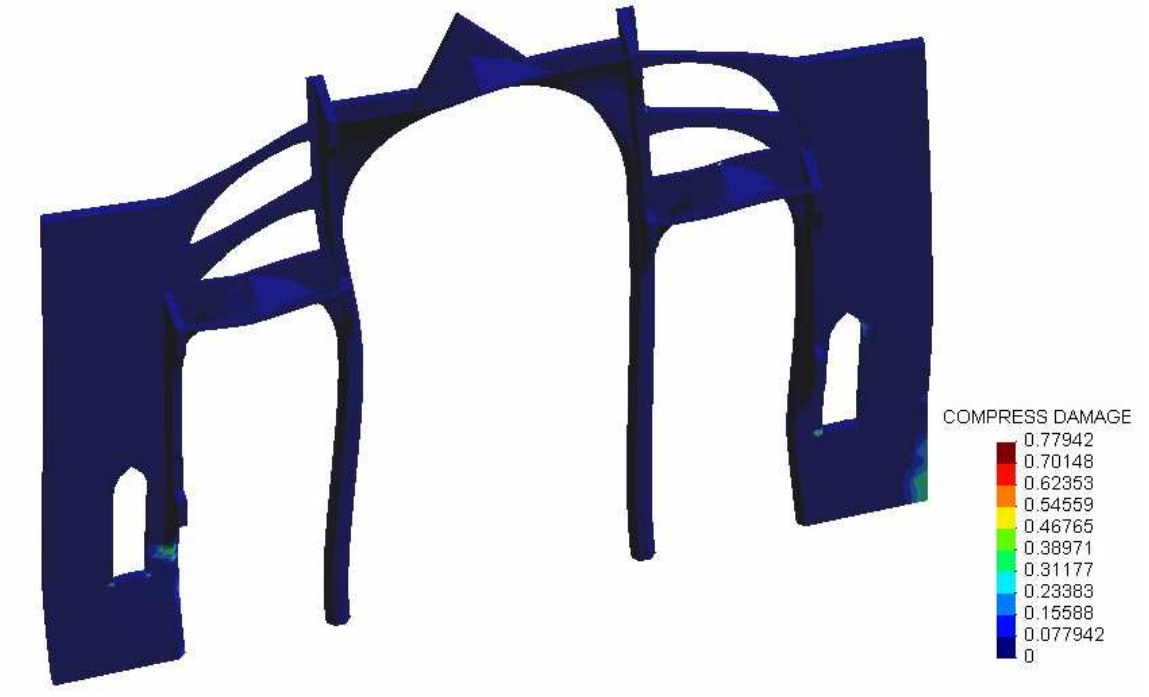

(c)

Figure 5.20: Demand displacement. 100 x (a) Deformed shape; (b) Tensile damage; (c) Compressive damage.

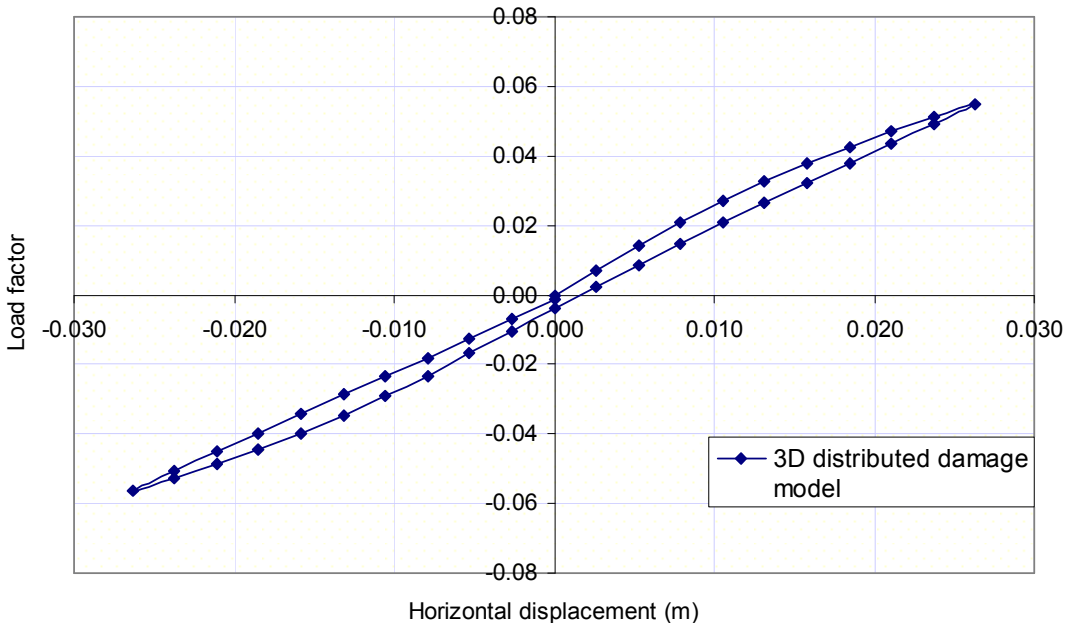

Figure 5.21: Single load-unload cycle for demand displacement.

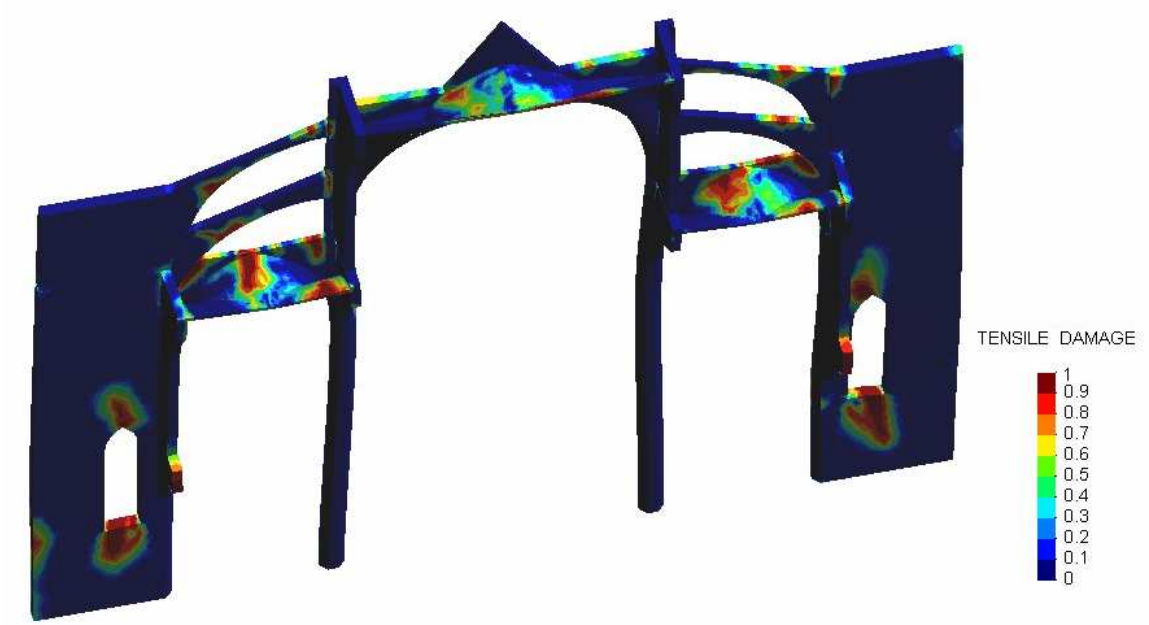

Figure 5.22: Tensile damage after removal of demand displacement.

6

Discussions and conclusions

6.1 Summary of woks done

Structural analysis of historical masonry construction and the challenges in this filed has been presented. The importance of research on masonry and the possible directions, in which it can help the mankind especially in the context of conserving the cultural heritage, has been discussed. Not only is to conserve the cultural heritage, but also analysis of masonry linked to other fields of engineering where prediction of material property is highly complicated. It has been pointed that masonry is a very environment friendly material and can last long in the nature if proper maintenance is done. Further more continuation of research in this field may provide more inspiration to build structures using this naturally available material.

A brief study on the structural analysis options of masonry has been presented. From static graphic analysis to modern numerical analysis, there are relative merits and demerits that should be kept in considerations while performing any task. Each method is suitable for a particular situation. Some procedures are robust but in cost of high computational time. Specifically complexity in terms of geometry and material should be avoided; otherwise a small mistake may result in high magnification of error. Present day research had been found to be very intensive in terms of material idealization. A careful understanding of it is important in the sense that the idealization

should reproduce most realistic response. Very brief discussion on the tension-compression distributed damage model, utilized in the present study, had been made to introduce the salient features of the model. Performance based structural analysis of masonry for seismic capacity evaluation had been introduced. This kind of analyses, although being very new to masonry field, had been discussed to give the idea the performance of a structure in case of dynamic demand.

Study on Mallorca cathedral in the island of Mallorca had been presented. Due to the long duration construction period, it had undergone significant changes. The importance of the study was to find consequence of the past construction and alterations in the present condition of the cathedral. Also information on the seismic actions in the island and the effect of it on the cathedral had been presented, the aim of which was to think of the present safety by comparing with similar earthquakes.

Detail information included previous analysis of the cathedral. This had been used for making comparison with the present analysis results. Results obtained by different authors in case of gravity load were comparable, but it did not confirm the present situation (except Clemente 2007 but considered infinite fracture energy). A careful inclusion of the effect of long term loading as well as simulating the construction phase in a model proved that the present deformation was a result of the self weight of the cathedral itself, but this needs again verification using low fracture energy.

Present structural analyses of Mallorca cathedral had been performed with aim to find the safety both for gravity load and lateral seismic load. But in this time consideration had been made to account a more realistic behaviour of masonry material by considering softening effect. The applicability was proved when the results varied from the results of previous analyses by Clemente (2007).

6.2 Summary of results obtained

The analyses were performed for a 3D model of a bay similar as used by Clemente, 2007. But this time the symmetry about the longitudinal axis passing through the key of the central vault had been eliminated. Symmetry consideration was about the transversal axis only. Young's modulus of elasticity had been improved by considering the values as adopted by Martinez (2008). In contrast to the infinite fracture energy used by Clemente (2007), this time very low fracture energy was used. The model with modified modulus of elasticity reproduced good dynamic property of the structure, nearer to that obtained in field experiment and that obtained for the global model prepared by Martinez. The difference of numerical frequency and experimental frequency was around 14.84%. Keeping in view that our model had been a simpler one and the global frequency of the whole

structure was influenced by the irregularity in plan (i.e. existence of additional structural elements at other location), the model with updated young's modulus had been accepted. The first mode frequency and corresponding mass participation factor were found to be 1.09 (unit rad/sec) and 80.09% respectively.

Analysis of the structure for gravity load considering both linear and non-linear material yielded maximum horizontal displacement of the pillar to be 3.06mm and 4.4mm respectively. Both values were lesser than that obtained by Clemente, 2007 due the improved of modulus of elasticity in the present case. But the structural behaviour was found to have a good agreement with that of Clemente.

Gravity load applied till collapse resulted in a load factor of 1.62 in terms existing gravity load which was 19% smaller than that obtained by Clemente (collapse load factor was 2.0) but close to that obtained by Salas (2002). The structure collapses both due to tensile damage and compressive damage (at the base of the large window inner side, clerestory wall and at the base of the abutment outer side).

Seismic load analysis performed by applying step by step increment load proportional to mass yielded collapse load factor of 0.056 (5.6% of the existing gravity load) with a maximum displacement of 40mm at the control point (i.e. top of the pillar). The structure mainly collapsed due to severe tensile damage at the base and top of the large windows, lateral vault and wall above it, central vault and battery of flying arches. Also the tensile damage was observed over a larger area in the damage parts. The battery of flying arches collapsed almost.

Seismic load analysis performed by applying force according to first mode at the representative points yielded peak load factor of 0.0874 (i.e. 8.74% of the existing gravity load). Displacement obtained at the top of the pillar was found to be 47mm. The deformation of the structure in this case was found to be different from previous method, especially the deformation was less for battery of flying arches. At the final condition of the structure almost all parts of the structure underwent severe tensile damage but minor compressive damage at the base and at the battery of flying arches.

The parametric analysis showed that the collapse load increases with the increase of the tensile resistance of material. According to the analysis, the increase of collapse followed two rising path - the initial path had been found to steeper than the later path. This signifies that even if the small value of tensile resistance play an important role for overall structural resistance.

Finally capacity spectrum had been applied to find the displacement demand corresponding to a demand earthquake acceleration. An earthquake of peak ground acceleration of 0.048g with a return period of 475 years, demanded spectral displacement of 0.0245m. Intersection of the demand spectrum with the capacity spectrum showed that the structure had a good resistance. The initial damage due to gravity load had been found to widen at this demand displacement. More over other parts like battery of the flying arches, central vault, outer side of the abutments and bottom of the clerestory wall had been found to undergo tension damage. Compressive damage was very insignificant. But this tensile damage was no so severe to change the structural behaviour significantly. Result proved that after removal of demand displacement the structure retain minor deformation (3.8%) but more or less followed a linear elastic path.

6.3 Discussion on structural performance

An intention had been kept to model the material in a more realistic way. Keeping in reference to similar kind of researches, a very small value of fracture energy had been considered. Even then the structure shows a capacity to bear a collapse load factor of 1.62 in terms of the existing gravity load. This means that the structure is in good condition and it can undergo vertical load more than the existing gravity load. Some damage at the base of the large window, also agreed by the numerical analysis, had already been repaired. So the current repair together with the capacity to bear more vertical load assure the safety against gravity load.

Two different procedures for seismic load analysis yielded two contradictory values of collapse load factors. Distribution of force according to first mode resulted higher collapse load than that resulted from distribution of force according to mass. But application of capacity spectrum method showed that the performance point is in the elastic range of the capacity spectrum, thereby assuring a good structural resistance during an earthquake of PGA = 0.048g and return period = 475 years. But certainly there would be limited tensile damage at the top and base of the large window. The top surfaces of lateral vaults, central vault, bottom of clerestory wall and walls above the lateral vault would undergo damage. In any case the structure would be safe for this earthquake as it followed nearly linear elastic behaviour in during a load-unload cycle of demand displacement.

6.4 Notes on future improvement

Geometrical improvement: 3D model of the whole bay

Symmetry of the structure with respect to the transversal axis has been considered in the current study. In the plane of symmetry suitable boundary conditions were implemented. These were in

terms of applying constraint on the displacements at the points in the plane of symmetry. This idealization can not reproduce bulging of material or crushing of material in the abutment. Therefore a 3D model can be prepared to find internal crushing of material, if any, inside the abutments.
Loose filling material can behave well in compression if it is constrained properly. The present model considered the effect of filling over the lateral vault by means of applying vertical load. In an improved model the filling material can be modelled with low stiffness to see if it can vary the tensile damage that was found on the top of the lateral vault during application of lateral load.

Closing of large window
In all the cases irrespective of the gravity load and seismic load, the damage initiate first at the base and top of the large window. A possible analysis can be performed without considering the windows, or closing the window with a material with low stiffness material. This may change the damage pattern around the windows.

Model for longitudinal direction
Seismic load analysis had been performed for the model prepared for the transverse bay of the structure. In a similar way, a longitudinal bay of the cathedral can be modelled to check if the vertical load yield same damage effect on the structure (i.e. on the central vault, lateral vault etc) and also to verify the safety for seismic load in longitudinal direction.

Limit analysis
Limit analysis can be performed considering possible collapse mechanism, initially obtained from finite element analysis of the structure. The force-displacement results obtained from FEM analysis and limit analysis can be compared. Because of the convergence problem, FEM analysis may not yield the exact value of collapse deformation, whereas limit analysis is robust for this. Information on the lateral deformation capacity is very important for dynamic loading.

Time history analysis
Though due to the computational cost, time-history analysis is not generally performed for structures that are having complex geometry, but in this case a non-linear time-history analysis can yield exact representation of the structural behaviour under dynamic loading. In the present case lateral load analysis had been performed by applying force according to mass or first mode. This gives the idea of the strength of the structure for load applied at one time and in one direction. But for load varying with time and also the direction, i.e. for seismic load, it is important to know strength reduction in each cycle and thereby the effect of duration of the earthquake on the strength of the structure because it is a well known fact that an earthquake of smaller magnitude of higher duration can be more dangerous than a higher magnitude but lower duration earthquake.

7

References

Binda, L., Saisi, A. (2005). *Research on historic structures in seismic areas in Italy*, Prog. Struct. Engg Mater., 7:71–85.

Casarin, P. (2006), *Structural assessment and seismic vulnerability analysis of a complex historical building*, Ph. D. thesis, University of Trento, University of Brescia, University of Padova, University of Trieste, University of Udine, University IUAV of Venezia.

Clemente, R. (2007). Análisis structural de edificios históricos mediante modelos localizados de fissuración (in Spanish), Ph. D. dissertation. Barcelona: Universitat Politècnica de Catalunya.

COMET data input manual (ver. 5.0). Release June 2002. by M. Carvera, C. Agelet de Saracibar and M. Chiumenti.

Detailed description of Mallorca cathedral, EU-India economic cross cultural programme, Project contract no. ALA/95/23/2003/077-122, Project benificiary: Universidade do Minho, Portugal. Available from *www.civil.uminho.pt/eu-india.*

Freeman, S. A., Nicoletti, J.P., Tyrell, J.V. (1975). *Evaluations of existing buildings for seismic risk - A case study of Puget Sound Naval Shipyard, Bremerton, Washington*, Proc. 1st ; .S. National Conf. Earthquake Engng., EERI, Berkeley, pp. 113-122.

Giménez, J., Gelabert, B. (2002). *Recent tectonic activity analysis of Mallorca Island,* EGS XXVII General Assembly, Nice, Bib. Code 2002EGSGA..27.4526G.

González, J. L., Roca, P. (2000). *Plan de estudios constructivos-estructurales de la catedral de Palma de Mallorca,* Universitat Politècnica de Catalunya, Barcelona.

González, J. L., Roca, P. (2003-2004). *Estudio del comportamiento constructivo-estructural de la catedral de Santa María, en la ciudad de Palma, isla de Mallorca (Baleares)*. Primera Fase. Parts I. (2003), Part II (2003), Part III (2004), Part IV (2004). Universitat Politècnica de Catalunya, Barcelona.

González, R., Cavallé, F., Domenge, J., Vendrell, M., Giráldez, P., Roca, P., González, J. L., *Construction process, damage and structural analysis: Two case studies.*

Lourenc¸o P.B., Rots J.G. & Blaauwendraad, J. (1998). *Continuum model for masonry: parameter estimation and validation*. Journal of Structural Engineering,124(6): 642–652.

Lourenco, P. B., Olivera, D. V., Roca, P., Orduna, A. (2005). *Dry joint stone masonry walls subjected to in-plane combined loading*, Journal of Structural Engineering, ASCE, 131(11), pp. 1665-1673.

Lourenço, P.B. (1996). *Computational strategies for masonry structures,* Doctoral hesis, Delft University Press, Netherlands.

Lourenço, P.B., Mourão, S. (2001). *Safety assessment of moastery of Jeronimos, Lisbon,* Proc. 3rd Int. Seminar on Structural Analysis of Historical Constructions, Guimarães, Portugal, pp 697-706.

Lourenço, P.B. (2002), *Computations on historic masonry structures,* Prog. Struct. Engg Mater., 4:301–319 (DOI: 10.1002/pse.120).

Lourenço, P.B. (2005), *Assessment, diagnosis and strengthening of Outeiro Church, Portugal,* Construction and Building Materials 19, pp 634-645.

Mark, R. (1982). *Experiments in Gothic structure*. The Massachusetts Institute of Technology Press, Massachusetts and London.

Martínez, G., 2008. *Vulnerabilidad sísmica de edificios históricos de obra de fábrica de mediana y gran luz. Aplicación a la cathedral de Mallorca*. Ph. D. dissertation. Universitat Politècnica de Catalunya: Barcelona.

Maynou, J. (2001). *Estudi estructural del pòrtic tipus de la Catedral de Mallorca mitjançan l'estàtica gràfica.* Graduation Thesis. Universitat Politècnica de Catalunya, Barcelona.

Modena, C., Valluzzi, M.R., Binda, L., Cardani, G., Saisi, A. (2004). *Vulnerability of historical centres in seismic area: reliability of assessment methods for different building typologies,* 13th International Brick/Block Masonry Conference RAI Amsterdam in CD-ROM.

Ramos, L. F. (2002). *Experimental and numerical analysis of historical masonry structures,* MSc thesis, Univ. of Minho, Guimarães, Portugal, available from (www.civil.uminho.pt/masonry) (in Portuguese).

Restoration of the Cathedral of Palma de Mallorca (1903-1914), Source: *http://www.gaudiclub.com/ingles/i_vida/mallorca.asp.*

RISK-UE: *An advanced approach to earthquake risk scenarioswith applications to different European town, WP4: Vulnerability of current buildings, by* Zoran V. Milutinovic & Goran S. Trendafiloski, Contract: EVK4-CT-2000-00014, September, 2003.

Roca, P. (2001). *Studies on the structure of Gothic cathedrals,* Historical Constructions, P.B. Lourenço, P. Roca (Eds.), Guimarães, pp. 71-90.

Roca, P. (2004). *Considerations on the significance of history for the structural analysis of ancient constructions*, Proc. 4th Int. Seminar on Structural Analysis of Historical Constructions, Padova, pp 63-73.

Rubió, J. (1912). *Conferencia acerca de los conceptos orgánicos, mecánicos y constructivos de la catedral de Mallorca*, Anuario de la Asociación de Arquitectos de Cataluña, Barcelona.

Salas, J. (2002). *Estudio estructrural de los porticos tipo de la Catedral de Mallorca*. Graduation Thesis. Universistat Politècnica de Catalunya.

Senthivel, R., Lourenco, P.B., Vasconcelos, G. (2006), *Analytical modeling of stone masonry wall under monotonic and reversed cyclic lading*, Structural Analysis of Monuments and Historical Constructions, New Delhi, pp. 1005-1012.

Silva, P.G., González Hernández, F.M., Goy, J.L., Zazo, C. and Carrasco, P. (2001). *Paleo and historical seismicity in Mallorca (Baleares, Spain): a preliminary approach*, Acta Geologicahispanica, v. 36, nº 3-4, pp. 245-266.